# Behaviour of Concrete Corbels Reinforced with GFRP Bent Bars

By

**Ankit Borgohain**

A Thesis submitted to the Faculty of Graduate Studies of

University of Manitoba

in partial fulfillment of the requirements of the degree of

**Master of Science**

Department of Civil Engineering

University of Manitoba

Winnipeg, MB, Canada

# Abstract

Steel-reinforced concrete (RC) corbels are one of the significant components in the precast buildings and superstructure of bridges, and they are used for load transfer from girders or slabs to columns. In North America, such elements are exposed to harsh weather, which makes them more susceptible to corrosion problems. This study focused on the behaviour and performance of reinforced concrete corbels using non-corrodible glass fibre reinforced polymer (GFRP). The study involved constructing and testing fourteen large-scale concrete double-sided corbel specimens to failure. Twelve out of the fourteen corbels were reinforced with GFRP bent bars, and the remaining two were reinforced with steel reinforcement as control specimens. Four out of the twelve GFRP-RC corbels were cast using high-strength concrete (HSC), while the remaining eight were constructed using normal-strength concrete (NSC). The corbel was tapered with cross-sectional dimensions of 450 mm deep × 300 mm wide at the corbel-column interface and 300 deep × 300 mm wide at the free edge. The overall length of each corbel, measured from the corbel-column interface, was 600 mm. All corbels were tested in an inverted position under displacement-controlled monotonic loading. The test variables were the shear span-to-depth ratio, main reinforcement ratio, crack-control horizontal reinforcement ratio, and concrete strength. The test results were presented in terms of the cracking and ultimate capacities, deflection and strains in reinforcement and were compared to predicted values by relevant Canadian Standards and American Codes.

The test results indicated the formation of the strut-and-tie-model (STM) and showed that increasing the concrete strength and main reinforcement ratio increased the stiffness and load-carrying capacity of the corbel to a large extent. Increasing the shear span-to-depth ratio and decreasing the crack-control horizontal reinforcement ratio led to a significant decrease in the load-carrying capacity of the corbel. Overall, this study contributes to a better understanding of the behaviour and performance of the non-corrodible GFRP reinforcement in concrete corbels. The results can lead to the development of design guidelines and

standards for corbels, especially in North America, where harsh weather makes such components more susceptible to corrosion problems.

# Acknowledgements

I am profoundly grateful to my advisor, Dr. Ehab F. El-Salakawy, Ph.D., PEng, FACI, FCSCE, FEIC, FIIFC, Professor of Structural Engineering in the Department of Civil Engineering at the University of Manitoba for his trust, encouragement, guidance, support and extreme patience throughout this work and his precious academic and personal advice.

I want to thank my colleagues and seniors for their continuous support, especially Yasser Selmy, Ibrahim Abdelwahed, Hasanur Rahman, Shukai Chen and Matthew Allen, whose comments and suggestions were remarkable. I would also like to thank Dr. Karam Mahmoud for his continuous help and encouragement. Also, I would like to thank Dr. Ahmed Bediwy for his support in editing and revising the two journal papers from this work.

I want to thank the technical staff of the W. R. McQuade structures laboratory: Dr. Chad Klowak, P.Eng., Samuel Abraha and Dan Szara for their support and help during the construction and testing of the specimens. Also, the financial support from the Natural Science and Engineering Research Council of Canada (NSERC), University of Manitoba Graduate Fellowship (UMGF) and MITACS is greatly appreciated.

Finally, no words can explain my love and gratitude to my parents and my sister (Ma, Deuta and Jharna), whose unconditional love, patience and support always kept me going through my life. This endeavour would not have been possible without elderly blessings (Koka, Aita, Anai, Putha, Dodo, Khuri, Mama and Mami) and love from my cousins (Borsha and Gupa) and my dearest friends. Lastly, I would like to thank the almighty Lord Shiva for giving me the strength and concentration to complete this project.

# Table of Contents

# List of Figures

# List of Tables

# List of Abbreviations

| | |
|---|---|
| ACI | American Concrete Institute |
| CSA | Canadian Standards Association |
| CCC | Node with Three Compression Struts |
| CCT | Node with Two Compression Struts and One Tension Tie |
| GFRP | Glass Fibre-Reinforced Polymers |
| HSC | High-Strength Concrete |
| NSC | Normal-Strength Concrete |
| RC | Reinforced Concrete |

# List of Notations

| | |
|---|---|
| $a$ | shear span, equal to distance from center of concentrated load to the face of support for cantilevered members |
| $a_g$ | Maximum aggregate size |
| $A_{cs}$ | Effective cross-sectional area of strut |
| $A_s$ | Area of non-prestressed reinforcement on the flexural tension side. |
| $A_{hx}$ | Cross-sectional area of horizontal stirrups |
| $A_{sw}$ | Area steel of web reinforcement |
| $A_1$ | Loaded area for consideration of bearing, strut, and node strength |
| $A_2$ | Area of the lower base of the largest frustum of a pyramid, cone, or tapered wedge contained wholly within the support and having its upper base equal to the loaded area. |
| $b_w$ | Width of the member |
| $d$ | Effective depth of the member |
| $E_c$ | Secant Modulus of Elasticity of concrete |
| $E_s$ | Modulus of elasticity of non-prestressed reinforcement |
| $f_{cr}$ | Cracking strength of concrete |
| $f'_c$ | Cylinder compressive strength of concrete |
| $f_{c2}$ | Compressive stress in diagonally cracked concrete in principal direction. |
| $f_{c2max}$ | Crushing Strength of diagonally cracked concrete at failure. |
| $f_{shx}$ | Stress in horizontal stirrups |
| $f_{shfinal}$ | Stress in the reinforcement at the surface of a crack due to mechanism II |
| $f_{cu}$ | Limiting compressive strength |
| $f_1$ | Principal tensile stress in concrete |
| $f_2$ | Principal compressive Stress in Concrete |

| | |
|---|---|
| $f_{ck}$ | Characteristic compressive cylinder strength of concrete at 28 days |
| $f_{cd}$ | Design value of concrete compressive strength |
| $f_{FU}$ | Ultimate strength of the FRP bar |
| $F_{nm}$ | Nominal compressive strength of a nodal zone |
| $F_{ns}$ | Strength of strut |
| $H$ | Overall Depth of the Member |
| $M$ | Bending Moment at the section of Interest |
| $P_{cr}$ | First flexural-cracking load of the failed side of the corbel |
| $P_u$ | Ultimate experimental capacity of the failed side of the corbel |
| $s_x$ | Transverse spacing of secondary horizontal crack-control reinforcement |
| $s_\theta$ | Spacing of diagonal cracks |
| $s_z$ | Crack spacing parameter dependent on crack control characteristics of longitudinal reinforcement |
| $s_{ze}$ | Equivalent value of $s_z$ that allows for influence of aggregate size |
| $\upsilon$ | Shear Stress at the section of interest |
| $\upsilon_{ci}$ | Shear stress on the crack interface |
| $V$ | Shear force at the section of interest |
| $V_{(1)}$ | Shear strength of corbel due to mechanism I (direct strut) |
| $V_{stirrups}$ | Shear strength of corbel due to horizontal crack-control reinforcement |
| $w$ | Crack width |
| $w_s$ | Width of a strut perpendicular to the axis of the strut |
| $w_t$ | Effective tie width in a strut-and-tie model |
| $\beta_c$ | Strut confinement modification factor |
| $\beta_s$ | Strut coefficient |

| | |
|---|---|
| $\delta_{max}$ | Mid-span deflection at failure |
| $\delta_{sl}$ | Deflection at service load |
| $\varepsilon_c'$ | Strain at Maximum compressive stress |
| $\varepsilon_1$ | Principal Tensile Strain |
| $\varepsilon_2$ | Principal Compressive Strain |
| $\varepsilon_{x,STM\ 1}$ | Strain in horizontal crack-control due to mechanism I (direct strut) |
| $\varepsilon_{final\ x,STM\ 2}$ | Strain at a crack-location in horizontal crack-control due to mechanism II |
| $\varepsilon_f$ | Tensile strain in the tie |
| $\phi_c$ | Resistance factor for concrete |
| $\phi_s$ | Resistance factor for steel |
| $\theta$ | Inclination of Principal average compressive stresses of the Strut to Tension Tie |
| $\sigma_{rd}$ | Allowable compressive stress of struts |
| $\rho_{sw}$ | Reinforcement ratio for Web reinforcement |
| $\rho_{main}$ | Main longitudinal reinforcement ratio |
| $\nu$ | Reduction factor for concrete strength |

# Chapter 1. Introduction

## 1.1 General

Reinforced concrete (RC) corbels are extensively used as load transfer elements from girders and primary beams to support members such as columns, walls, and piers. The position of loads and support locations in a structural member influence shear behaviour, determining the presence of bending regions (B) or disturbed regions (D). Bending or Bernoulli (B) regions in a structural member are those parts where plane sections remain plane after bending. This assumption implies a linear or plane strain profile due to the linearly varying strain trajectories. For members with B-regions, sectional forces can be easily used to obtain the stress state of the cross-section using section equilibrium. Disturbed (D) regions are those in which the Bernoulli hypothesis can no longer be applied. In these regions, a non-linear strain distribution is caused by static (e.g., presence of concentrated loads) and geometric (e.g., abrupt change of cross-section) discontinuities. The flow of stresses is disturbed, and plane sections no longer remain plane after loading. As a result, a regional design approach, for instance, the strut-and-tie model (STM) method, can be followed instead of a sectional analysis. The details of the STM method can be found in the following Section 2.6. STM is extensively used to design D-regions such as corbels, pier-cap, dapped beams, and deep beams (Figs. 1.1 – 1.3). The STM method can also be used to design members in the B-regions as well.

Steel-RC corbels can be designed with the empirical method using shear friction theory or the STM method (ACI 318-19 2019). The STM method is specially used for designing D-regions, which treats the problem of shear and flexure in a single approach. The STM method uses load paths, also called “stress trajectories,” and idealizes them as compression and tension members forming a truss. Compression members are called struts, and tension members are called ties.

Figure 1.1. Pier-cap supporting the deck is designed by Strut-and-Tie Modelling (STM)

Figure 1.2. Corbel under column load is also designed as an STM.

Figure 1.3. Corbels are used in the construction of precast buildings[1].

According to the STM methodology, load paths with the lowest number and lengths of tension ties are more feasible as the loads use the paths with the least forces and deformation since the reinforced ties are much more deformable than the concrete struts (Schlaich et al. 1987). On the other hand, the traditional design method of corbels uses the section's shear friction and flexural capacity to carry the load. After the formation of a shear crack, the reinforcement passing through the crack experiences a tension force, which

[1] Snapshot taken from https://www.youtube.com/@PeikkoGroupCorp (URL: https://youtu.be/WsL-xkAO67Q )

applies a clamping force, controlling the crack opening. This clamping/compressive force, which is normal to the surface of the crack, gives rise to the frictional force, resisting slippage of the two faces of the crack.

Reinforced Concrete structures are usually reinforced with conventional steel reinforcement. In the presence of moisture, steel is subjected to a significant durability problem: corrosion. Corrosion of steel reinforcement is one of the significant durability issues resulting in the deterioration of structures which increases the number of repair cycles required for a structure to achieve its service life and, consequently, increases the repair and maintenance costs over the service life of the structure. The National Association of Corrosion Engineers (NACE) started the International Measures of Prevention, Application and Economics of Corrosion Technologies (IMPACT) report (Koch *et al.* 2016, IMPACT Canada Study - AMPP 2021) to examine the role of corrosion management in industry. In this recent report, the total annual direct cost of corrosion in Canada is estimated to be USD 51.9 billion, approximately 2.98% of the nation's Gross Domestic Product "GDP".

When used as internal reinforcement for concrete structures in harsh environments, fibre-reinforced polymers (FRP) reduce any possible durability concerns related to steel reinforcement. Design equations and code requirements for steel-RC structures have been developed based on the characteristics and behaviour of steel. Therefore, it should be noted that current equations cannot be readily applied to FRP-RC design. The primary distinction between FRP and steel is that the former does not have a yield point. The FRP material exhibits elastic deformation to failure and does not exhibit steel's stress-strain plateau. For FRP reinforcement, a select few fibre types have been employed, including carbon, aramid, glass, and basalt. However, glass FRP (GFRP) is the most desirable due to its excellent strain capacity and relatively cheaper cost.

To have a safe and less brittle failure using the GFRP reinforcement, the standards and codes need to ensure that the corbel undergoes a ductile or deformable mode of failure such that no premature failure occurs. The steel-RC corbels rely on reinforcement yielding for a safe and ductile failure mode. This type of failure

is impossible for GFRP-RC corbels due to their linear behaviour and brittle failure state of the GFRP reinforcement. Therefore, the primary load-carrying mechanism should fail using the least brittle method - members undergoing concrete compression crushing. Studies need to be conducted to check the applicability of the STM to GFRP-RC, particularly if the horizontal crack-control reinforcement was adopted. The crack-control reinforcement is an essential requirement as it helps transfer stresses throughout the corbel's depth and prevents the premature failure of the compression struts. The GFRP reinforcement has a lower modulus of elasticity and will undergo more strains for the same stress than steel reinforcement. The minimum requirements for horizontal crack-control reinforcements need to be investigated in the case of GFRP.

The next essential aspect of this research is to look at the impact of concrete strength on the failure of GFRP-RC. Over the last few decades, there has been progressive and continuous growth in the application and definition of high-strength concrete (HSC). Concrete with a compressive strength of 34 MPa (5,000 psi) was regarded as high strength in the 1950s. In the early 1970s, 62 MPa (9,000 psi) concrete was created. Laboratory researchers using unique materials and processes have achieved “concretes” with compressive strengths of more than 800 MPa (116,000 psi) (Schmidt and Fehling 2005). It is probable that the maximum compressive strength of concrete will continue to rise, and that HSC will be employed in more applications as materials technology and manufacturing techniques advance with time. Compressive strength of 55 MPa or more is considered HSC according to current standards (ACI Committee 363 2011, ACI Committee 222 2019). Its failure due to shear can be significantly different from the normal-strength concrete (NSC), where the HSC has lower aggregate interlock resistance due to the shear plane passing through the coarse aggregates, where the aggregate interlock is the primary shear resistance mechanism. In conclusion, the HSC exhibits a more brittle behaviour, necessitating unique design considerations (ACI Committee 363 2010), particularly in shear design for D-regions when GFRP reinforcement is applied.

## 1.2 Problem Definition

The STM uses struts as compression members and ties as tension-carrying members. While a strut constantly undergoes compression in its longitudinal direction, depending on its *H/d* and *D/d* ratios (where *D* is the width of confinement, *d* is the width of the strut bearing, and *H* is the height of the strut), it may also develop transverse tensile strains at mid-height of the struts (Adebar and Zhou 1993). If a strut under compression develops longitudinal tensile cracking at mid-height, it may never reach its design capacity and may undergo early failure. This is the reason why various code provisions have requirements to provide secondary horizontal reinforcement throughout the depth of the corbel. This reinforcement should be ideally provided in the transverse direction of the strut. However, struts are usually inclined, which makes them receive a component of the secondary horizontal reinforcement in the direction of transverse tensile forces. On a plane stress field, the spreading of compressive stresses over the length of the strut significantly affects the strength of the strut before tensile splitting. When the compressive stresses spread over a longer strut length, the limiting tensile strength of the strut decreases.

This would be worsened in case of using GFRP as main or secondary reinforcement due to its lower modulus of elasticity, leading to large deformations under the same load as steel. This may lead to some compatibility issues, especially for high-strength concrete (HSC) because of its lower deformability (brittleness). The Canadian Standards such as CSA S806-12 (CSA 2021), CSA A23.3-19(CSA 2019a) and CSA S6-19 (CSA 2019b) follow an analytical method of design. The American codes and guidelines such as ACI 440.1R-15 (ACI Committee 440 2015), ACI 318-19 (ACI Committee 318 2019) and ACI PRC 445.2-21 (ACI-ASCE Committee 445 2021) and ACI 440.11R-22 (ACI Committee 440 2022) have shear equations derived from an extensive database of parametric testing done in shear during experimental investigations. These equations to design for shear are empirical in nature. On the other hand, CSA Standards shear equations are much more intuitive because the theory is based on the mechanics of cracked RC. The STM design provisions in ACI 318-19 (ACI Committee 318 2019) for steel-RC corbels need to be reviewed well before applying it to GFRP-RC corbels because of the differences in the mechanical

properties of the reinforcement and consequently, the change in the mode of failure of the STM. Even though the CSA S806-12 (CSA 2021) has its existing STM provisions from the Canadian Standards for steel-RC corbels (CSA 2019a, b), these provisions have been only reviewed for certain slender elements and deep beams reinforced with GFRP. Therefore, the existing design provisions for the GFRP-RC corbels in Canadian Standards CSA S806-12 (CSA 2021) must be validated.

## 1.3 Research Significance

Based on the problem definition, research is needed to investigate the feasibility and applicability of GFRP-RC STM in the context of corbel design. Only one study, with limited scope, has been reported on concrete corbels reinforced with straight GFRP bars (Abu-Obaida *et al.* 2018), even though significant research has been carried out on other D-Region components reinforced with GFRP, such as deep beams; both simply supported (El-Sayed *et al.* 2012; Andermatt and Lubell 2013; Mohamed *et al.* 2017; Mohamed et al. 2021) and continuous (Mohamed et al. 2021). Also, previous research on GFRP-RC deep beams has shed light on the importance of crack-control horizontal reinforcement to prevent premature brittle failure, which needs further investigation. Furthermore, an analytical model based on the CSA standards needs to be developed to help predict diagonal tension failure and calculate additional corbel capacity due to horizontal crack-control reinforcement. This pioneering research project builds on the systematic experimental and analytical investigation of other D-regions structures (e.g., steel-RC corbels, GFRP-RC deep beams) to identify the critical parameters controlling corbels' behaviour when reinforced with GFRP bent bars.

## 1.4 Scope of Work

Corbels could be one-sided or two-sided based on their location in the structure (Figure 1.3). Due to the simplicity of the test setup, which is statically determinate (Kriz and Raths 1965, Mattock et al. 1976, Fattuhi 1990a, 1990b, 1994a, 1994b), double-sided corbels were selected in this study. The corbels were selected for an intermediate-storey interior column, which has an extension of the column stub beyond the tension side of the corbel. This extension of the column stub is almost equal to the depth of the column to

study the effect of external loads in the D-regions of the column-corbel assembly. The shear-span has been varied from 133 to 265 mm to mimic varying shear span-to-depth ratios (*a/d*) of 0.33 and 0.66, respectively.

## 1.5 Objectives

This research study has the following main objectives:

1. Examining the behaviour of GFRP-RC corbels reinforced with GFRP bent bars under monotonic loads, considering key parameters, which are known to affect such behaviour.
2. Determining the difference between the behaviour of GFRP-RC corbels and steel-RC corbels.
3. Validate the shear provisions in the Canadian Standards Association, CSA S806-12, and CSA S6-19, the American Concrete Institute code ACI 318-19, and the European code (EC2) against test results of large size GFRP-RC corbels.
4. Develop an add-on analytical model to allow accurate prediction of shear capacity due to horizontal web reinforcement and to predict diagonal tension failure.
5. Provide recommendations for designers and researchers to predict the ultimate capacity of GFRP-RC corbels.

The influence of the following specific parameters on the shear behaviour of double-sided corbel has been investigated to attain these key goals:

1. Shear span-to-depth ratio (*a/d*) of 0.33 and 0.66.
2. Flexural/main tie reinforcement ratio (0.5 and 0.7%)
3. Reinforcement ratio of horizontal stirrups (0.7 and 1.3 %).
4. Concrete compressive strength (35 MPa for NSC and 60 MPa for HSC)

## 1.6 Work Methodology

Based on the objectives of this study, an experimental program was conducted. The results of fourteen (14) full-scale GFRP-RC corbels were analyzed to understand their performance and behaviour better. All the corbels were fabricated and tested at the McQuade's Structural Laboratory of the University of Manitoba. It was necessary to test specimens roughly the same size as commonly used corbels to achieve the study's objectives and accurately characterize the behaviour and performance of GFRP-reinforced corbels. The corbels had 300 mm in width and 450 mm in height. All the tested specimens in the current study were designed according to the Canadian standards CSA S806-12 (CSA 2021) and CSA A23.3-19 (CSA 2019), as appropriate.

The experimental program was divided according to the objectives of the current study as follows: all the fourteen specimens were equally divided, having two different *a/d* ratios (0.33 and 0.66); and four specimens, out of the fourteen, did not contain any web reinforcement, while the remaining ten specimens contained horizontal crack-control reinforcement. The main reinforcement ratio was 0.5% for half of the specimens and 0.7% for the remaining. Five specimens, out of the fourteen, were constructed with HSC, while the others were built with NSC. The list of specimens, along with their parametric variations, are listed in Table 6.1 of Appendix A. The experimental results were analyzed to evaluate the effect of *a/d* ratio, concrete strength ($f'_c$), type of reinforcement (steel and GFRP), main tie reinforcement ratio and, crack-control horizontal reinforcement ratio on the crack pattern and mode of failure, the load-deflection response, the ultimate capacity, the crack width and strains in reinforcement on the GFRP-RC corbels. In addition, the formation of arch action and the development of STM were also investigated. Then, the experimental results were compared to the STMs proposed by different codes and standards. Finally, a new strut-and-tie ad-on analytical model was proposed based on the provisions of the CSA standards using postulates of modified compression field theory and validated with the experimental results in the current study.

## 1.7 Thesis Organisation

The thesis consists of six chapters and three appendices. The contents of each chapter can be summarized as follows:

**Chapter 1** presents background information on the research topic, the problem definition, research significance, the scope of the work, objectives and the adopted methodology.

**Chapter 2** introduces a literature review reporting the documented mechanism of steel-RC corbels under flexure and shear. The code provisions and analytical models for steel-RC corbels from the literature are also demonstrated. The effect of *a/d* ratio, crack-control horizontal reinforcement with different main reinforcement configurations on the behaviour of steel-RC corbels, concrete strength and the effect of column load is presented. Furthermore, the chapter provides a summary of relevant design codes and guidelines with regard to the use of GFRP materials in deep members such as corbels.

The following chapters (3 and 4) are presented in journal article format. The articles have been submitted to the respective journals and are currently under review.

**Chapter 3** (Article 1) exclusively deals with the two major parameters: crack-control reinforcement ratio ($\rho_{sw}$) and shear span-to-depth (*a/d*) ratio and their impact on the ultimate capacity of the GFRP-RC corbels. It also discusses the effects of main tie reinforcement ratio coupled and uncoupled with parameters like horizontal crack-control reinforcement ratio on its impact on ultimate capacity. Also, the serviceability state for GFRP-RC corbels with respect to steel-RC corbels has been discussed. Finally, various code and standards predictions have been compared with ultimate load capacities. Article 1 integrates the results of Series I and II (Appendix A) and the first nine out of the fourteen corbel specimens tested in this research program.

Borgohain, A., Bediwy, A. and El-Salakawy, E.F. “Performance of GFRP-Reinforced Concrete Corbels under Monotonic Loading,” ASCE, Journal of Composites for Construction, under review.

**Chapter 4** (Article 2) provides an in-depth analysis of two primary parameters, concrete strength ($f'_c$) and shear-span-to-depth (*a/d*) ratio, and their impact on the load-carrying capacity of the specimens. Additionally, the study investigates the effects of combined parameters, such as longitudinal and horizontal crack-control reinforcement ratios, on the ultimate capacity of the corbels. Moreover, this chapter discusses the serviceability state of GFRP-RC corbels, and various code and standards predictions are compared to the actual ultimate load capacities. Overall, this chapter offers a comprehensive overview of the factors that affect the ultimate capacity of corbel specimens, with a particular focus on GFRP-RC corbels. This chapter focuses on Series II and III (Appendix A), encompassing nine out of the fourteen corbel specimens examined in the research program.

Borgohain, A., Bediwy, A., and El-Salakawy, E.F. "Practical Evaluation of High-Strength Concrete Corbels Reinforced with GFRP Bars." Engineering Structures, Elsevier, under review.

**Chapter 5** addresses the uncertainties in predicting the ultimate strength of corbels with horizontal crack-control reinforcement. An analytical model for calculating additional strength due to horizontal crack-control reinforcement in corbels is developed using the Modified Compression Field Theory. The model can also predict the type of failure either strut-crushing or diagonal-tension. It also shows the flow chart and how this analytical model can be incorporated into spreadsheets or computer codes.

**Chapter 6** summarizes the significant findings of the work and essential conclusions. Recommendation for future work is also included.

Both Article 1 in Chapter 3 and Article 2 in Chapter 4 have their stand-alone sections dedicated to the experimental program. Table 6.1 in Appendix A lists all the specimens in the program. Appendix A also contains information on the design, fabrication, and testing procedure of the specimens. Sample calculations with the CSA S806-12 and ACI 318-19 are shown in Appendix B and Appendix C, respectively.

# Chapter 2. Literature Review

## 2.1 Bernoulli versus Discontinuity Regions

The shear behaviour of steel-RC members shows a change in the failure mode at an *a/d* ratio of 2.0 to 2.5 (Wight and MacGregor 2009b). Slender members are RC members with higher shear span-to-depth ratios (*a/d* > 2.5). In contrast, deep or non-slender members have an *a/d* ratio of less than 2.5 (Kani 1966). Collins and Kuchma (1999) found that the *a/d* ratio significantly influences the shear capacity of an RC component, as shown in Figure 2.1 and Figure 2.2. When the *a/d* ratio falls below 2.5, the shear stress at failure rapidly increases, suggesting a shift in the shear transfer mechanism.

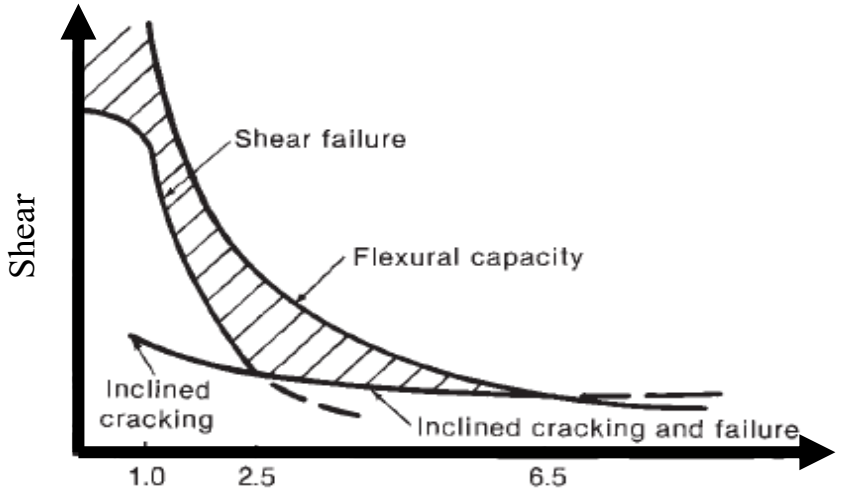


Figure 2.1. Effects of shear-span-to-depth ratio on Shear capacity of members (Wight and MacGregor 2009b))

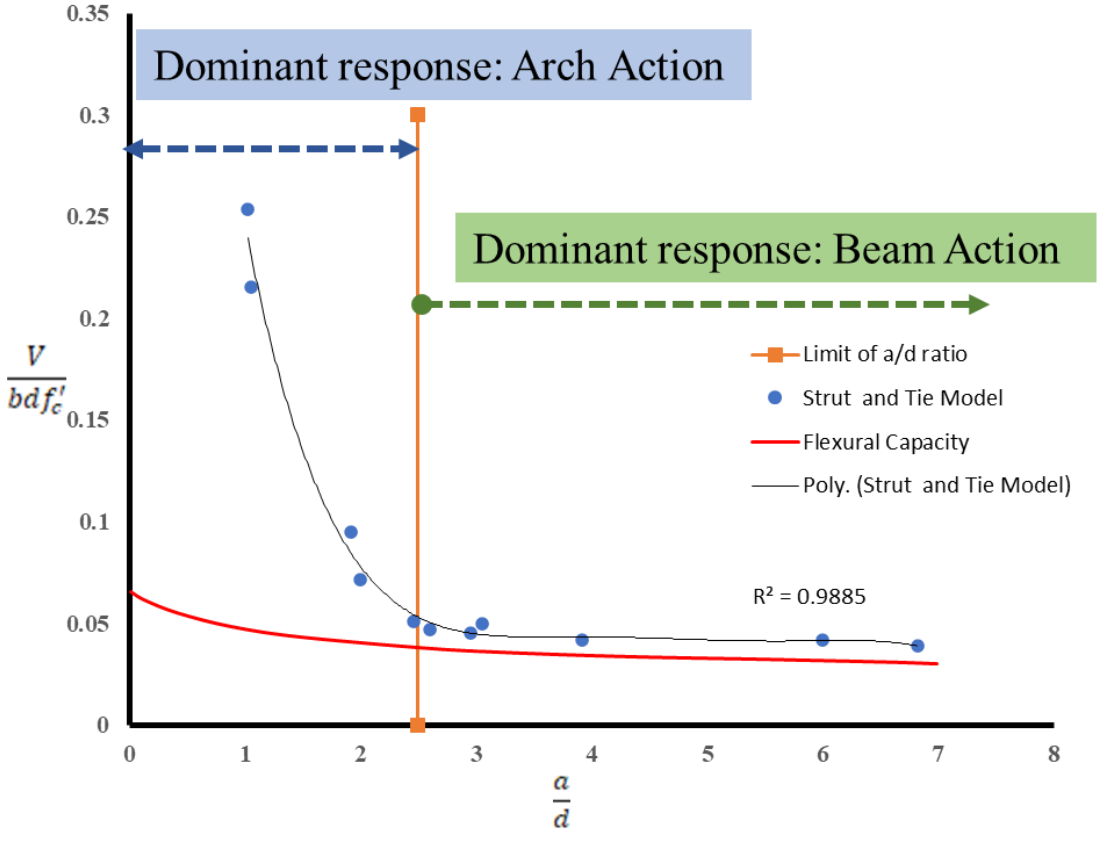


Figure 2.2. Shear strength of a simply supported RC beam varying with shear -span-to-depth ratio (*a/d*). (Adapted from (Kani *et al.* 1979) )

Depending on the *a/d* ratio, different analytical methodologies are employed for the design and analysis of steel-RC members due to these variations in observed behaviour. Sectional flexural and shear models are commonly used to analyze thin members with $a/d > 2.5$. As further stated in Section 2.3, one technique for assessing deep members with $a/d \leq 2.5$ uses strut-and-tie (STM) models.

Due to these differences in observed behaviour, different analysis approaches are used for steel-RC members depending on the *a/d* ratio. For slender members with $a/d > 2.5$, the analysis typically uses sectional flexural and shear models. Strut-and-tie models analyze deep members with $a/d < 2.5$ as further discussed in STM Modelling, Section 2.6.

Kriz and Raths (1965) conducted the first experimental and analytical studies on the behaviour of RC corbels using normal strength concrete (NSC), involving the following parameters: main reinforcement

ratio, shear span-to-depth ratio (*a/d*), concrete strength ($f'_c$), and the applied horizontal load to vertical load ratio ($N_u/V_u$). The authors observed that tension reinforcement and horizontal stirrups had the same impact on corbel strength when subjected to vertical stress. Whereas the presence of horizontal load drastically reduced corbel strength. All forms of failure mentioned above tend to converge into a single category of beam-shear failure in corbels with supplementary reinforcement (stirrups), which is always recommended. This type of beam-shear failure is distinguished by the formation of one or more diagonal cracks, followed by shear failure in the compressed zone of the strut. The researchers also found the stress state at which bearing failures occurred. They concluded that a stress of $0.34f'_c$ was the ultimate strength of a node when the *a/d* ratios were larger. The research also showed that the effect of crack-control reinforcement on increasing the ultimate strength of corbels kept decreasing as the ($N_u/V_u$) kept increasing.

Mattock et al. (1976) conducted a substantial study on corbels, focusing on the shear friction approach. The research used a certain quantity of minimal secondary reinforcement to minimize early diagonal failure and yield the primary reinforcement (steel). According to the study, the yield strength of horizontal stirrups is half that of the primary reinforcement, which resists vertical shear but not horizontal stresses. If the primary reinforcement yields, any form of failure is acceptable, according to the report (flexural or beam shear). The article compared several approaches for designing corbels, including shear friction provisions, improved shear friction equations previously provided (for both standard and lightweight concrete corbels), and flexural capacity. An intriguing finding was that the primary reinforcement yielded a load lower than the ultimate capacity of the corbels. This behaviour was observed in specimens with lower *a/d* and reinforcement ratios. The load at which the primary reinforcement yielded or the maximum load at which the main reinforcement did not yield was used to calculate the ultimate functional strength of the corbels.

Adebar and Zhou (1993) concluded from experimental and numerical investigations that while a strut always experiences longitudinal compression, based on its *H*/*d* and *D*/*d* ratios (where *D* is the width of confinement, *d* is the width of the strut bearing, and *H* is the height of the strut), it may also experience transverse tensile stresses at mid-height (Adebar and Zhou 1993). Suppose a compression strut develops

transverse tensile cracking at the mid-height. In that case, it may never achieve its intended capacity and break prematurely. This is why various code standards require supplementary horizontal reinforcement to be provided along the depth of the corbel. This reinforcement should preferably be applied in the strut's transverse direction. Struts, on the other hand, are typically inclined, allowing them to receive a component of secondary horizontal reinforcement in the direction of transverse tensile stresses.

Abdul-Razzaq and Dawood (2021) evaluated the performance of STM models by comparing standard STM models to novel reference frame models consisting solely of struts and ties that were strengthened and tested at *a/d* ratios of 0.5, 1.0, and 1.5. The conventional STM specimens were built using an orthogonal grid. However, strut-and-tie confinement restricted the suggested frame STM specimens. Only at greater loads did the steel-RC specimen SN-0.33-0.5-10 exhibit fractures. The primary reinforcement was secured to the steel plates to eliminate the chance of anchoring failure. Corbels with larger *a/d* ratios failed at lower loads because of the reduced vertical component of strength that the struts could provide. Furthermore, cracking showed soon for the same specimens because the horizontal component of strut strength was significantly greater than that of the smaller *a/d* ratios. Strut cracking caused the failure of the specimen with a lower *a/d* ratio of 0.5. The failure of a compressive strut was shown to be more ductile than diagonal splitting. Furthermore, compressive strut failure was observed to have finer cracks that were more equally distributed than strut splitting failure. Some suggested framed STM specimens lacked a concrete cover (uncovered tie). The uncovered tie specimens yielded faster than the reference STM specimens, which were built following the ACI 318-14 (ACI 2014) orthogonal grid crack-control standards.

## 2.2 D-Regions (Double-sided RC Corbels and Deep Beams)

There are several factors affecting the behaviour and strength of RC corbels, which are listed below:

1. Shear-span-to-depth ratio
2. Web reinforcement or crack-control reinforcement.
3. Concrete strength

4. Longitudinal reinforcement ratio.
5. Presence of column-load

### *2.2.1 Effect of shear-span-to-depth ratio*

The shear span-to-depth (*a/d*) ratio determines the inclination of the struts, which transfer compression from the bearing region to the support location. An increase in the above parameter makes the struts more inclined to the direction of the longitudinal ties. In an STM with struts as its weakest link, the strut controls the strength of the mechanism. As a result, the vertical load capacity of STM decreases with the increase of *a/d* ratio.

Both the proposed and the conventional corbel specimens in the study by (Abdul-Razzaq and Dawood 2021) showed a decrease in the strength of corbels with an increase in *a/d* ratio. Also, the deflection increased from 15% to 55% for the proposed specimens, while the conventional specimens increased from 10 to 36%.

El-Sayed et al. (2012) tested ten full-scale RC deep beams reinforced with GFRP and CFRP reinforcement. The test variables included the main reinforcement ratio, shear-span-to-depth ratio (*a/d*) and modulus of Elasticity of the main reinforcement. The *a/d* ratio varied from 1.69, 1.3 and 0.92 for all the specimens. Decreasing *a/d* ratio from 1.69 to 1.3 for GFRP specimens increased the ultimate strength by 54%. Further, decreasing the *a/d* ratio from 1.6 to 0.92 showed that the capacities increased by 157%. Decreasing *a/d* was attributed to the fact that the tied arching action became more effective with decreasing *a/d* because of the increased angle between the inclined strut and the longitudinal direction of the main reinforcement. The decrease in *a/d* decreased the distance between the supports and the applied loads and hence increased the effectiveness of the arching mechanism by transmitting a greater part of the load directly to the support by diagonal compression.

Nagrodzka-Godycka (1999) studied nine corbels with various *a/d* ratios of 1,0.6 and 0.3 and had external prestressing or external passive steel bars. The specimens were tested first without any external prestressing

or passive reinforcement. After reaching about 60% of the ultimate capacity, they were unloaded and strengthened using prestressed or passive reinforcement. The studies investigated the parameters such as cracking and the load-carrying capacity of the corbels. The specimens with *a/d* of 0.3, 0.6 and 1.0 showed ultimate strength as 650, 475 and 250 kN, respectively.

### *2.2.2 Effect of web-reinforcement or crack-control reinforcement*

Web-reinforcement is required to regulate the crack-widths and prevents premature diagonal tension failure in the struts. Supposing the web reinforcement is laid in the direction of the main reinforcement or perpendicular to the main reinforcement, as in the case of vertical stirrups. In that case, only a component of the total reinforcement area is engaged in the orthogonal direction of the strut's longitudinal axis. This component is responsible for resisting the tensile strains in the struts. When the angle of the strut is very steep with the main reinforcement, the web-reinforcement in the direction of the main reinforcement resists much more tensile stresses than the web-reinforcement in the vertical direction and vice-versa.

Mohamed et al. (2017) tested ten full-scale deep beams reinforced with GFRP main reinforcement until failure under two-point loading apparatus. The test variables were the layout of crack-control reinforcement and shear span-to-depth ratio (*a/d* of 1.47, 1.13 and 0.83). The research showed that web-reinforcement had no apparent impact on the ultimate capacity of the specimens. The research also found that web reinforcement provided significant crack-control by 77% compared to deep beams without crack-control reinforcement. The first flexural crack occurred between 11-18% of the ultimate load, and the flexural cracks kept occurring at the constant moment region of the beam. The failure mode for all the specimens included the strut crushing fully or partially. The specimens with larger *a/d* of 1.47 and 1.13 with horizontal web-reinforcement showed premature strut failure before the ultimate strength because of the lower component of the cross-section area of the web-reinforcement being utilized in the confining action of the strut. The steeper strut with *a/d* of 0.83 had reached its ultimate strength without any premature failure.

### *2.2.3 Effect of compressive strength of concrete*

The STM, which has its compression members (struts) as the weakest members, depends on the compressive strength of the concrete. The increased strut compressive strength will directly increase its ultimate load-carrying capacity if the ties are over-reinforced. This is generally true for the GFRP-RC STM models, which are often over-reinforced. The increasing concrete strength will result in higher stresses in Ties and other nodal surfaces which must be checked during design.

For Steel-RC corbels, the specimens are under-reinforced, and increasing concrete strength might do very little in increasing the overall load-carrying capacity of the corbels as the weakest link are the tensile ties in such STM.

Andermatt and Lubell (2013) tested 12 large-scale concrete deep beams under shear in a four-point bending test where the primary test variables included shear span-to-depth ratio (*a/d*), reinforcement ratio, member height and concrete strength. The specimens had *a/d* ratio of 1.48, and the ultimate strength varied by 28% when the concrete strength was increased from 40.7 to 66.4 MPa. Both specimens had a main reinforcement ratio of 2.13%. This was not observed in the third specimen, which had a concrete strength of 39.9 MPa and reinforcement ratio of 1.7 % and *a/d* ratio of 1.48. This specimen showed brittle failure, and its ultimate capacity was 799 kN as compared to the other normal strength ($f_c' = 40.7$ MPa) specimen of 830 kN. This can be attributed to the fact that the specimen failed by strut failure and more reinforcement in the ties did not affect the corbel's ultimate capacity.

Fattuhi (1994b) performed Vertical load tests on concrete corbels with main reinforcements and various forms of web-reinforcement like steel or monofilament polypropylene fibres or with main bars and plastic mesh. The fibres or strips of plastic mesh were used as crack-control reinforcement, and both volume of the main bars and shear span-to-depth (*a/d*) ratio were varied. The tests indicated that corbels reinforced with main bars and without crack-control reinforcement failed explosively by diagonal splitting. The

addition of secondary reinforcements generally resulted in gains in terms of corbels' ultimate strength and ductility.

Corbels reinforced with steel fibres with smaller crack widths achieved high strengths and failed in a gradual and controlled manner. The results also show that the strength of corbels failing in flexure can be predicted with reasonable accuracy using simple beam theory while accounting for the secondary reinforcement.

### *2.2.4 Effect of longitudinal Reinforcement ratio*

The increase in main reinforcement ratio according to the strut-and-tie modelling (STM) should ideally show no difference in case of corbels and deep beams reinforced with GFRP. This is opposite to the specimens reinforced with steel reinforcement due to the change in the mode of failure. Steel-RC specimens failure occurs due to the yielding of ties, the weakest link in the truss model. If this member is strengthened and the concrete struts do not fail, the specimens in D-regions (corbels or deep beams) will have increased strengths. In contrast, the GFRP-RC specimens have the struts as the weakest links, which can be the bottleneck even though the main reinforcement is increased. If higher concrete strengths are used, the specimens will still show higher ultimate capacities.

Andermatt and Lubell (2013) did an extensive study of twelve simply supported deep beam specimens reinforced with GFRP and which studied test variables such as *a/d*, the reinforcement ratio, concrete strength, and depth of the section. It was found that increasing the main reinforcement steel by 24% resulted in a 3% increase in the normalized shear capacity w.r.t concrete strength.

### *2.2.5 Effect of column load*

Fattuhi (1990a) tested eighteen corbel specimens with varying main reinforcement, web reinforcement and shear span-to-depth ratio. The tests indicated that neither column load nor unequal corbel loads significantly contributed to corbel ultimate strength capacity. The web reinforcement was steel-fibres, which helped in reducing crack-widths and increasing ductility. The study showed that when corbels were

only reinforced with main reinforcement, it failed suddenly after reaching ultimate capacity. The presence of steel fibres as a web reinforcement prevented diagonal tension failure or shear-compression failure. They also found that the presence of column load delayed the occurrence of the first crack on the corbels.

## 2.3 Modified Compression Field Theory (MCFT)

The MCFT is an analytical model for predicting the response of two-dimensional RC structures subjected to in-plane shear and normal stresses. This method considers cracked concrete as a new orthotropic material using a smeared rotating crack approach. The smeared approach is used mostly for structural engineering applications, and it uses cracked concrete as a continuum. The strains in cracked regions are average strains which are spread out over an area. In this approach, as dictated by the loading or material response, the crack direction reorients gradually as opposed to the fixed crack approach, where the crack orientation remains fixed in the direction of the first crack. Another postulate of this rotating crack model is the assumption that the principal stress and principal strain directions remain coincident. Even though cracks are smeared and stress and strain values are averaged, consideration is also given to the local stresses and strains at cracks. The theory consists of three sets of relationships: compatibility, equilibrium, and constitutive relationships. The stress-strain relationships (constitutive relationships) were derived empirically from tests of 30 RC panels subjected to uniform in-plane normal and shear stresses, as shown in Equation 2-13 and Equation 2-14. Since then, the constitutive relationships of the theory have been validated by more than 200 RC panel element tests.

1. Reinforcement is uniformly distributed across the element.
2. Cracks are smeared and able to rotate.
3. Loads are applied uniformly on the element.
4. Formulations are based on average stresses and strains over a distance, including several cracks.
5. The direction of principal strain is the same as that of principal stress.
6. Independent of loading history, each strain state has a unique stress state.

7. A perfect bond between the reinforcement and the concrete exists.
8. Shear stresses on the reinforcement are negligible.
9. Average tensile stress in the concrete is limited to the reserve strength of the reinforcement at the cracks.
10. Independent constitutive relationships are considered for concrete and reinforcement.

The equations for MCFT:

For compatibility between concrete and reinforcement, any deformation experienced by the concrete must be identical to the deformation experienced by the reinforcement, as the perfect bond between the reinforcement and the concrete is assumed. Therefore, for non-prestressed reinforcement, the average strain in the reinforcement is equal to the average strain in the

concrete. Figure 2.3 shows the state of stresses that occurs on an exterior surface of a flexural member under shear and flexural stresses.

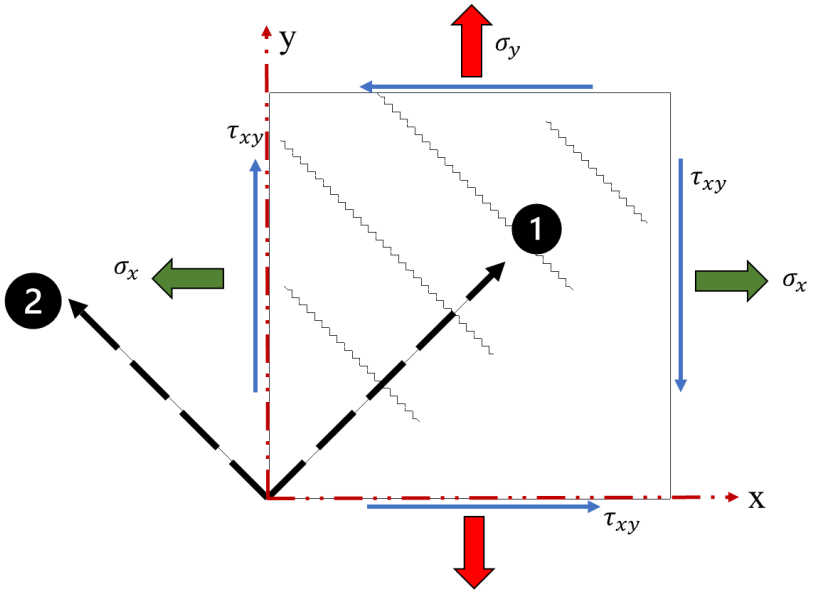


Figure 2.3. Stress state on a reinforced concrete (RC) shear-panel.

### *2.3.1 Equilibrium equations*

To establish the equilibrium of forces, the resultant of the externally applied normal stresses in the x-and y-direction,$(\sigma_x, \sigma_y)$ should be resisted by average concrete stresses $(f_{cx}, f_{cy})$ and average reinforcement $(f_{sx}, f_{sy})$ stresses in the x- and y-directions. Equilibrium of moment requires that the externally applied shear stress be entirely balanced by average shear stress ( $v_{cxy}$ ) in the concrete. Dowel action was not considered here.

Using the Mohr circle of stress, the compressive stress at the boundaries of the beam can be calculated as

$$f_{cx} = f_1 - v_{cxy} \times \cot(90 - \theta)$$

Equation 2-1

$$f_{cy} = f_1 - v_{cxy} \times \tan(90 - \theta)$$

Equation 2-2

From force equilibrium

$$\sigma_x = f_{cx} + \rho_x f_{sx}$$

Equation 2-3

$$\sigma_y = f_{cy} + \rho_y f_{sy}$$

Equation 2-4

The two equations combined yielded the equilibrium equations shown below:

$$f_x = \rho_x f_{sx} + f_1 - v \cot\theta$$

Equation 2-5

$$f_y = \rho_z f_{sy} + f_1 - v \tan\theta$$

Equation 2-6

$$v = (f_1 + f_2)/(\tan\theta + \cot\theta)$$

Equation 2-7

Stresses at cracks are as follows:

$$f_{sxcr} = (f_x + v\cot\theta + v_{ci}\cot\theta)/\rho_x$$

Equation 2-8

$$f_{sycr} = (f_y + v\tan\theta - v_{ci}\tan\theta)/\rho_y$$

Equation 2-9

### *2.3.2 Geometric strain conditions*

The principal concrete strains and stresses and their orientation in a Mohr Circle are shown in Figure 2.4 below. The Mohr circle of strain was skewed to the positive side of the x-axis due to the strain characteristic of RC members where tensile strains are always larger in magnitude compared to compression strains. The circle of strain is always skewed to the compression side because the stresses in compression are way more significant in magnitudes than those in tension.

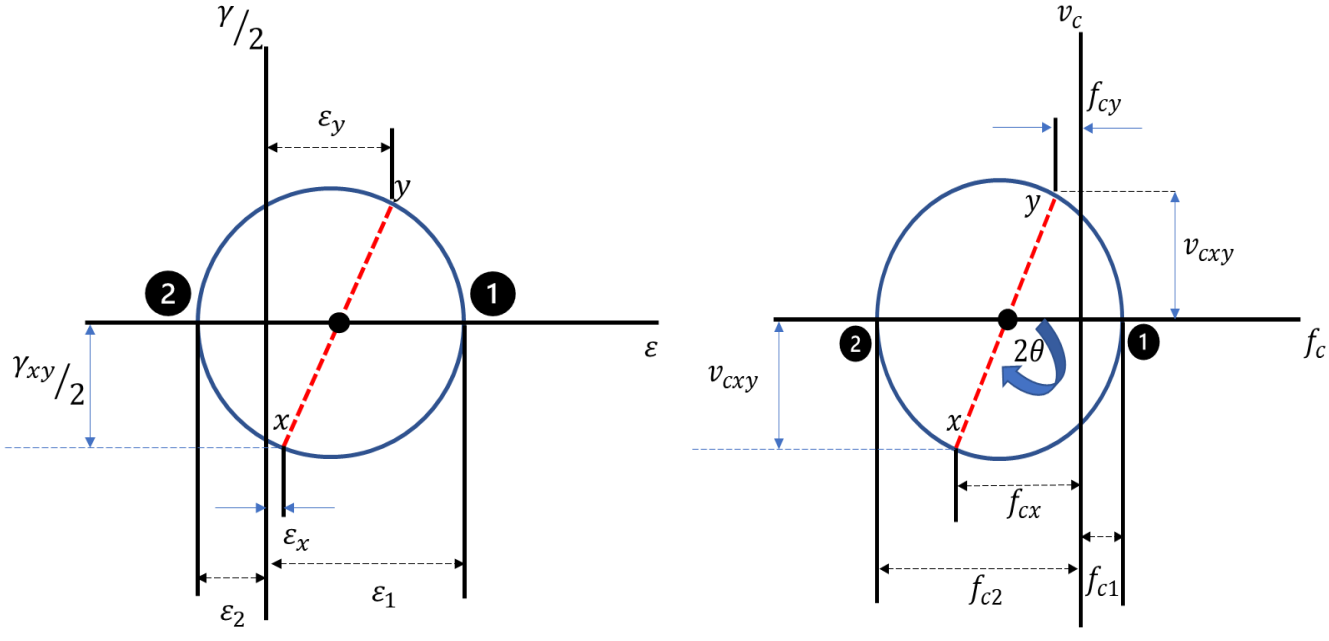


**(A) Mohr circle of Strain** **(B) Mohr circle of Stress**

Figure 2.4. Mohr circle for strain and stress at the exterior face of a flexural member for reinforced concrete.

The geometric strain combinations are derived from the Mohr circle of strains.

$$\mathrm{Tan}^2\,\theta = \frac{(\epsilon_x + \epsilon_2)}{(\epsilon_y + \epsilon_2)}$$

Equation 2-10

$$\epsilon_1 = \epsilon_x + \epsilon_y + \epsilon_2$$

Equation 2-11

$$\gamma_{xy} = 2(\epsilon_x + \epsilon_2)\cot\theta$$

Crack widths:

$$w = s_\theta \epsilon_1$$

$$s_\theta = 1/\left(\frac{\sin\theta}{s_x} + \frac{\cos\theta}{s_y}\right)$$

Equation 2-12

### *2.3.3 Stress-strain Relationships.*

Constitutive relations associated average stresses with average strains for concrete and reinforcement. They were derived from a comprehensive series of panel element tests.

*Concrete Compression:*

During the panel element tests (Vecchio and Collins 1982, 1986), it was found that the average stress-strain relations in cracked RC are substantially different than those obtained from uniaxial element tests. When along with compression simultaneously high tensile strains in the direction normal to the compression acts in concrete, cracked concrete exhibited a softer and weaker response compared to uncracked uniaxially compressed concrete. The above-mentioned property is called compression softening.

$$f_{sx} = E_s \epsilon_x \leq f_{yx}$$

$$f_{sy} = E_s \epsilon_y \leq f_{yy}$$

$$f_2 = \frac{f'_c}{0.8 + 170\epsilon_1}\left[2\frac{\epsilon_2}{\epsilon_c'} - \left(\frac{\epsilon_2}{\epsilon_c'}\right)^2\right]$$

Equation 2-13

The concrete carried significant tensile stresses between the cracks even at very high values of average tensile strain. This was due to the bond effects with the reinforcement. This observation was called tension stiffening and was empirically derived as the following:

$$f_1 = 0.33\sqrt{f'_c}/\left(1 + \sqrt{500\epsilon_1}\right)$$

Equation 2-14

Shear stress on crack was shown as the

$$v_{ci} \leq \frac{0.18\sqrt{f'_c}}{0.31 + \frac{24w}{a_g + 16}}$$

Equation 2-15

The diagonal compression field theory was developed from the postulates of the post-buckling shear resistance of thin webbed metal beams. The original theory assumed that after buckling, the metal would not resist any compression, and the shear would be carried by a field of diagonal tension. The adaptation in RC concrete meant that the concrete, after cracking due to tension, carried no load while the shear was carried by a field of diagonal compression.

For beams under shear and flexure, there is no compression or tensile action on the transverse direction of the beam and therefore in the equations of the stresses at crack:

$$f_{sycr} = (f_y + v\tan\theta - v_{ci}\tan\theta)/\rho_y$$

Equation 2-16

While $f_z = 0$, and the local strain at the crack in the reinforcement assumes yielding $f_{sycr} = f_y$ results in the above equation to converge to a form

$$\rho_y f_y \cot\theta = (v - v_{ci})$$

This form of shear strength $v$ has two parts the concrete contribution $v_c$ and the other part $v_s$ which can be equated to the following form respectively.

$$v = v_c + v_s = \beta\sqrt{f'_c} + \rho_y f_y \cot\theta$$

Equation 2-17

This results in the following equations for $\beta = \frac{0.33\cot\theta}{1+\sqrt{500\epsilon_1}}$

Numerous models for the shear behaviour of slender concrete components reinforced with GFRP have been presented. Furthermore, shear models for slender and deep steel-RC may be relevant to GFRP-RC members. This section highlights some shear design models developed or used in codes for GFRP and steel-RC members. Sections 2.5.1 and 2.5.2 describe sectional shear models for steel-reinforced and GFRP-reinforced members.

## 2.4 Slender Steel-RC Members

### *2.4.1 CSA A23.3-19*

The following formulae depict the general approach for determining the shear capacity of concrete components when subjected to extreme tension.

$$V_c{}^{[ii]} = \phi_c \lambda \beta \sqrt{f'_c} b_w d_v$$

Equation 2-18

$$\beta^{[iii]} = \frac{0.40}{(1 + 1500\varepsilon_x)} \frac{1300}{(1000 + s_{ze})}$$

Equation 2-19

[ii] $V_c$=shear resistance attributed to the concrete
[iii] $\beta$= factor accounting for shear resistance of cracked concrete

$$\varepsilon_x = \frac{\frac{M_f}{d_v} + V_f - V_p + 0.5\,N_f - A_p f_{po}}{2\left(E_s A_s + E_p A_p\right)}$$

Equation 2-20

$$s_{ze} = \frac{35 s_z}{15 + a_g} \geq 0.85 s_z$$

Equation 2-21

$s_z$ *is lesser of* $d_v$ *or maximum distance between layers of longitudinal reinforcement.*

The model by Bentz and Collins (2006), which was employed in CSA A23.3-19 proposes that the aggregate interlock mechanism for shear force transfer across a crack can forecast shear capacity at failure. The model is based on modified compression field theory (MCFT) simplifications (Vecchio and Collins 1986). The MCFT is a cracked RC model considering equilibrium, compatibility, stress-strain relationships, and tension stresses.

$V_c$ is calculated from an average shear stress in concrete acting across a region defined by the beam width, $b_w$, and effective shear depth, $d_v$. The value of $V_c$ was proportionate to the concrete's tensile strength. To maintain vertical equilibrium between cracked surface and uncracked surface, the principal tensile stress in concrete must be less than shear stress due to aggregate interlock times the tangent of the angle of the crack. The aggregate interlock mechanism is determined by the average crack width, computed by the product of the average principal strain and effective crack spacing, included by the factor $\beta$ in Equation 2-19. As the longitudinal strain at mid-depth of the concrete section (Equation 2-20) or effective crack spacing (Equation 2-21 ) rises, so do crack widths and the stress that may be transferred across the cracks by aggregate interlock.

The Equation 2-19 was created by utilizing a linear equation to approximate the nonlinear relationship between crack width and longitudinal strain and focussing the equation on strains less than 0.001. Since $\varepsilon_x$ is determined at mid-depth, this strain corresponds to the beginning yielding of Grade 400 steel ($f_y$ = 400 MPa)(Bentz and Collins 2006). Hoult *et al.* (2008) proved that for large tensile stresses, the equation

becomes increasingly conservative when the linear crack width approximation deviates further from the nonlinear relationship established from the MCFT. The effective crack spacing, $s_{ze}$, is a function of the average crack spacing and the maximum aggregate size and accounts for the so-called size impact in shear. The crack spacing grows as the effective depth grows, which reduces.

The effective crack spacing, $s_{ze}$, is a function of the average crack spacing and the maximum aggregate size and accounts for the so-called size impact in shear. As the effective depth increases, so does the crack spacing, reducing aggregate interlock and shear capacity. For concrete with a compressive strength greater than 70 MPa, the aggregate size no longer has significant affect on shear strength because fractures prefer to travel through the aggregate rather than around it.

The aggregate size value, $a_g$, in Equation 2-21 is treated as zero if $f_c'$ is larger than 70 MPa and is linearly decreased to zero as $f_c'$ climbs from 60 to 70 MPa according to the CSA A23.3-04 shear model.

### *2.4.2 CSA S6-19*

The factored shear resistance $V_r$ is the sum of there components $V_c, V_s$ and $V_p$ which are factored shear resistance provided by concrete due to tensile stresses, factored shear resistance by shear reinforcement and factored component of the effective prestressing force crossing the critical section in the direction of the applied shear. Figure 2.5 and Figure 2.6 show the various possible $s_z$ values for different layouts of main reinforcement.

The concrete component can further be simplified into the following equation,

$$V_c = 0.25\beta\phi_c f_{cr} b_v d_v = 2.5 \times \frac{0.4}{(1 + 1500\varepsilon_x)} \cdot \frac{1300}{(1000 + s_{ze})} f_{cr} b_w d_v$$

Equation 2-22

Where $f_{cr} \leq 3.2\ MPa$

$$s_{ze} = \frac{35 d_v}{15 + a_g} \geq 0.85 s_z \text{ where } s_z \leq \begin{cases} d_v \\ Distance\ between\ layers\ of\ longitudinal\ reinforcement \end{cases}$$

$$\varepsilon_x = \frac{M_f/d_v + V_f - V_p + 0.5N_f - A_{ps}f_{po}}{2\left(E_sA_s + E_pA_{ps}\right)}$$

Equation 2-23

$$\theta = (29 + 7000\varepsilon_x)$$

- $A_s$ and $A_{ps}$ are the areas of reinforcing bars and prestressing tendons at half-depth of the section under flexural tension.
- If the longitudinal strain $\varepsilon_x$comes out to be negative it will take the value of zero or new strain should be calculated using the denominator $2\left(E_sA_s + E_pA_{ps} + E_cA_{ct}\right)$

The factored shear resistance provided by the stirrups was calculated as $V_s = \frac{\phi_s f_y A_v d_v \cot\theta}{s}$ when the stirrups are perpendicular to the longitudinal axis of the member.

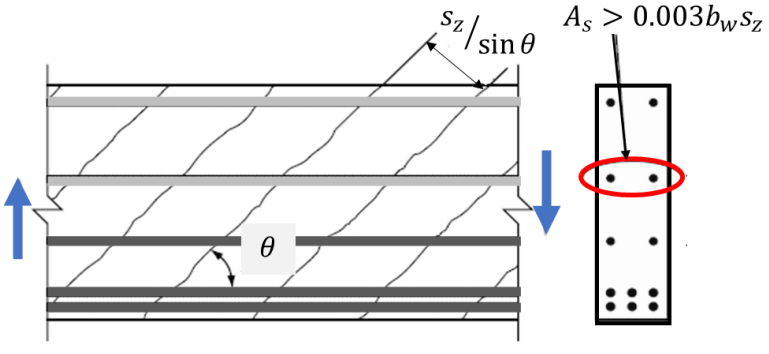


Figure 2.5. Influence of reinforcement on spacing of diagonal cracks for well distributed web-reinforcement (Reproduced from CSA S6-19 (CSA 2019b)).

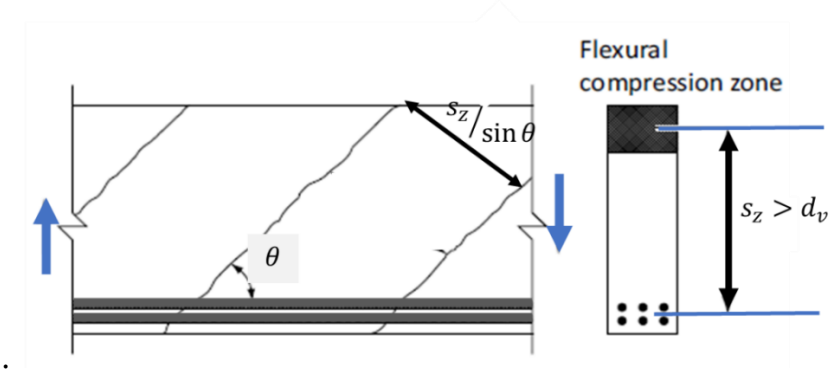


Figure 2.6. Influence of reinforcement on spacing of diagonal cracks for concentrated longitudinal reinforcement (Reproduced from CSA S6-19 (CSA 2019b))

## 2.5 Deep Beams and Corbel Design

### *2.5.1 Empirical Method in ACI 318-19*

Depending on the shear span-to-depth ratio, there are two ways to design corbels according to ACI 318-19 (ACI 2019).

When the shear-span-to-depth ratio is less than unity, the code provisions allow the design of corbels using empirical methods found in Chapter 16 and Chapter 22 of the code.

The following equation holds true if the reinforcement is perpendicular to the shear plane.

$$V_n = \mu A_{vf} f_y$$

Equation 2-24

Whereas if the reinforcement is inclined at an angle $\alpha$ to the shear plane, the following equations are used,

$$V_n = A_{vf} f_y (\mu \sin\alpha + \cos\alpha)$$

Equation 2-25

Where, $V_n$ is the nominal shear strength of the assumed shear plane, $A_{vf}$ is the area of shear friction reinforcement, and μ is the coefficient of friction according to the values of Table 22.9.4.2 (Coefficients of friction) of ACI 318.

The area of primary reinforcement in corbels not subjected to horizontal forces as per the empirical method is determined as the greatest of the following:

1. The sum of the area required to resist flexural demands $A_f$ and area of reinforcement $A_n$ required to resist a restraint force $N_{uc}$ applied perpendicular to the shear force $V_u$ at a bearing surface.
2. The sum of two third of the shear friction reinforcement and the area of reinforcement for restraint force.
3. $0.04(f_c'/f_y)(b_w d)$, where $f_c'$ is the compressive strength and $f_y$ is the yield strength of steel and $d$ and $b_w$ are the effective depth and width of the corbel.

The steel-RC corbel is designed to have enough sectional moment capacity and shear-friction resistance at the shear plane, which is the plane of intersection of the column and the corbel. As mentioned above, the design provides adequate reinforcement for a given strength of concrete. The flexural theory assumes a planar section after bending and is used to compute sectional moment capacity. Shear friction assumes that shear force is carried across a cracked interface because of friction, which is produced by normal forces equivalent to the component of the tensile forces in the reinforcement crossing that interface (Birkeland & Birkeland, 1966). Shear friction, aggregate interlock, and interface shear transfer are terms used to describe the shear-carrying mechanism. The shear or slip plane is the interface on which the shear friction occurs as shown in the Figure 2.7.

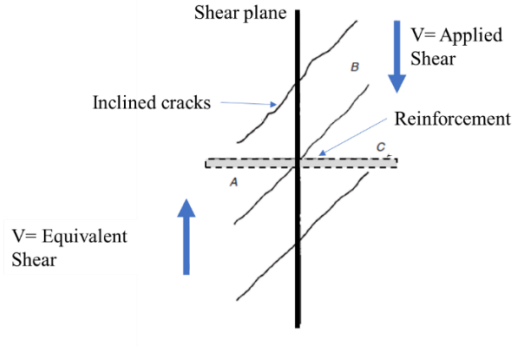


Figure 2.7. Diagonal Tension cracking at a previously uncracked shear-plane. (Adapted from (Wight and MacGregor 2009b))

## 2.6 STM Modelling

This section will only provide a brief description on the use of STMs before introducing the strut-and-tie modelling techniques and provisions design provisions from the two design codes and Standards used extensively in this study.

The strut-and-tie technique is a method for evaluating or designing structural concrete that involves breaking down complicated states of stress inside a structural part into simple load paths.(ACI-ASCE Committee 445 2021). These load pathways are modeled as two-dimensional or three-dimensional networks of straight, pin-connected, axially loaded elements that connect all applied loads to supports or adjacent nodes in the structures. Strut-and-tie modelling is a technique used to analyze regions of nonlinear strain distributions and is described in detail by (Schlaich *et al.* 1987), ACI-ASCE Committee 445 (1999) and (Wight and MacGregor 2009b).

Changes in the geometry or loading of the structure induces nonlinear strain distributions in concrete members and are commonly referred to as disturbed/ discontinuity regions or D-regions. St. Venant's principle suggests that the effect of a disturbance will only affect a region diverging from the point of application of load at a slope of 45 degrees from the point of load or about one member depth away from the load or geometric discontinuity.

The structural member portions not subjected to the above discontinuities are called Bernoulli -regions (B-regions). According to the fundamental concepts of beam theory, plane sections are supposed to remain plane within B-regions, meaning that a linear distribution of strains occurs through the member depth. As a result, sectional behaviour dominates the beam, and design can proceed section-by-section (i.e., sectional design). Compressive stresses are conventionally assumed to occur over a rectangular stress block in the flexural design of a B-region, whereas tensile loads (shown by blue lines in Figure 2.8) are expected to be carried by the longitudinal steel reinforcement.

The load path method or the elastic analysis of the stresses and principal stress directions are required to analyse a structure for STM modelling.(Schlaich *et al.* 1987) . The load path method is the most economic solution in terms of computing power and can be performed just following a few basic steps or rules of thumb.

Depending on the uniformity of the stress fields in which they are positioned, struts can be prismatic, or bottle shaped. Prismatic struts are concentrated in areas with more uniform and streamlined stresses or loads, like the compression zone for slender member under pure bending or members under uniform compression such as columns. Bottle-shaped struts are placed in areas where compressive forces can extend laterally.

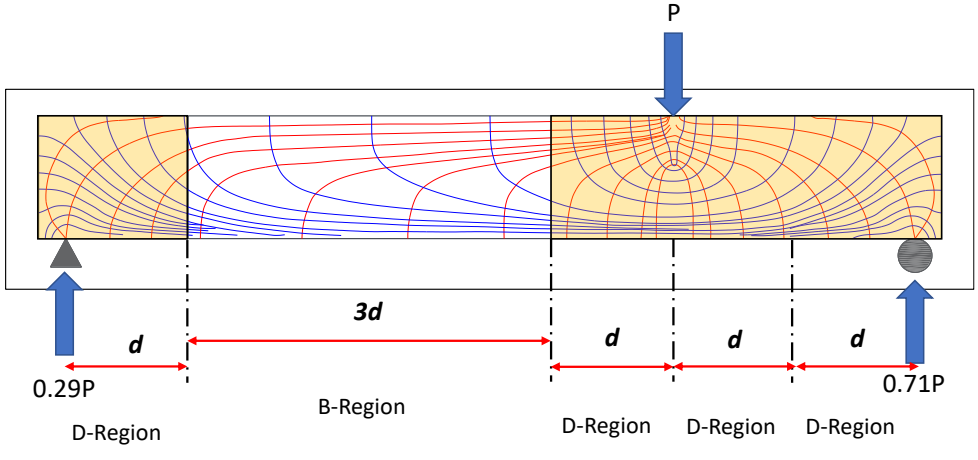


Figure 2.8. Stress trajectories within B- and D-regions of a member under flexure. (Adapted from (Williams et al. 2012) )

The strut-and-tie Method (STM) can be used for the design of structural concrete members, or regions of members, where load or geometric discontinuities cause a nonlinear distribution of longitudinal strains within the cross section.

Any structural concrete member, or discontinuity region in a member, is modeled as an idealized truss in accordance with this chapter. Figure 2.9 shows the steps involved in a general STM design according to North American Codes and Standards.

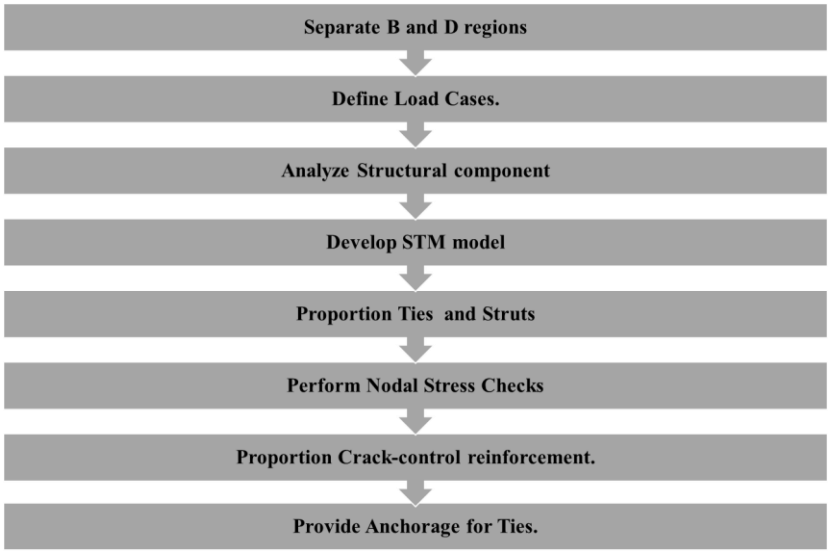


Figure 2.9. Generalized STM design procedure for corbels in codes and standards in North America.

The STM is a method of using Trusses for calculating the ultimate limit state of a member. Different modes of failure can be assumed during the analysis or design of concrete elements. The predicted ultimate capacity of a concrete member designed by STMs can be governed by:

- Crushing of the struts,
- Yielding of the tension ties (Steel) or rupture of Ties (GFRP),
- Failure of the nodes by reaching stresses larger than the allowable nodal stresses
- Anchorage failure of the reinforcement.

Nodes are the point of intersection of struts and ties where the forces are transferred between the struts and ties or where struts and ties intersect. The classification of the nodes is given according to the forces that

they connect, developing three different states of stress in the nodal zone, as CCC, CCT and CTT nodes as shown in a Figure 2.10.

A node that connects only compressive forces is called CCC node which is the strongest type of node. CCT is a node under the action of one tension force and two (or more) compression forces which is weaker node. A CTT node connects one compression force and two (or more) tension forces which is the weakest.

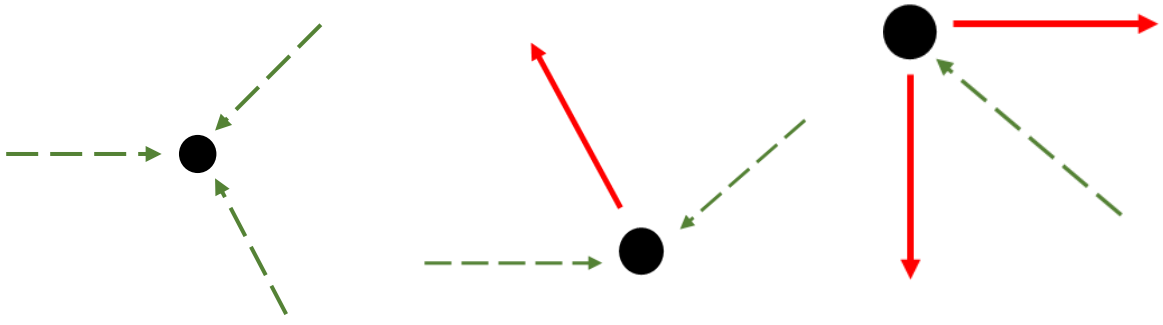

(A) CCC (B) CCT (C) CTT

Figure 2.10. Various types of Nodes in STM.

### *2.6.1 ACI Approach*

According to ACI 318 (2019), the internal forces in STM model should be in equilibrium with the loads and reactions at supports. Also, the angle between strut-and-tie cannot be less than 25 degrees (Clause 23.2.7).

The compressive strength of strut is calculated by $F_{ns} = f_{ce}A_{cs}$ and if longitudinal reinforcement is present is calculated accordingly,

$$F_{ns} = f_{ce}A_{cs} + A'_s f'_s$$

Equation 2-26

Where the notations mean the following:

$F_{ns} = Nominal\ strength\ of\ the\ strut\ at\ the\ end\ of\ each\ strut.$

$A_{cs} = cross - sectional\ area\ at\ the\ end\ of\ each\ strut\ under\ consideration.$

$A'_s = area\ of\ compression\ reinforceement\ along\ the\ direction\ of\ the\ strut$

Also $f_{ce}$ is the effective strength of the strut.

$$f_{ce} = 0.85\beta_c\beta_s f'_c$$

Equation 2-27

where $\beta_c$ and $\beta_s$ are Strut and node confinement modification factor and strut coefficient respectively.

In order to prevent diagonal tension failure, the Clause 23.4.4 allows the ultimate loads acting on the D-region to be lower than the following expression.

$$V_u \leq 0.42\phi \tan\theta\, \lambda\lambda_s \sqrt{f'_c} b_w d$$

Equation 2-28

Where $\lambda_s = \begin{cases} 1, & If\ the\ distributed\ reinforcement\ is\ provided\ according\ to\ the\ Clause\ 23.5. \\ \sqrt{\frac{2}{1+0.004d}} \leq 1 \end{cases}$

According to ACI 318 (2019), confining the strut increases the value of $f_{ce}$ by increasing the web reinforcement in corbels and deep beams which, in turn, increases the value of $F_{ns}$.

In struts, $\beta_s$ increase from 0.4 to 0.75 in case of using web reinforcement which helps in resisting the transverse tension forces of struts resulting from spreading of the compressive force in the strut.

The web reinforcement is calculated using the minimum distributed reinforcement in Clause 23.5. If an orthogonal grid is used then a web reinforcement ratio of 0.25% should be used whereas if the web reinforcement is along the main reinforcement crossing the strut at an angle of $\alpha_1$, the web reinforcement will be equal to $\frac{0.0025}{\sin^2 \alpha_1}$. The maximum spacing between the web reinforcement should not exceed 300 mm and the $\alpha_1$ should be more than 40 degrees.

According to ACI 318 (2019), the tie reinforcement can be non-prestressed or prestressed and the strength of ties $F_{nt}$ is calculated by $F_{nt} = A_{ts}f_y + A_{tp}(f_{se} + \Delta f_p)$

Where $(f_{se} + \Delta f_p)$ shall not increase $f_{py}$, and $A_{tp}$ is zero for non -prestressed members.

Also, the centroid of the tie reinforcement should be corresponding to the assumed tie in the STM.

The reinforcement of the tie should be anchored by mechanical devices, post-tensioning anchorage devices, standard hooks, or straight bar development.

Curved bars on Nodes are designed and detailed for anchorage when the bends are less than 180 degrees as the following inequality $r_b \geq \frac{2A_{ts}f_y}{b_s f_c'}$ where the bent radius is represented by $r_b$ and $b_s$is the width of the strut transverse to the plane of the strut-and-tie model. When ties are anchored with 180 degrees bend then the following expression can be used for evaluating tie development. $r_b \geq \frac{1.5A_{ts}f_y}{w_t f_c'}$

### *2.6.2 CSA Approach*

The Canadian standards (CSA 2019a) allows the use of STM for deep beam design in members with non-linear distribution of strain. The STM is defined as a method of investigating strength of RC members by idealizing the member as a series of reinforcing steel tensile ties and concrete compressive struts connected at nodes to form a truss able to transfer loads to supports directly.

The limiting compressive stresses in struts is shown below.

$$f_{cu} = \frac{f_c'}{0.8 + 170\varepsilon_1} \leq 0.85f_c' \ (MPa)$$

Equation 2-29

Where $\varepsilon_1 = \varepsilon_s + (\varepsilon_s + 0.002)\cot^2\theta_s$

$\theta_s$ is the smallest angle between strut and the tie.

$\varepsilon_s$ is the tensile strain in the horizontal tie.

Reinforced compressive struts strength is evaluated as following $F_{strut} = \phi_c f_{cu} A_{cs} + \phi_s f_y A_{ss}$

Strength of Ties should not exceed the following $F_{ties} = \phi_s f_y A_{st} + \phi_p (f_{po} + 400) A_p$

The calculated compressive strength on the nodes is limited by the following stress levels:

- $0.85\phi_c m f_c'$ in regions bounded by struts and bearing area.
- $0.75\phi_c m f_c'$ in regions bounded by struts and only one tie.
- $0.65\phi_c m f_c'$ in regions bounded by ties in at least two directions.

Where m is the confinement modification factor taken as $\sqrt{\frac{A_2}{A_1}}$ but not more than 2.0

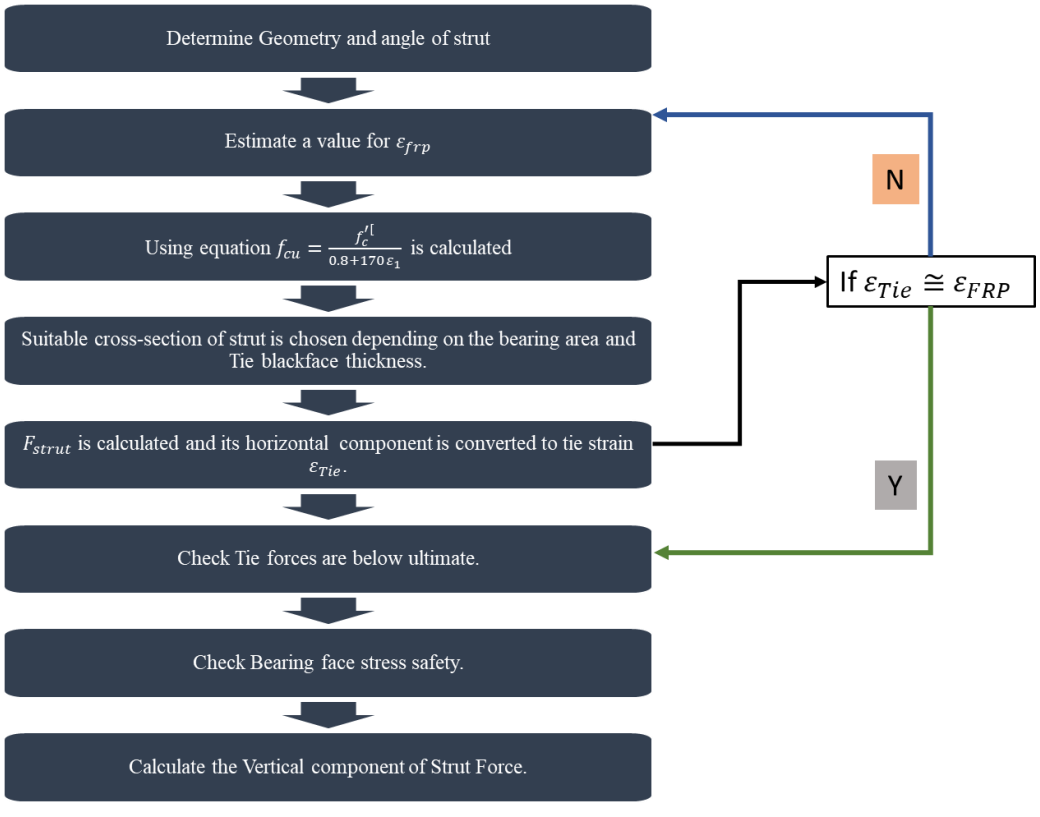


Figure 2.11. STM analysis procedure for corbels in CSA A23.3-19 (CSA 2019a).

It is evident from the studies reviewed in this chapter that the behaviour of reinforced concrete (RC) corbels under monotonic loading is influenced by several parameters including the shear span-to-depth ratio (*a/d*),

horizontal crack-control reinforcement, concrete compressive strength ($f'_c$), and longitudinal reinforcement ratio ($\rho_{main}$). To further investigate the impact of these above factors on simply supported double-sided glass fiber-reinforced polymer (GFRP)-RC corbels, this study examined corbels considering the following parameters:

1. Shear span-to-depth ratio (*a/d)* of 0.33 and 0.66.
2. Concrete strength at target strength of 35 MPa and 60 MPa.
3. Main reinforcement type (steel or GFRP) and main reinforcement ratio $\rho_{main}$ of 0.5% and 0.7%.
4. Crack-control horizontal reinforcement ratio of 0% (absence), 0.7% and 1.3%.

# Chapter 3. Performance of GFRP-Reinforced Concrete Corbels under Monotonic Loading

**Authors and Affiliations**

- Ankit Borgohain, M.Sc. Student, Department of Civil Engineering, University of Manitoba.
- Ahmed G. Bediwy, Assistant Professor, Department of Civil Engineering, Lakehead University.
- Ehab F. El-Salakawy, Professor, Department of Civil Engineering, University of Manitoba.

**Journal and Status:** American Society of Civil Engineers, Journal of Composites for Construction, under review.

**Reference:**

Borgohain, A., Bediwy, A. and El-Salakawy, E. "Performance of GFRP-Reinforced concrete Corbels under Monotonic Loading", ASCE, Journal of Composites for Construction, Submitted in April 2023.

**Note:**

The manuscript had been slightly edited from the original paper by renumbering the tables and figures to include the chapter number. The abbreviations of the specimen names are explained in the Appendix A under Section A.1. In addition, the reference list and list of notations have been moved to the appropriate sections in the thesis as indicated in the Table of Contents.

## 3.1 Abstract

Reinforced concrete (RC) corbels are commonly utilized in bridges and industrial buildings to support primary beams and girders. The use of glass fiber-reinforced polymer (GFRP) reinforcement in corbels can be advantageous due to its corrosion-resistance properties. However, GFRP reinforcement, with lower modulus of elasticity and shear strength compared to steel, could affect the capacity in direct shear. This paper presents the experimental results of nine full-scale, double-sided corbels reinforced with either GFRP or steel bent bars. Large-scale double-sided corbels were constructed and tested to failure under monotonic concentric loads. The test parameters included the reinforcement type (GFRP and steel), the main reinforcement ratio (0.5% and 0.7%), the shear span-to-depth ratio ($a/d$ = 0.33 and 0.66), and the amount of crack-control horizontal reinforcement (0.7% and 1.3%). The predictions of corbel capacity using the Canadian standards for FRP-RC structures were conservative, especially for the corbels with crack-control reinforcement. While the predictions of the American and European codes were overestimating the corbel strength particularly for the higher $a/d$ ratio of 0.66.

**Keywords:** Corbels, GFRP bars, shear span-to-depth ratio, transverse reinforcement, strut failure.

## 3.2 Introduction

Reinforced concrete (RC) corbels are extensively used as load transfer elements from girders and primary beams to columns and piers. The position of loads and location of supports influence the shear design resulting in either bending regions (B) or disturbed regions (D). Bending or Bernoulli (B) regions in a structural member are those regions where plane cross-sections remain plane after bending. This assumption implies a linear or plane strain profile due to the constant stress trajectories. For members with B-regions, sectional load effects can be obtained using an elastic analysis and section properties. Disturbed (D) regions are those in which the Bernoulli hypothesis can no longer be applied. In these regions, a non-linear strain distribution is caused by static (e.g., presence of concentrated loads) or geometric (e.g., abrupt

change of cross-section) discontinuities. The flow of stresses is disturbed, and plane sections no longer remain plane after loading.

Due to the geometrical dimensions (shear-span-to-depth ratio, *a/d*, less than 1.0) and the presence of a concentrated load, RC corbels are usually categorized as D-regions. As a result, a regional design approach, for instance, the strut-and-tie model (STM) approach, should be followed instead of a sectional analysis. Steel-RC corbels can be designed with the empirical method using shear friction theory or the STM Method (ACI 318-19 2019) (ACI Committee 318 2019). The STM method uses load paths, also called stress trajectories, and idealizes it as compression and tension members forming a truss. Compression members are called struts, and tension members are called ties. According to the STM methodology, load paths with the lowest number and lengths of tension ties are more feasible as the loads try to use the paths with least forces and deformation since the ties are more deformable than the concrete struts (Schlaich *et al.* 1987).

Nowadays, the glass fibre-reinforced polymer (GFRP) reinforcement is used as a practical substitution to traditional steel in RC structures, particularly those in extreme weather conditions. This is due to the exceptional behavior of GFRP in corrosive environments (e.g., North America), which is attributable to its inherent non-corrodible nature. In addition to the corrosion resistivity, the new generation of the GFRP has high tensile strength, lightweight and ease of installation. However, the linear stress-strain relationship of the GFRP may hinder its application in RC members, dominated by a brittle/abrupt behaviour upon failure (e.g., corbels). In addition, the low modulus of elasticity of GFRP would lead to large deformations for GFRP-RC members with the same reinforcement ratio as their steel-RC counterparts, which in turn may produce some compatibility issues.

To reap the benefits of the nonlinearity of concrete when STM is used, GFRP-RC structures better be designed based on having the failure in concrete strut prior to the tie for a safe and less abrupt/catastrophic failure, which is opposite to steel-RC counterparts. In this context, the existence of secondary reinforcement is deemed crucial for crack control, as it reduces the probability of the undesired premature strut failure

that may trigger from the in-plane tensile strains pertained to the heterogenous nature of concrete. Moreover, secondary reinforcement is employed to resist the tensile strains perpendicular to the strut axis according to the modified compression field theory (MCFT) that accounts for the strain within the cracked concrete (Vecchio and Collins 1986). Previous research conducted by Tan et al. (1997) and Campione et al. (2012) on steel-RC STM-based structures (e.g., corbels and deep beam) has confirmed the importance of including secondary reinforcement for crack control. However, the effect of including such secondary reinforcement on the strength of structures designed based on the STM (e.g., corbels) is still controversial between researchers and in code provisions as well. For example, Abdul-Razzaq and Dawood (2021) and Mohamed et al. (2017) indicated that the inclusion of web reinforcement had a positive impact on the strength of the inclined strut. On the other hand, other research reported that the addition of such web reinforcement had minimal or no effect on the strength.

An example for the discrepancy in code provisions, the new code for GFRP-RC structures released by the American Concrete Institution, ACI 440.11-22(ACI Committee 440 2015) , did not include any provisions for the design of corbels. On the other hand, providing the minimum secondary reinforcement that is stipulated in the steel-RC standards ACI 318-19 (ACI Committee 318 2019) in structural elements designed by STM would lead to improving the capacity by 67% (Mohamed et al. 2017). The minimum crack control reinforcement shall be more than $A_{si} \times Sin\ \alpha_i / b \times s_{i,}$, where $A_{si}$, $\alpha_i$, $b$, and $s_i$ are the cross-sectional area of the bar, angle to the strut axis, the strut width, and the reinforcement spacing, respectively. On the other hand, the current Canadian standards for FRP-RC buildings CSA S806-12 (CSA 2021) specified a minimum secondary reinforcement ratio of more than 0.004 for GFRP reinforcement as crack control distributed on two-thirds of the depth, without any influence on the predicted strength.

Much research has been conducted on steel-RC corbels with and without secondary reinforcement to evaluate its effect on the shear capacity (Mattock et al. 1976; Fattuhi 1994; Yong and Balaguru 1994; Hwang et al. 2000). However, there is a significant gap in the current literature on how to apply the STM in GFRP-RC corbels, and to the authors' knowledge there are no comprehensive studies carried out to

investigate the role of changing the secondary reinforcement ratio on the strength of FRP-RC corbels. This paper is a part of ongoing research investigation at the University of Manitoba to evaluate the overall behavior of GFRP-RC corbels. To fulfil this objective, experimental and analytical attempts were dedicated to demonstrating that concrete corbels reinforced with GFRP bars as main and secondary reinforcement can achieve an acceptable strength. In the experimental phase, nine large-scale double-sided corbels were cast and tested until failure, eight were reinforced with GFRP and one was reinforced with steel. All corbels were tapered with a cross section of 300 by 450 mm at the corbel-column interface and 300 by 300 mm at the free end. Besides the type of reinforcement, the main and secondary reinforcement ratios and the shear span-to-depth ratio were investigated in this study. In the analytical phase, a critical examination was conducted on the current provisions specified in the Canadian standards and American codes to predict the capacity of GFRP-RC corbels.

## 3.3 Experimental Program

### *3.3.1 Test specimens*

In this study, nine large-scale double corbels were constructed and tested to failure. The tapered corbels had a rectangular cross-section measuring 300 mm wide by 450 mm high at the corbel-column interface and 300 mm wide by 300 mm high at the free end. The test variables included shear span-to-depth (*a/d*) ratio (0.33 and 0.66), main reinforcement ratio (0.5% and 0.7%) and the amount of crack control horizontal reinforcement (0.7% and 1.3%). The column segment of the specimen had dimensions of 300 × 350 mm and extended 400 and 600 mm below and above the corbel surfaces, respectively, as shown in Figure 3.1. All test specimens were internally reinforced with sand coated GFRP bent bars, except for the control specimen, which was reinforced with steel bars. the conventional steel-RC corbel was designed according to the CSA A23.3-19 code provisions (CSA 2019a) with an *a/d* ratio of 0.33. In addition, three closed stirrups representing the horizontal crack control reinforcement spaced at 65 mm were used. The column segment was adequately reinforced with four No. 20M longitudinal bars and No. 10M closed stirrups spaced at 250 mm, irrespective of the type of reinforcement used in the corbels, as shown in Figure 3.1. To

prevent any premature anchorage failure of the GFRP bars (e.g., slippage), the corbel reinforcement was extended beyond the point of load application.

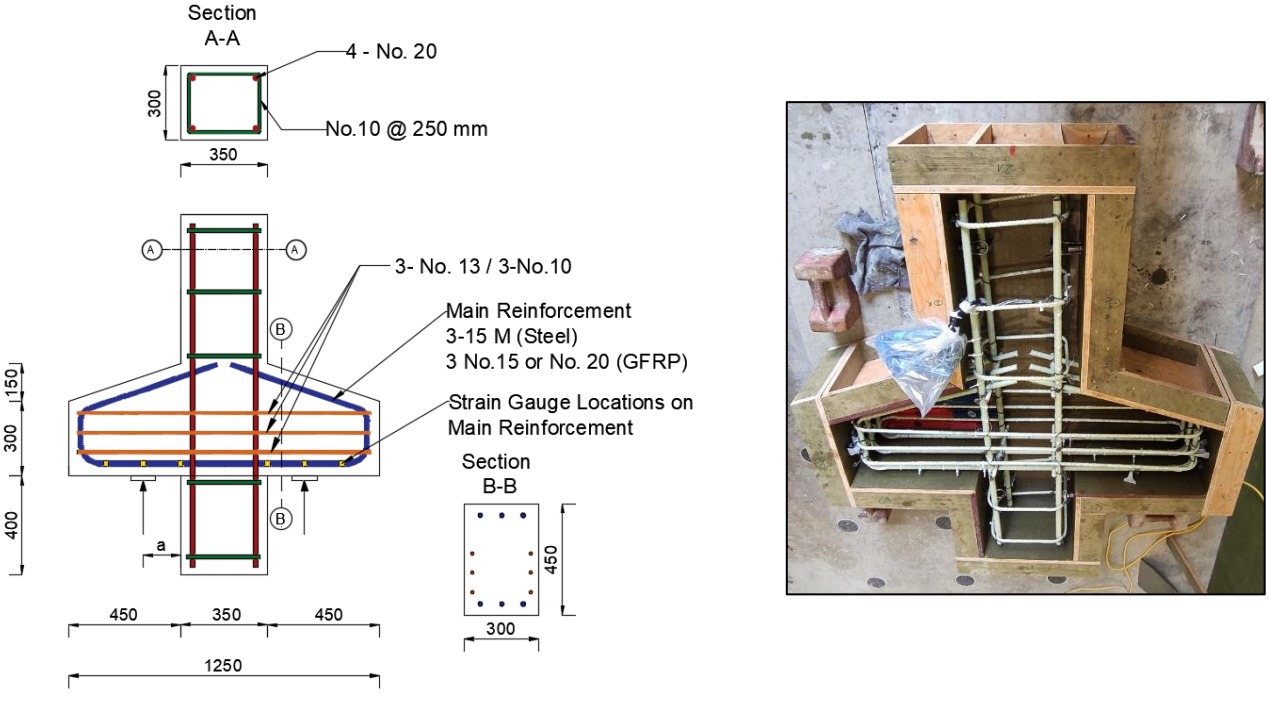


Figure 3.1.Geometry and reinforcement details of the corbel. (Dimensions in mm.)

The corbel name had four terms. The first term denotes the type of reinforcement ("S" for steel and "G" for GFRP), the second term is the *a/d* ratio (0.33 and 0.66), the third term indicates the main reinforcement ratio (0.5% and 0.7%) while the last term defines the amount of horizontal crack-control reinforcement ("0" for no stirrups, "10" for three horizontal stirrups of No.10 and "13" for three stirrups of No 12). For example, *S-0.33-0.5-10* refers to a steel-RC corbel with an *a/d* ratio of 0.33, a main reinforcement ratio of 0.5% and 3 No. 10M horizontal stirrups. Table 3.1 presents the details of the tested corbels.

Table 3.1.Details of test corbels

| Specimen ID | *a/d* | *d* (mm) | Main reinforcement | Transverse reinforcement | | $f'_c$ (MPa) |
|---|---|---|---|---|---|---|
| | | | | Size and number of bars | Spacing (mm) | |
| S-0.33-0.5-10 | 0.33 | 404.0 | 3-15M | 3-10M | 65 | 45.2 |
| G-0.33-0.5-0 | 0.33 | 403.5 | 3-No. 15 | - | - | 39.1 |
| G-0.33-0.5-10 | 0.33 | 403.5 | 3-No. 15 | 3 No. 10 | 65 | 39.9 |
| G-0.33-0.7-0 | 0.33 | 401.7 | 3-No. 20 | - | - | 42.0 |
| G-0.33-0.7-13 | 0.33 | 401.7 | 3-No. 20 | 3 No. 13 | 65 | 44.0 |
| G-0.66-0.5-0 | 0.66 | 403.5 | 3-No. 15 | - | - | 42.5 |
| G-0.66-0.5-10 | 0.66 | 403.5 | 3-No. 15 | 3 No. 10 | 65 | 40.8 |
| G-0.66-0.7-0 | 0.66 | 401.7 | 3-No. 20 | - | - | 43.0 |
| G-0.66-0.7-13 | 0.66 | 401.7 | 3-No. 20 | 3 No. 13 | 65 | 41.5 |

*$a$ is the shear span, $d$ is the effective depth of main flexural reinforcement, $f'_c$ is the concrete compressive strength.

### *3.3.2 Material properties*

All corbels were constructed at the McQuade Heavy Structures Laboratory at the University of Manitoba using ready-mix normal weight concrete with a target 28-day compressive strength of 35 MPa. The concrete had a nominal maximum aggregate size of 20 mm and a target slump ranging between 120 and 150 mm. The actual compressive strength of the specimens was obtained by testing standard 100 × 200 mm cylinders on the day of testing according to CSA A23.1/A23.2-19 (CSA 2019c), as listed in Table 3.1. The corbel and the cylinders were demolded after 24 h from casting, covered with wet burlap for 7 days and stored in the laboratory conditions before proceeding to the testing stage.

For all GFRP-RC specimens, either size No. 15 or No. 20 GFRP bent bars as the main reinforcement along with size No. 13 or No. 10 GFRP as horizontal closed stirrups were used. Size No. 20 GFRP straight bars

and No. 10 GFRP stirrups were used in the column segment. All the GFRP reinforcement used in this study was sand coated.

For the steel-RC control specimen, sizes 10M, 15M and 20M deformed steel bars were used as shown in Figure 3.1. The mechanical properties of the used GFRP bent bars were provided by the manufacturer through certified tests that were carried out according to the CSA S807-19 (CSA 2019d) standards. While the properties of the straight GFRP straight bars and steel reinforcement were obtained/confirmed in the laboratory according to ASTM A370-17 (ASTM 2017) and ASTM D7205-06 (ASTM 2016), as applicable. The properties of the used reinforcement are listed in Table 3.2.

### *3.3.3 Test Setup and Instrumentation*

The vertical monotonic load was applied using a 5000-kN closed loop hydraulic actuator at a displacement-controlled rate of 0.25 mm/minute (Fattuhi 1994; Andermatt and Lubell 2013). The vertical load was applied to the top of the column through a steel loading plate (350×300×50 mm), and the two corbels was supported on two identical bearing plates (150×300×50 mm). The actuator was equipped with a built-in load cell to measure the total load applied to the column, while a load cell was installed under the bearing plate of one corbel. The specimens were tested in an inverted position as a simply supported double-corbel with a hinged support on one side and a roller on the other one. Figure 3.2 shows a schematic drawing and a photo of the test setup.

To measure strains, electrical strain gauges were attached to the main reinforcement at critical locations as shown in Figure 3.1. Linear variable-displacement transducers (LVDTs) were used to measure deflection at both sides of the column. In addition, four 200-mm PI gauges were used to measure crack width at two different locations: the mid-height of the struts and the column-corbel interface at main reinforcement level to monitor the strut and flexural crack widths, respectively. All strains, displacements, and loads were automatically logged into a Data Acquisition System (DAQ) and were recorded and stored on a personal computer.

Table 3.2.Mechanical properties of the corbel reinforcement

| Bar size | Bar type | Nominal diameter (mm) | Area ($mm^2$) | | Modulus of elasticity (GPa) | Tensile strength (MPa) | Ultimate strain (%) |
|---|---|---|---|---|---|---|---|
| | | | Nominal | CSA S806-12 Annex A | | | |
| No. 10M | Steel | 11.3 | 100 | - | 200 | 460[a] | 0.230 [a] |
| No. 15M | Steel | 15.9 | 200 | - | 200 | 450 [a] | 0.225 [a] |
| No. 20M | Steel | 19.9 | 300 | - | 200 | 450* | 0.225* |
| No. 10 | GFRP | 9.50 | 71 | 98 | 54.3 | 1,199 | 2.210 |
| No. 13 | GFRP | 12.7 | 127 | 175 | 54.7 | 1,209 | 2.210 |
| No. 15 | GFRP | 15.9 | 198 | 291 | 55.6 | 1,194 | 2.150 |
| No. 20 | GFRP | 19.0 | 285 | 394 | 55.6 | 1,197 | 2.140 |

[a] Yield stress/strain for steel reinforcement

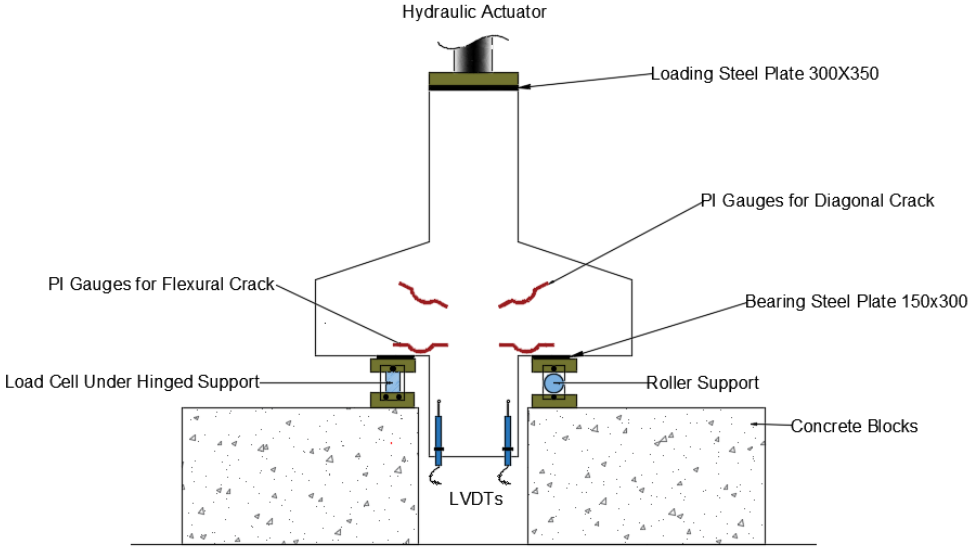


(a)

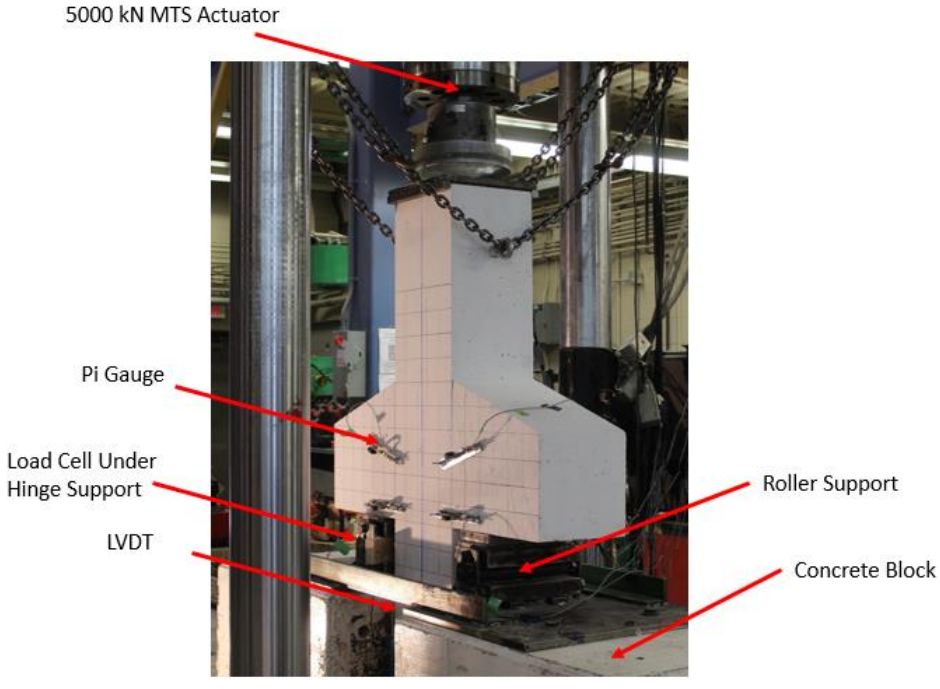


(b)

Figure 3.2. Test set-up. (a) Schematic drawing, (b) photo

## 3.4 Experimental Results and Discussions

### *3.4.1 Mode of failure and crack pattern*

The results of the tested corbels at different loading stages are summarized and tabularized in Table 3.3. Throughout the testing process, no undesired local failure originated at the supporting or loading plates or the slippage of the bars for all corbels was observed. Three modes of failure were identified including shear compression failure (SH-C), diagonal-compression strut failure (DC-ST) and splitting failure (SP-F). Such failures are in good agreement with those that were previously reported by Abu-Obida et al. (2018) and Andermatt and Lubell (2013), who investigated GFRP-RC corbels and deep beams with various *a/d* ratios, respectively. The shear-compression failure occurred in three specimens G-0.66-0.5-10, G-0.33-0.7-0 and G-0.66-0.7-13. This failure was characterized by a major diagonal crack accompanied by crushing of the concrete in the compression zone at the upper end of the crack near the column-corbel junction. This main crack links the inside edge of the supporting plate and the intersection point between the column and the

corbel. On the other hand, two corbels (G-0.66-0.7-0 and G-0.66-0.5-0) experienced a splitting tensile failure, which was characterized by a diagonal crack (resulting from transverse tensile stresses) that split the corbel in a direction perpendicular to the strut trajectory. Diagonal-compression strut failure took place in four specimens, namely, G-0.33-0.5-10, G-0.33-0.5-0, G-0.33-0.7-13, and S-0.33-0.5-10 due to the compression stresses in the strut (ASCE-ACI Committee 426 1973; Wight and MacGregor 2009), confirming that this was the most dominant failure mode. Diagonal-compression strut failure was the most stiff and brittle failure, which was characterized by numerous closely spaced cracks in the region of the main compression strut. Finally, it is worth mentioning that the tie (main steel reinforcement) had already reached yield strains near ultimate loads in specimen S-0.33-0.5-10. This was the least brittle failure and showed good ductility. Figure 3.3 shows the mode of failure for all corbels.

The propagation of cracks was closely traced and marked on the surface of each specimen at 50 kN intervals. To improve the appearance of cracks, the concrete surface was covered with white paint and gridded into a 75 mm squares. Figure 3.4 shows the cracks pattern for all tested specimens at failure. In the early stage of loading within 14-20% of the ultimate load, the initial flexural crack appeared, which was predominantly vertical and propagated up to reach 80-90% of the corbel depth. With increasing the load, additional flexural cracks were developed adjacent to the initial one; in addition to, the formation of new inclined/diagonal flexural-shear cracks at the mid height of the corbel in the shear span (between the outer edge of the supporting plate and the column-corbel interface). With further load increase, the latter cracks propagated diagonally towards the loading plate. At approximately 30-45% of the failure load, the main diagonal crack formed, defining the direction and location of the main strut, and indicating the activation of the arch action. No further diagonal cracks were observed after reaching a load level of approximately 65-75% of the ultimate load; however, the width of the existing cracks was increased with the increase in the load level, until the failure of the specimen occurred. Generally, the specimens with a lower *a/d* ratio of 0.33 showed a more brittle and catastrophic failure, which was accompanied by abrupt/explosive sound of the concrete crushing. In addition, the specimens with horizontal (crack-control) reinforcement showed

higher intensity, narrower and more uniformly distributed cracks compared to that of the counterpart corbels without horizontal reinforcement.

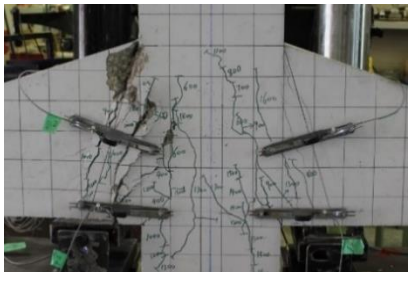
G-0.33-0.5-10 (DC-ST)

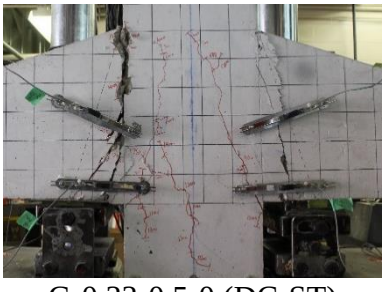
G-0.33-0.5-0 (DC-ST)

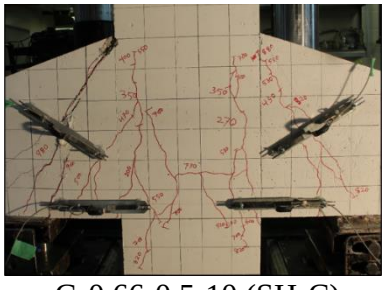
G-0.66-0.5-10 (SH-C)


G-0.66-0.7-0 (SP-F)

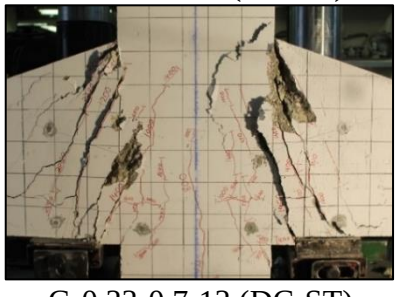
G-0.33-0.7-13 (DC-ST)

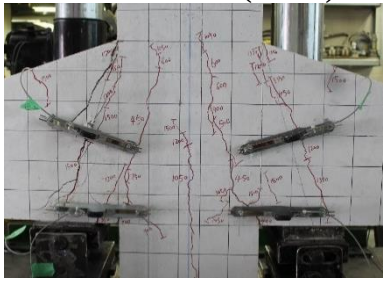
G-0.33-0.7-0 (SH-C)

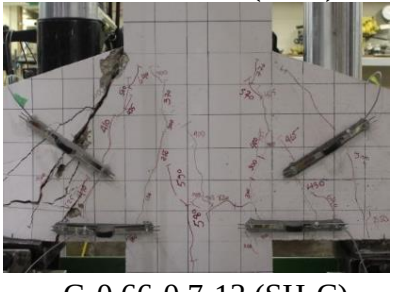
G-0.66-0.7-13 (SH-C)

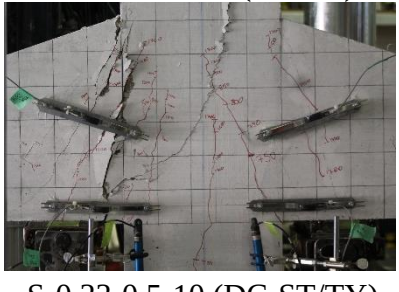
S-0.33-0.5-10 (DC-ST/TY)

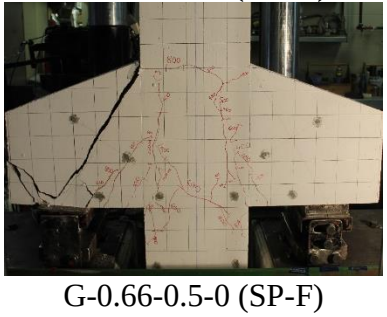
G-0.66-0.5-0 (SP-F)

Figure 3.3. Mode of failure of test corbels

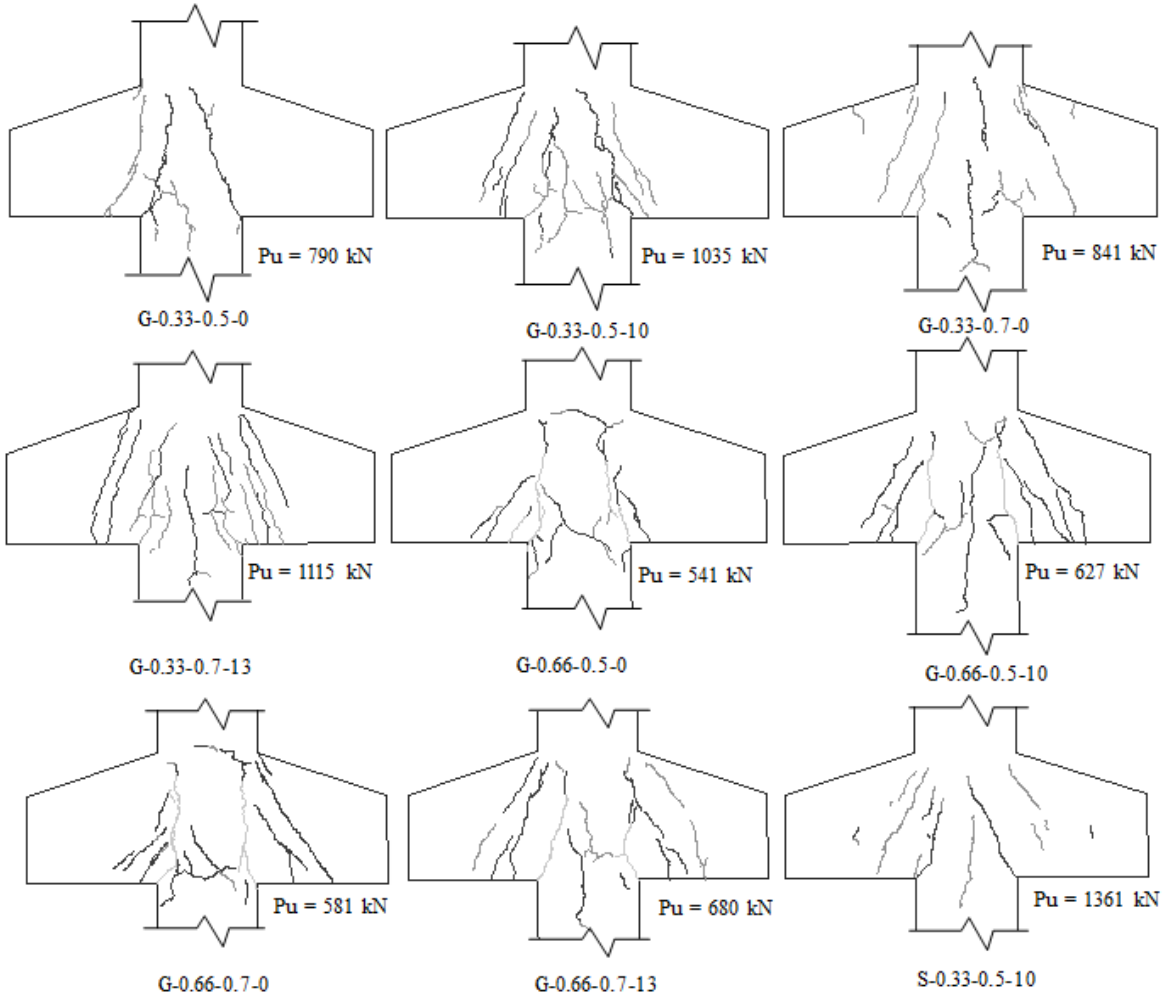


Figure 3.4. Cracking pattern of the tested corbels.

### *3.4.2 Cracking and ultimate loads*

The cracking and ultimate loads for the tested corbels reinforced with either steel or GFRP are listed in Table 3.3. It is worth mentioning that the flexural cracking load was recorded when the first crack appeared on the white-washed surface of the tested corbels. On the other hand, the corbel was considered failed, when the applied load dropped to 75% of its ultimate load, which was captured by the load cells. The flexural cracking load did not depend on the presence of crack control reinforcement or the *a/d* ratio but rather on the compressive strength of the concrete at the tie zone. For example, the average flexural cracking load for the GFRP-RC specimens with an *a/d* of 0.33 (G-0.33-0.5-0, G-0.33-0.5-10, G-0.33-0.7-0, G-0.33-

0.7-13) was 131 kN, and for the specimens with an *a/d* of 0.66 (G-0.66-0.5-0, G-0.66-0.5-10, G-0.66-0.7-0, G-0.66-0.7-13) was 120 kN, for an average compressive strength of 40 MPa and 42 MPa, respectively. For example, comparing specimens G-0.33-0.5-0 and G-0.33-0.5-10 would examine the effect of adding crack-control reinforcement on the cracking load. Thus, adding three size No. 10 horizontal stirrups in specimen G-0.33-0.5-10 showed insignificant effect on the cracking load with an increase of 3%, compared to the control specimen without stirrups (G-0.33-0.5-0), confirming the previous notion. Similarly, increasing the reinforcement ratio of the GFRP bars showed insignificant effect on the cracking load. For instance, the flexural cracking loads for the specimens with *a/d* of 0.33, G-0.33-0.5-0 and G-0.33-0.7-0, were 121 and 136 kN, respectively, and for the corbels with *a/d* of 0.66, G-0.66-0.5-0 and G-0.66-0.7-0, were 125 and 127 kN, respectively. In this study, replacing the main GFRP reinforcement with steel bars and maintaining all other parameters unchanged, yielded a significant effect on the cracking load. For example, using steel bars as main reinforcement in specimen S-0.33-0.5-10 yielded a significant increase of 94% in the cracking load compared to the GFRP-RC counterpart specimen G-0.33-0.5-10. This was mainly attributed to the variation in the compressive strength between both corbels, which were 45.2 and 39.9 MPa, respectively.

Nevertheless, the abovementioned parameters (e.g., the main reinforcement ratio, the presence of crack-control reinforcement, and the *a/d* ratio) that did not show any effect on the cracking load, had a clear effect on the ultimate load. Figure 3.5 presents the effect of the investigated parameters on the ultimate load-carrying capacity. Irrespective of the reinforcement ratio of the main reinforcement, the inclusion of horizontal reinforcement in the tested corbels with an *a/d* ratio of 0.33, improved the load-carrying capacity of the corbel. For instance, adding three horizontal stirrups with diameters of No. 10 and No. 13 in specimens G-0.33-0.5-10 and G-0.33-0.7-13 increased the load-carrying capacity by 23 and 33%, respectively, compared to their counterparts G-0.33-0.5-0 and G-0.33-0.7-0 horizontal reinforcement. On the other hand, such parameter showed less effect when it was added to the specimens with the *a/d* ratio of 0.66. For instance, adding horizontal reinforcement in specimens G-0.66-0.5-10 and G-0.66-0.7-13

obtained ultimate loads of 627 and 680 kN, respectively. These loads were 541 and 581 kN for the counterpart specimens G-0.66-0.5-0 and G-0.66-0.7-0, respectively, without horizontal reinforcement. This may be attributed to that increasing the *a/d* ratio reduced the angle between the horizontal stirrups and the axis of the strut, decreasing the efficiency of such reinforcement that is most efficient when placed perpendicular to the strut axis (Brown and Bayrak 2006).

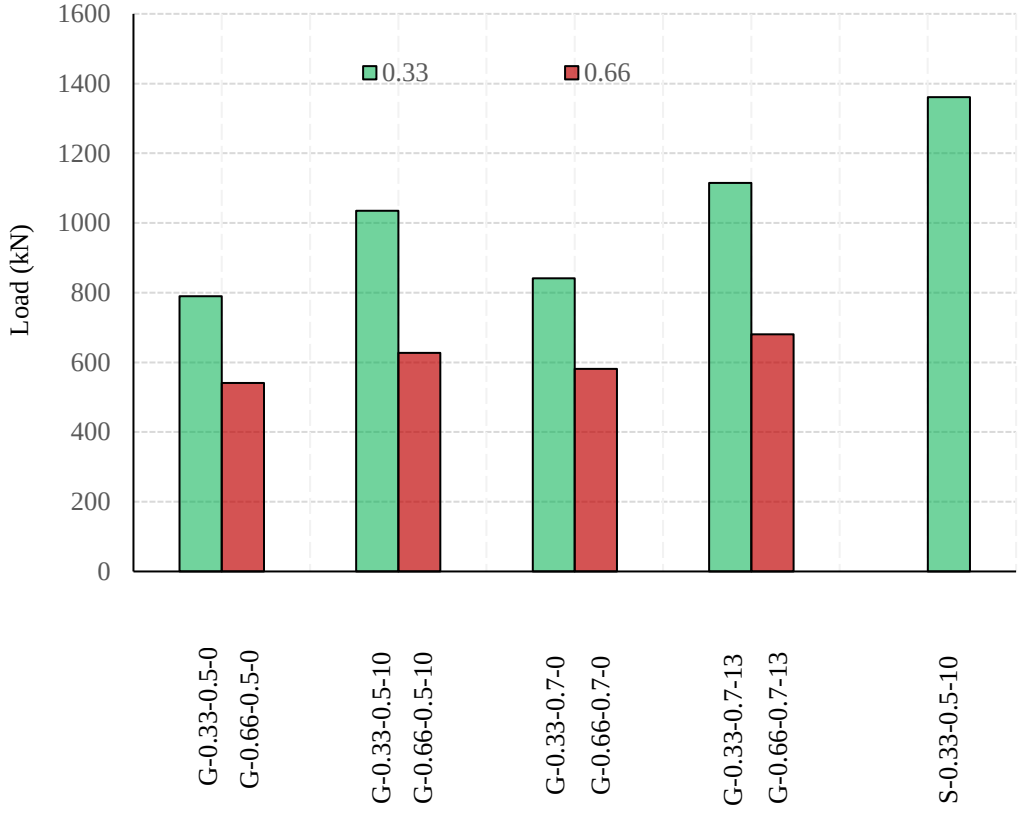


Figure 3.5. Effect of investigated parameters on the capacity of the test specimens

On the other hand, the *a*/*d* ratio was considered as one of the main parameters that remarkably affect the ultimate capacity of the tested corbel. For instance, when the *a*/*d* ratio increased from 0.33 to 0.66, the average ultimate capacity of specimens G-0.66-0.5-0, G-0.66-0.5-10, G-0.66-0.7-0, and G-0.66-0.7-13 was significantly decreased by approximately 36%, compared to the average capacity of the counterpart

specimens with an *a*/*d* ratio of 0.33. This may be attributed to that the increase in the *a*/*d* ratio was accompanied by a reduction in the inclination angle of the strut, which led to a reduction in the effect of the arch action mechanism (Omeman et al. 2008). Accordingly, the load carrying capacity of the compression strut was reduced, and the main tie started to carry a more significant part of the applied load. The ultimate load carrying capacity of the steel-RC specimen S-0.33-0.5-10 (1,361 kN) was higher than the GFRP-RC counterpart, G-0.33-0.5-10 (1,035 kN), considering that the other parameters (*a/d* ratio, reinforcement ratio of main and secondary reinforcements) were maintained constant. This was ascribed to the fact that the axial rigidity of the steel is significantly greater than the GFRP, which consequently led to a significant reduction in the transverse stresses generated in the compression strut under the same load level.

### *3.4.3 Load-deflection response*

Figure 3.6 categorizes the specimens according to *a/d* ratios to illustrate the response of the load-deflection relationship. The deflection was measured under the column with two LVDTs, which produced identical readings until a diagonal crack formed at one of the two corbels, which affected the readings of one of the two LVDTs. Thus, the deflection in Figure 3.6 was plotted based on the readings from the LVDT mounted near the failed corbel. All corbels showed bilinear response up to the ultimate load. Prior to the formation of the flexural crack, all specimens showed small values of deflection. After the initiation of the first crack, a reduction in the overall stiffness of the tested corbel was noticed, representing a cracked specimen and reduced moment of inertia, but with different tendencies based on the presence of transverse reinforcement and *a/d.* ratio with further increase in the load, shear cracks propagated in the shear span of the specimens, followed by the formation of the main diagonal crack which enhanced the stiffness due the activation of the arching action (the redistribution of the internal stresses). As expected, all corbels without crack-control horizontal reinforcement did not show any post-peak behaviour, and failed in an abrupt brittle manner, particularly for the specimens with *a/d* of 0.33. Table 3.3 gives the maximum deflection under the column upon failure and the deflection corresponding to the service load. It is worth mentioning that the service

load of the corbel (SL =532 kN) was considered as the load corresponding to a strain in the main tension steel reinforcement of 0.00135 (60% of the yield strain of 0.00231) of the steel-RC corbel. Irrespective of the *a/d* for the tested corbels, as the amount of reinforcement increased, the corresponding deflection at the service load level was reduced. Similarly, the addition of crack-control horizontal reinforcement was accompanied by an increase in the stiffness of the specimens due to the confining effect provided by the stirrups, which consequently led to a reduction in the measured deflection at the SL level. Similarly, the behavior for specimens with *a/d* ratio of 0.66 showed a similar trend with much less load-carrying capacity and corresponding deflection (Figure 3.6b). This may be attributed to that the full capacity of the diagonal struts was not reached and failure occurred due to either splitting tensile failure or shear compression failures.

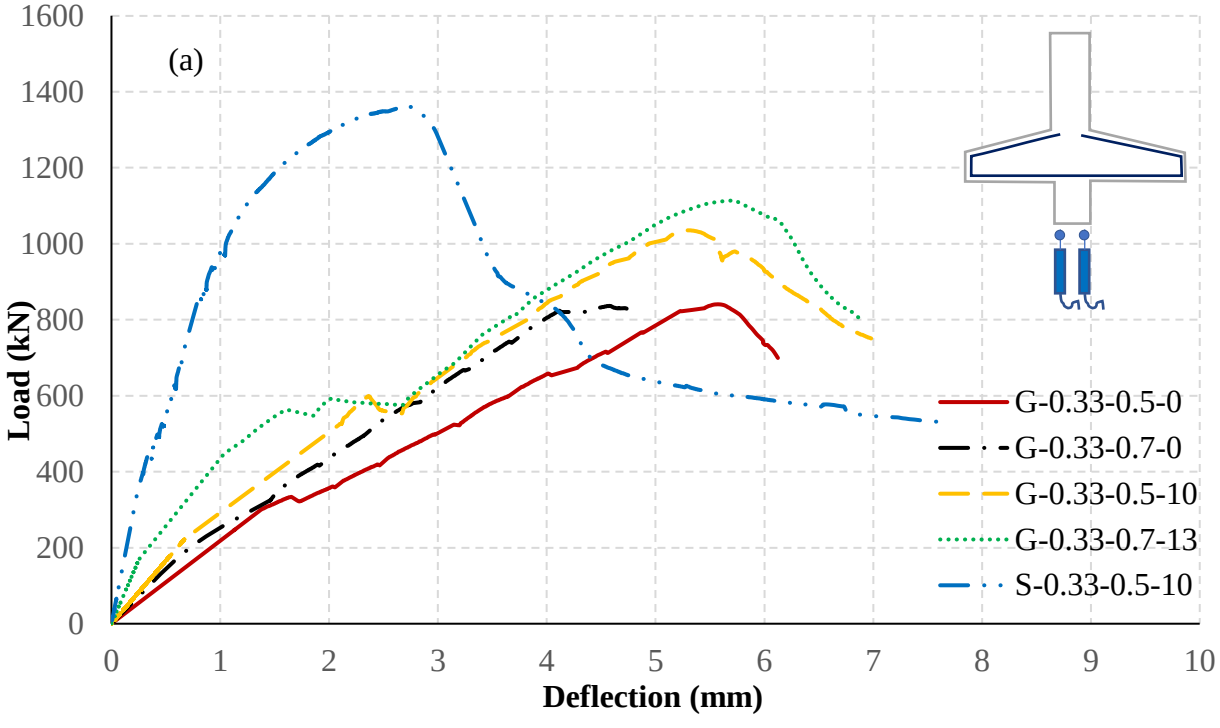

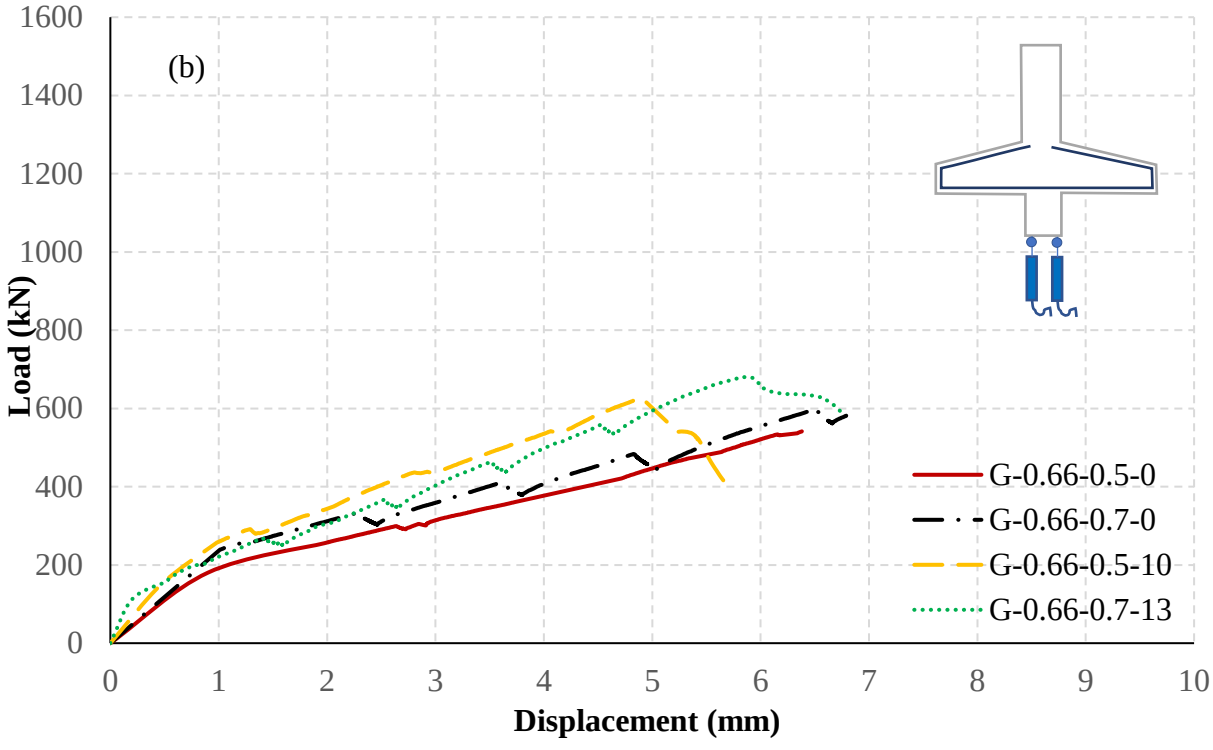


Figure 3.6. Load-deflection relationship for corbels with *a/d* ratio of (a) 0.33, and (b) 0.66

### *3.4.4 Crack width*

The flexural crack width throughout the loading process was captured and plotted in Figure 3.7. The maximum crack width allowed by the Canadian standards for bridges, CSA S6-19 (CSA 2019d), is 0.5 mm for exterior exposure. Irrespective of the *a/d* ratio for the tested corbel, increasing the reinforcement ratio of the main bars had a significant effect on controlling the crack width. At the service load level, the crack width for the control corbels G-0.33-0.5-0 and G-0.33-0.7-0 was 0.93 and 0.71 mm, respectively. These values were 2.30 and 2.17 mm for the counterpart corbels G-0.66-0.5-0 and G-0.66-0.7-0, respectively. Furthermore, the addition of crack-control horizontal reinforcement showed a clear positive effect in controlling the crack width, particularly for the specimens with *a/d* ratio of 0.33. For instance, at the service load level, adding three horizontal stirrups distributed in two-thirds of the effective depth as specified in the Canadian standards in specimens G-0.33-0.5-10 and G-0.33-0.7-13 showed an enhancement in reducing

the flexural crack width by 15 and 27%, respectively, compared with the control corbels without transverse reinforcement (G-0.33-0.5-0 and G-0.33-0.7-0).

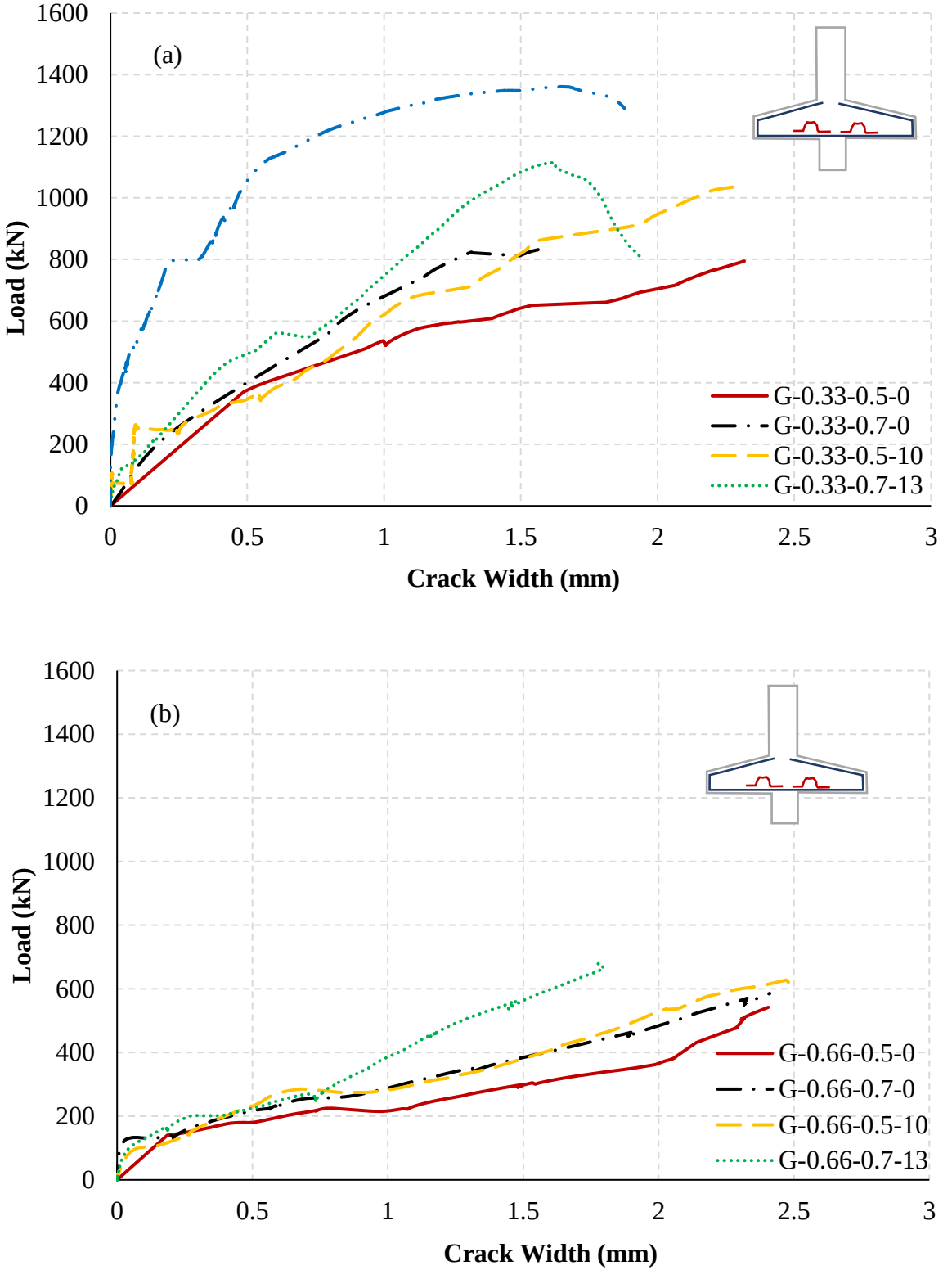


Figure 3.7. Load-flexural crack width relationship for corbels with *a/d* ratio of (a) 0.33, and (b) 0.66

Table 3.3. Summary of test results

| Specimens | $a$ (mm) | $d$ (mm) | $P_{cr}$ (kN) | $P_u$ (kN) | $f'_c$ (MPa) | $w_c$ (mm) | $\delta_{max}$ (mm) | $\delta_{sl}$ (mm) | Mode of Failure |
|---|---|---|---|---|---|---|---|---|---|
| S-0.33-0.5-10 | 133.1 | 404.0 | 235 | 1,361 | 45.2 | 0.21 | 7.6 | 0.4 | DC-ST/TY |
| G-0.33-0.5-0 | 133.1 | 403.5 | 121 | 790 | 39.1 | 0.93 | 6.1 | 1.2 | DC-ST |
| G-0.33-0.5-10 | 132.6 | 403.5 | 123 | 1,035 | 39.9 | 0.79 | 6.9 | 1.8 | DC-ST |
| G-0.33-0.7-0 | 132.6 | 401.7 | 136 | 841 | 42.0 | 0.71 | 4.8 | 2.2 | SH-C |
| G-0.33-0.7-13 | 132.6 | 401.7 | 145 | 1,115 | 44.0 | 0.52 | 6.8 | 2.8 | DC-ST |
| G-0.66-0.5-0 | 266.3 | 403.5 | 125 | 541 | 42.5 | 2.30 | 6.4 | 6.1 | SP-F |
| G-0.66-0.5-10 | 265.1 | 403.5 | 108 | 627 | 40.8 | 2.00 | 5.7 | 4.0 | SH-C |
| G-0.66-0.7-0 | 265.1 | 401.7 | 131 | 581 | 43.0 | 2.17 | 6.8 | 5.6 | SP-F |
| G-0.66-0.7-13 | 266.6 | 401.7 | 112 | 680 | 41.5 | 1.34 | 6.7 | 4.2 | SH-C |

*Note: $P_{cr}$ = first flexural-cracking load; $P_u$ = ultimate load; $w_c$ flexural crack width at service load; $\delta_{max}$ = maximum deflection at failure; $\delta_{sl}$ = deflection at service load; DC-ST is diagonal compression-strut failure; SH-C is shear-compression failure; SP-F is splitting failure; TY is tie yielding.*

This is mainly attributed to the confining effect that enabled forces to be redistributed. On the other hand, such confining effect resulted from the horizontal stirrups was diluted in the specimens with the *a/d* ratio of 0.66. For instance, at the service load level, specimens G-0.66-0.5-10 and G-0.66-0.7-13 experienced a crack width of 2.0 and 1.34 mm, respectively, while the crack width for the control corbels G-0.66-0.5-0 and G-0.66-0.7-0 was 2.3 and 2.17 mm, respectively. This was attributed to the reduction in the angle between the strut and the stirrups, as the strut with higher *a/d* is more flattened.

### *3.4.5 Strain Profile*

The mechanism of shear transfer in corbels or brackets is predominantly caused by the arch action of the diagonal strut. An arch action develops when a truss model is formed and is in an equilibrium state, where the stresses in all its elements are not more than their capacities. The development of arch action in other types of GFRP-RC structures that were designed using the STM (e.g., deep beams) was confirmed by Andermatt and Lubell (2013), Farghaly and Benmokrane (2013), and Mohamed et al. (2017).

Figure 3.8 illustrates the load versus measured strain at the column-corbel interface for the tested corbels. The load–strain plots for the corbels exhibited similar characteristics for both *a/d* ratios of 0.33 and 0.66. For all GFRP-RC corbels after cracking, the strains varied linearly with increased load up to failure. In addition, the results showed that increasing the reinforcement ratio decreased the strains in the bars measured at the same load level. For instance, at the ultimate load level of corbel G-0.33-0.5-0, increasing the reinforcement ratio to 0.7 in specimen G-0.33-0.7-0 led to 33% reduction in the measured strains. For the test corbels and at the same SL level, the corbel reinforced with GFRP bars showed larger strains than the corbel reinforced with steel bars, which showed a yielding plateau at a strain of 2,300 με. This was attributed to the lower modulus of elasticity of GFRP compared to steel bars. On the other hand, the decrease in the *a/d* ratio decreased the strains in bars measured at the same load level.

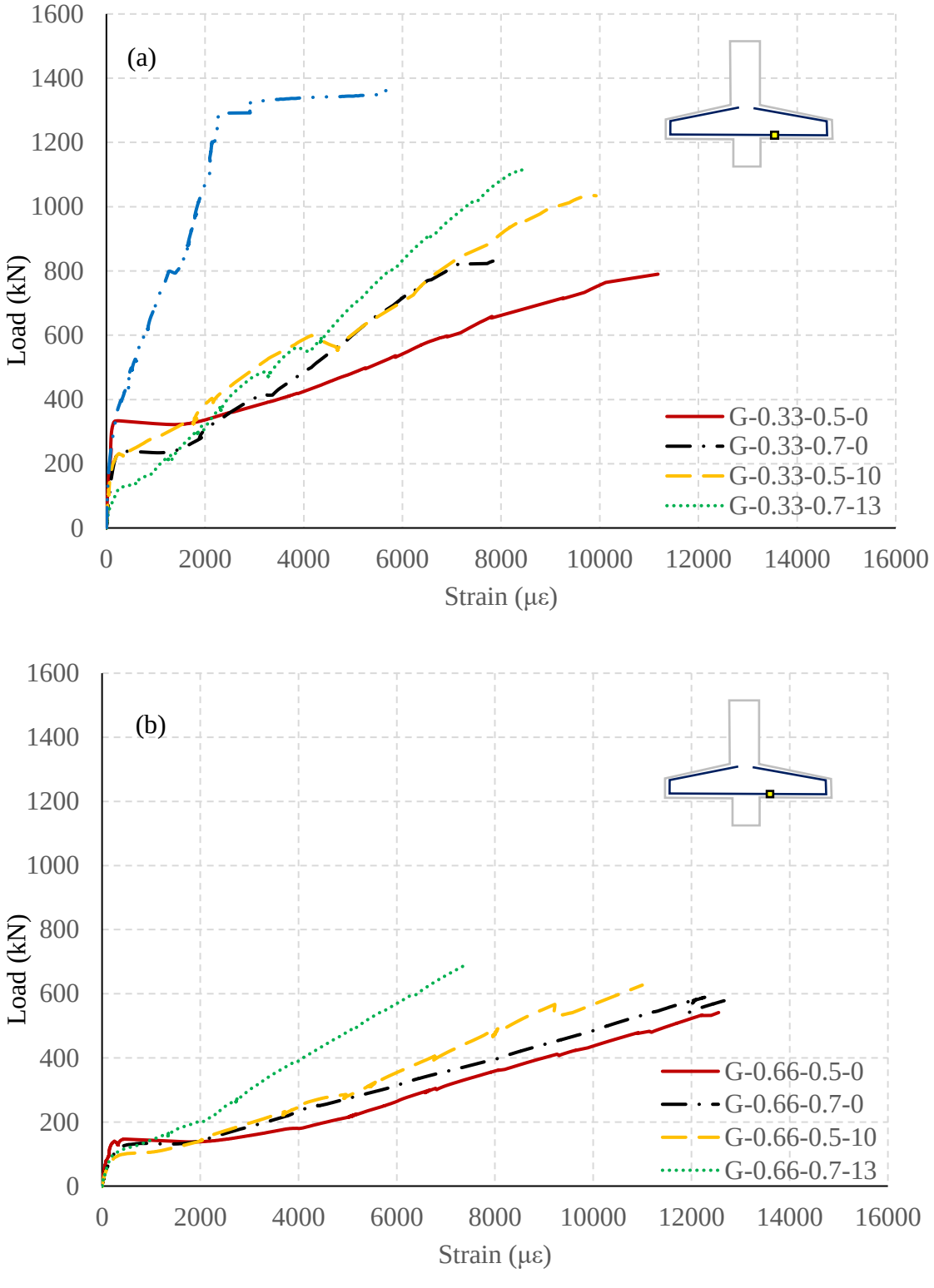


Figure 3.8. Strains at column-corbel interface in tested corbels with *a/d* ratio of (a) 0.33, and (b) 0.66

In a well-developed arching action (STM) for such corbels, the strain in the main reinforcement (tie) is expected to be uniform. In this context, the distribution of strains was determined by measuring the strains in the main longitudinal bars at three different locations 150-mm apart starting at the column-corbel interface. The strain profile at different stages of loading (20, 40, 60, 80, 90, and 100% of the corbel ultimate load) is presented in Figure 3.9. Prior to the initiation of the inclined cracks, where the beam action was still applicable, the distribution of the strains was following the shape of the elastic bending moment of a cantilever. At early loading level (20% of the ultimate load), no visible variation in the strain was noticed along the reinforcement. However, at the location of the maximum bending moment, close to the column-corbel interface, the rate of increase of strains was higher than the other locations. However, once the major inclined crack was initiated an increase in the strains near the support plate was recorded trying to reach a uniform strain distribution in the reinforcement along the corbel. In the locations without major cracks, no variation in the strain was observed. In addition, the increase in the measured strains in the GFRP bars past the edge of the support plate were minimal as indicated by the readings of the strain gauges located at 150 or 300 mm from the edge of the support plate for the specimens with *a/d* ratio of 0.33 or 0.66, respectively. These strain measurements confirm the development of the arching mechanism, in the tested corbels once the inclined cracks have formed. Another methodology previously applied by Mohamed et al. (2017) and Bediwy et al. (2021) was adopted in this study, by computing the predicted ultimate load using the average of the measured strains, the axial stiffness of the GFRP longitudinal bars, and the angle between the strut and tie, and compare it to the experimental failure load. It was found out that the mean ratio between the experimental failure load to the predicted load was 84% for the corbels reinforced with GFRP bars only, which proved the applicability of using the STM for the tested corbels.

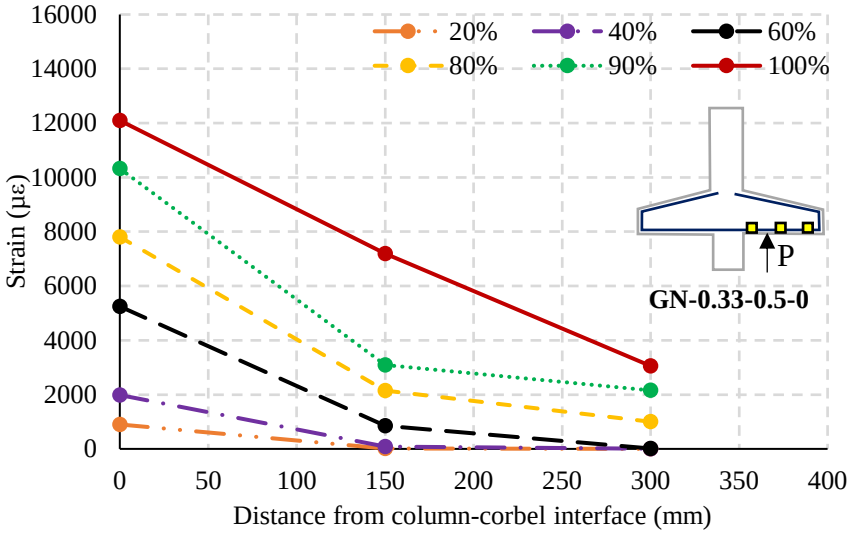
20%
40%
60%
80%
90%
100%
Strain (με)
16000
14000
12000
10000
8000
6000
4000
2000
0
0
50
100
150
200
250
300
350
400
Distance from column-corbel interface (mm)
P
GN-0.33-0.5-0

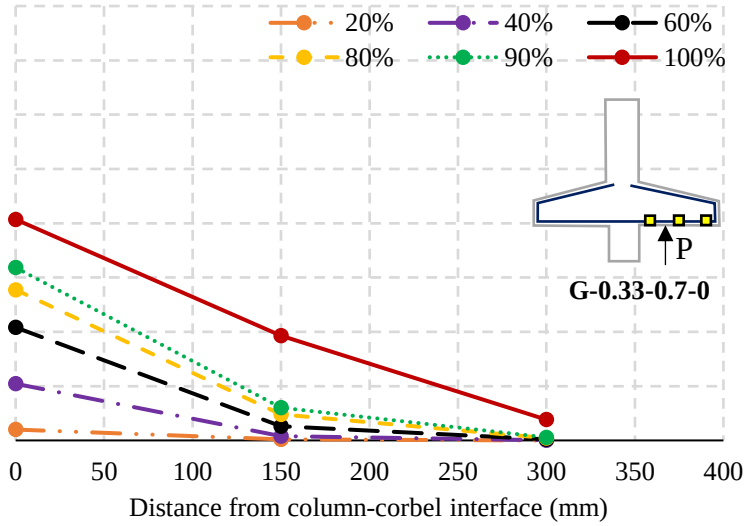
20%
40%
60%
80%
90%
100%
0
50
100
150
200
250
300
350
400
Distance from column-corbel interface (mm)
P
G-0.33-0.7-0

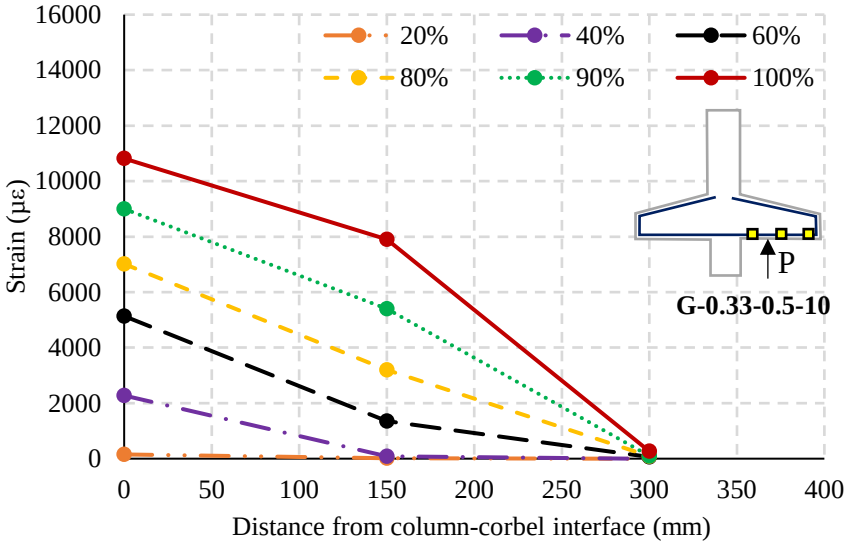
20%
40%
60%
80%
90%
100%
Strain (με)
16000
14000
12000
10000
8000
6000
4000
2000
0
0
50
100
150
200
250
300
350
400
Distance from column-corbel interface (mm)
P
G-0.33-0.5-10

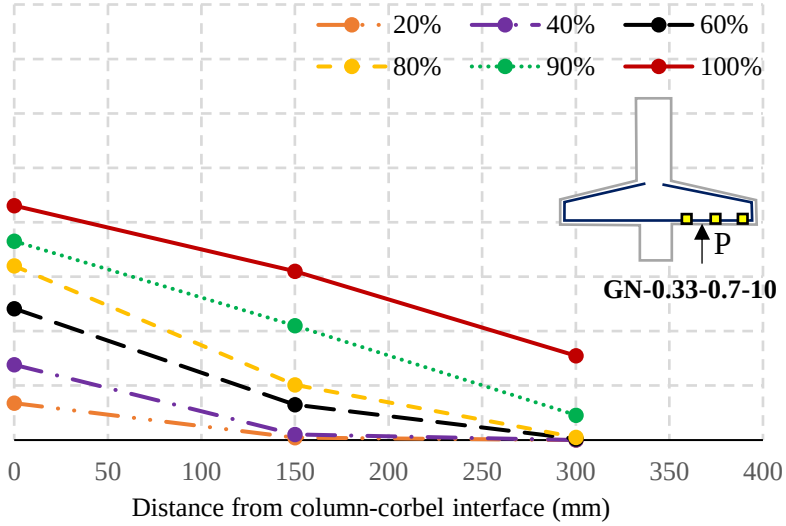
20%
40%
60%
80%
90%
100%
0
50
100
150
200
250
300
350
400
Distance from column-corbel interface (mm)
P
GN-0.33-0.7-10

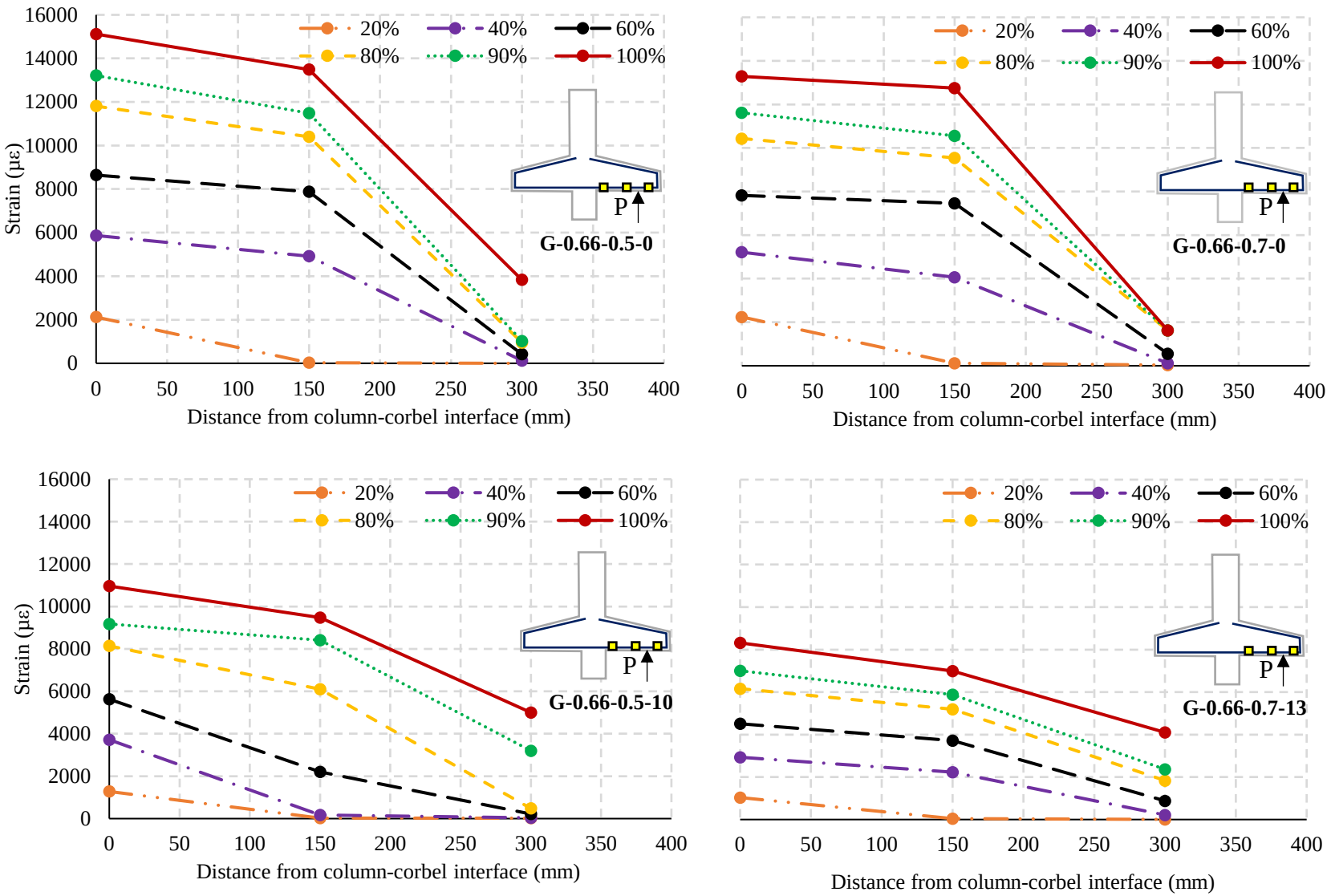


Figure 3.9. Strain profile in corbels

### *3.4.6 Evaluation of Code provisions for strut and tie model*

The Canadian standards for FRP-RC building structures, CSA S806-12 (CSA 2021), and bridges CSA S6-19 (CSA 2019d), provided special provisions to adopt the STM for FRP-RC structures with an *a/d* ratio less than 1.0, such as corbels and brackets. In these standards, the capacity of the struct primarily depends on the compressive strength of the concrete, the transverse strains developed in the strut that triggered by the strains in the main reinforcement, and the type of reinforcement of the tie. It is worth mentioning that the objectives of these special provisions, which were reproduced form the Canadian standards for steel-RC structures CSA A23.3-19 (CSA 2019a), are to control the corbel's effective depth and regulate the use of crack control reinforcement. On the other hand, the recently published code for GFRP-RC structures, ACI 440.11-22 (ACI Committee 440 2022); does not include design provisions for corbels or brackets due to the significant lack of knowledge in this subject. However, since the capacity of the concrete strut is considered as the governing factor in defining the overall capacity of the corbels reinforced with FRP bars, unlike the steel-RC corbels, where yielding of the steel in the tie is the governing mode of failure, the authors believe that using the provisions stipulated in the American code for steel-RC structures, ACI 318-19 (ACI 2019), is practicable for the FRP-RC corbels. Particularly, the STM specified in the ACI code correlated the capacity of the corbels with only the concrete compressive strength within the strut region and the struct geometry and did not count for the transvers strains in the strut that generated from the strains in the main reinforcement. In addition, the special requirements to apply the STM in corbels or brackets in the American code were satisfied, where the shear force shall not exceed the least of (i) $0.2f'_c\, b_w\, d$, (ii) $(480+.08\, f'_c\,)b_w\, d$, or (iii) $1600\, b_w\, d$, where the $f'_c$ is the concrete compressive strength, $b_w$ is the width of the corbel, and $d$ is the effective depth of the corbel. Similarly, the Eurocode (EN 1992-1-1:2004), Committee CEN/TS 250, issued the first version for the design of FRP-RC structures; however, similar to the ACI code, no provisions were included to use the STM in designing the corbels, but the application of the equations in the steel version on FRP-RC structures is still fitting due to the same reasons previously mentioned for the ACI code.

In this study, the load carrying capacity of the tested corbels was computed using the STM provisions in the CSA S806-12 (CSA 2021), CSA S6-19 (CSA 2019d), the ACI 318-19 (ACI 2019), and Eurocode 2 (EN 1992-1-1:2004). Afterwards, a critical comparison between the calculated and the experimental capacities of the tested corbels were conducted. A summary of the STM equations in the standards and codes adopted in this study is listed in Table 3.4. The strength reduction and the material resistance factor, $\phi$, in all equations were set to unity. The STM adopted in this study to analyze the tested corbels was set to be a single panel, as depicted in Figure 3.10. Table 3.5 shows the comparisons between the experimental and the code predicted capacity for the tested corbels. The results indicate that the Eurocode and the ACI code overestimated the failure load with a mean ratio predicted-to-experimental, $P_{pre}/P_{exp,}$ of 1.10 and 1.32, and coefficient of variation (CoV) of 0.22 and 0.14, respectively. This might be attributed to that the ACI and the Eurocode 2 neglect the effect of concrete softening in the diagonal strut resulting from the high longitudinal strains experienced by the GFRP longitudinal reinforcement. On the other hand, the Canadian standards CSA S806-12 (CSA 2021) and CSA S6-19 (CSA 2019d) showed conservative estimates of the ultimate capacity of the GFRP-RC corbels with average values of $P_{pre}/P_{exp}$ = 0.66, and CoV of 0.14. This was attributed to that the capacity of the compression strut in the Canadian standards is adversely affected by the amount of longitudinal strain ($\varepsilon_1$) that could reach 0.01 or more in GFRP bars, which leads to sensible predictions. In addition, despite the minimum amount of the horizontal reinforcement as a crack-control specified in the Canadian standards, it was not reflected in the equations that predict the strength of the corbel.

Table 3.4. Design standards and code provisions for STM

| STM Component | CSA S806-12 / CSA S6-19 | Eurocode 2 | ACI 318-19 |
|---|---|---|---|
| Strut | Compressive force in the strut = $\phi_c f_{cu} A_{cs}$<br>$f_{cu}$ is the limiting compressive stress<br>$f_{cu} = \frac{f_c'}{0.8+170\varepsilon_1}$ where,<br>$\varepsilon_1 = \varepsilon_f + (\varepsilon_f + 0.002)\cot^2\theta_s$<br>$f_c'$ = concrete strength<br>$\varepsilon_1$ = transverse tensile strain<br>$\varepsilon_f$ = tensile strain in the tie<br>$\theta_s$ = the smallest angle between the strut and the adjoining ties | The allowable compressive stress of struts<br>$\sigma_{Rd,max} = 0.6\nu f_{cd}$ (no transverse compressive stress)<br>$\sigma_{Rd,max} = f_{cd}$ (with transverse compressive stress)<br>$f_{cd}$ is design value of concrete compressive strength = $\alpha_{cc} f_{ck}/\gamma_c$<br>Where $f_{ck}$ is characteristic compressive cylinder strength of concrete at 28 days<br>$\alpha_{cc}$ is the coefficient taking account of long-term effects on the compressive strength (Recommended value is 1.0)<br>$\gamma_c$ is the partial safety factor for concrete<br>$\nu = 1 - f_{ck}/250$ | Strength of struts = $F_{ns} = f_{ce} A_{cs}$ and<br>$f_{ce} = 0.85\beta_s\beta_c f_c'$ where<br>• $\beta_s$ is strut coefficient = 1.0 for boundary struts, 0.75 for interior struts satisfying one of the following equations $\frac{0.0025}{\sin^2\alpha_1}$ & $V_u \le \phi 5 \tan\phi\lambda\lambda_s\sqrt{f_c'} b_w d$ and 0.4 for other cases<br>• $\beta_c$ is strut confinement factor, which is the lesser of: $\sqrt{\frac{A_2}{A_1}}$ or 2.0, where $A_1$ is the loaded area and $A_2$ is the area of the lower base of the largest frustum of a pyramid, cone, or tapered wedge contained wholly within the support and having its upper base equal to the loaded area |
| Tie | Tensile force in the tie $\le 0.65\phi_F A_{FT} f_{FU}$<br>$\phi_F$ = resistance factor for FRP, $A_{FT}$ = area of reinforcement, $f_{FU}$ = ultimate strength of the bar | The nominal tensile strength of a tie, $F_{nt}$, shall be calculated by $F_{nt} = A_{st} f_y$, $A_{st}$ = area of steel reinforcement<br>$f_y$ = yield strength of steel reinforcement | |

| | | | |
|---|---|---|---|
| Node | Compressive stress in the node regions ≤ $0.85\phi_c m f_c^{'}$ in node regions bounded by struts and nearing areas, $0.75\phi_c m f_c^{'}$ in node regions anchoring a tie in only one direction and $0.65\phi_c m f_c^{'}$ in node regions anchoring ties in more than one direction | Compressive stress in the node regions ≤ $vf_{cd}$ in node regions bounded by struts and nearing areas, 0.85 $v f_{cd}$ in node regions anchoring a tie in only one direction and 0.75 $v f_{cd}$ in node regions anchoring ties in more than one direction | The nominal compressive strength of a nodal zone, $F_{nn}$, is calculated by $F_{nn} = f_{ce} A_{nz}$<br>where $f_{ce} = 0.85\beta_n f_c^{'}$, $\beta_n$ is nodal zone coefficient<br>• $\beta_n$ =1.0, nodal zones bounded by struts and bearing areas or both, $\beta_n$ = 0.8, nodal zones anchoring one tie, and $\beta_n$ = 0.6, nodal zones anchoring two or more ties. |
| Special Provisions for Corbels | • Closed stirrups or ties parallel to the primary tensile tie reinforcement, and having a total area of not less than 0.65 $A_{FT}$, shall be distributed within two-thirds of the effective depth adjacent to $A_{FT}$<br>• The ratio $A_{FT}^*/bd$ calculated at the face of the support shall be not less than 0.04 ($f_c'/0.01E_f$), where $E_f$ is the design modulus for FRP reinforcement. | • If $a_c < 0.5\ h_c$, closed horizontal stirrups should be provided with $A_{shorizontal}$ more than $k_1\ A_{s,main}$, and If $a_c > 0.5\ h_c$, closed vertical stirrups should be used<br>• $a_c$ is shear span, and $h_c$ is the height of the corbel<br>• The main tension reinforcement should be anchored at both ends | • Primary tension reinforcement shall be developed at the face of the support<br>• Closed stirrups or ties shall be spaced such that $A_h$ is uniformly distributed within (2/3) $d$ measured from the main tension reinforcement |

* $A_{FT}$ = area of reinforcement

Table 3.5. Comparison between experimental and predicted failure loads

| Corbel ID | $P_{exp}$ (kN) | Strut-and-tie-model (STM) | | | | | |
|---|---|---|---|---|---|---|---|
| | | CSA S806-12 / CSA S6-19 | | ACI 318-19 | | Eurocode 2 | |
| | | $P_{CSA}$ (kN) | $P_{CSA}/P_{exp}$ | $P_{ACI}$ (kN) | $P_{ACI}/P_{exp}$ | $P_{EC2}$ (kN) | $P_{EC2}/P_{exp}$ |
| S-0.33-0.5-10 | 1,361 | *465 | 0.34 | 465 | 0.34 | 465 | 0.34 |
| G-0.33-0.5-0 | 790 | 564 | 0.71 | 607 | 0.77 | 903 | 1.14 |
| G-0.33-0.5-10 | 1,035 | 568 | 0.55 | 1,161 | 1.12 | 1,223 | 1.18 |
| G-0.33-0.7-0 | 841 | 681 | 0.81 | 658 | 0.78 | 965 | 1.15 |
| G-0.33-0.7-13 | 1,115 | 700 | 0.63 | 1292 | 1.16 | 1745 | 1.56 |
| G-0.66-0.5-0 | 541 | 358 | 0.66 | 541 | 1.00 | 746 | 1.38 |
| G-0.66-0.5-10 | 627 | 349 | 0.56 | 746 | 1.19 | 746 | 1.19 |
| G-0.66-0.7-0 | 581 | 419 | 0.72 | 552 | 0.95 | 807 | 1.39 |
| G-0.66-0.7-13 | 680 | 410 | 0.6 | 999 | 1.47 | 1,065 | 1.57 |
| **Mean | | | 0.66 | | 1.10 | | 1.32 |
| ***CoV | | | 0.14 | | 0.22 | | 0.14 |

*The steel specimen (S-0.33-0.5-10) was computed using CSA A23.3 (CSA 2019a)

**The mean value was calculated based on the GFRP specimens only

***CoV = Coefficient of variation

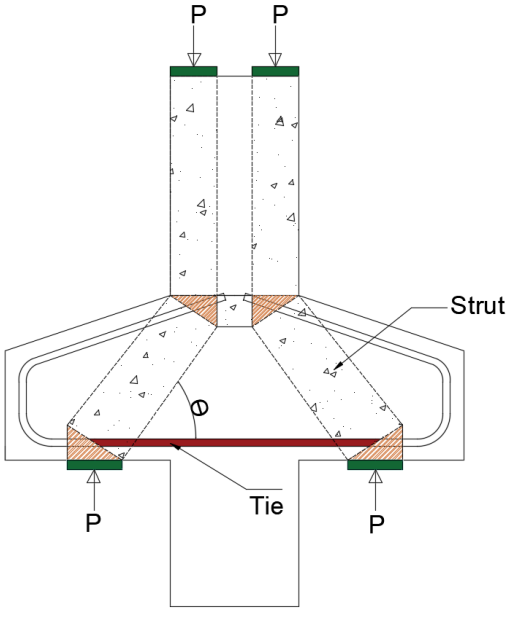


Figure 3.10. Strut-and-tie model (STM) for double-sided corbels

## 3.5 Conclusions

Eight GFRP-RC and one steel-RC full-scale corbels with *a/d* ratios of 0.33 and 0.66 were constructed and tested to failure to investigate the behavior of GFRP-RC corbels, emphasizing the effect of crack-control horizontal reinforcement for such structural elements. Based on the presented results and analysis, the following conclusions can be drawn:

1. The steel-RC corbel experienced the highest load-carrying capacity of 1,361 kN, while the counterpart GFRP-RC corbel failed at 1,035 kN. For the steel-RC corbel, the main (tie) reinforcement yielded at ultimate load resulting in the least brittle failure among all tested specimens.
2. The development of the arching action in the tested GFRP-RC corbels was substantiated by the essentially uniform strain distribution in the main reinforcement (tie). After the initiation of the main diagonal crack, significant reserve capacity was available, indicating the development of an arch action mechanism.

3. The main or horizontal reinforcement had no effect on the formation of initial flexural or shear cracks; however, it clearly affected the ultimate load capacity of the corbel. Similarly, the presence of crack-control horizontal reinforcement distributed within two-third of the effective depth had a notable effect on the ultimate capacity of the specimens.
4. The predictions of the CSA S806-12 (CSA 2021) and CSA S6-19 (CSA 2019d) were conservative with an average value of $P_{pre}/P_{exp}$ of 0.66 and a CoV of 14%. On the other hand, the predictions of the ACI 318-19 (ACI 2019) and Eurocode (EN 1992-1-1:2004) were over-estimating the experimental capacities with a mean value of $P_{exp}/P_{pre}$ of 1.10 and 1.32 and CoV of 22 and 14%, respectively.

# Chapter 4. Practical Evaluation of High-Strength Concrete Corbels Reinforced with GFRP Bars

**Authors and Affiliations**

- Ankit Borgohain, M.Sc. Student, Department of Civil Engineering, University of Manitoba.
- Ahmed G. Bediwy, Assistant Professor, Department of Civil Engineering, Lakehead University.
- Ehab F. El-Salakawy, Professor, Department of Civil Engineering, University of Manitoba.

**Journal and Status:** Engineering Structures, Elsevier, under review.

**Reference:**

Borgohain, A., Bediwy, A. and El-Salakawy, E. "Practical Evaluation of High-Strength Concrete Corbels Reinforced with GFRP bars." Engineering Structures, Submitted in March 2023.

**Note:**

The manuscript had been slightly edited from the original paper by renumbering the tables and figures to include the chapter number. The abbreviations of the specimen names are explained in the Appendix A under Section A.1. In addition, the reference list and list of notations have been moved to the appropriate sections in the thesis as indicated in the Table of Contents.

## 4.1 Abstract

Corbels, designed primarily as discontinuity-region structural elements, are often used as components of bridges and buildings to support beams and girders. There has been extensive research on steel-reinforced concrete (RC) corbels; however, there is a noticeable gap in research to investigate the behavior of glass fiber-reinforced polymer (GFRP)-RC corbels. Considering the linear stress-strain relationship up to failure of GFRP, the use of high-strength concrete (HSC) in lieu of the normal-strength concrete (NSC) in corbels would reduce their sizes considerably; yet it will aggravate their brittle nature. In this study, nine full-scale concrete corbels were constructed and tested until failure. One reference specimen was reinforced with steel bars, while the other eight were GFRP-RC corbels. The main test parameters were the type of concrete (HSC or NSC), the shear span-to-depth ratio, and the total reinforcement ratio of the main and horizontal bars. The tests showed that the principal mode of failure was concrete strut crushing for specimens with a shorter shear-span-to-depth ratio. The steel-RC corbels failed by tension tie yielding, which showed large ductility. The Canadian standards for FRP-RC building structures predicted a conservative mean capacity with $P_{pre}/P_{exp}$ ratio of 0.59 compared to the American code and Eurocode, which overestimated the capacities with a ratio of 1.18 and 1.25, respectively.

**Keywords**: Corbels, glass fiber-reinforced polymer, high-strength concrete, shear capacity, strut-and-tie model

## 4.2 Introduction

Corbels are deep reinforced concrete (RC) cantilevers with a shear span-to-depth ($a/d$) ratio less than unity(ACI Committee 318 2019, CSA 2019a) such that the behavior is shear dominated. Unlike the beam action in Bernoulli (B) regions (e.g., slender beams), the arch action that involves the transmission of the vertical loads to the supports through the concrete compression struts while the reinforcement acts as a tie, is the main load transfer mechanism in Discontinuity (D) regions (e.g., corbels)(Collins and Mitchell 1986, Wight and MacGregor 2009b). While analyzing the arch action, the traditional sectional design approaches

based on the plane sections theory are no longer applicable' thus, the strut-and-tie model (STM) and some empirical methods (shear friction) are among the approaches extensively used in corbels design and has been included in several standards and codes of practice(ACI Committee 318 2019, CSA 2019a, 2019b, 2021). An STM idealizes the complex flow of stresses in a structural member by aligning uniaxial truss elements. The applied load is transmitted directly to the support by in-plane compression through an inclined concrete strut and constant tension in the reinforcement. The point of intersection of struts, ties, or a combination of both forms a node. Struts, ties, and nodes are the three elements that shape an STM, and they must be proportioned to resist the applied forces(Schlaich *et al.* 1987, Wight and MacGregor 2009b)

Corbels are structural members conventionally used in RC bridges, parking garages and industrial buildings. Structures located in aggressive conditions and reinforced with conventional steel bars are susceptible to a reduced service life due to steel corrosion(Abu-Obaida *et al.* 2018, Mohamed *et al.* 2021). In addition, this situation would be much aggravated in North America, especially with the use of de-icing salts to remove the hazardous ice/snow accumulation off roads and pave the way for safe driving conditions. Thus, the utilization of glass fiber-reinforced polymer (GFRP) reinforcement is deemed a prime substitute to overcome the costly repair expenses resulting from corrosion-led damages in RC structures(ACI Committee 440 2022). In addition to the permanent immunity to the corrosion-related problems, GFRP bars, compared to steel, have higher tensile strength, lighter weight, easier installation, and handling process, leading to lower construction labor and long-term costs (Berg *et al.* 2006). Nevertheless, the linear elastic stress-strain relationship (unlike the yielding plateau in steel), along with the lower modulus of elasticity would usually lead to larger strains and wider concrete cracks in GFRP-RC structures. Thus, using GFRP bars in structural members that had a shear-dominated failure mode/nature, such as deep beams or corbels, would lead to abrupt/catastrophic failure without ample warning (Andermatt and Lubell 2013; Bediwy and El-Salakawy 2021; Mohamed *et al.* 2021)

Corbels are constructed and cast monolithically with other structural members (e.g., columns and walls) to bear heavy concentrated loads. In some cases, corbels can be subjected to additional loads resulting from

heavy traffic or can be exposed to a high concentration of chloride or carbon, which will accordingly lead to cover spalling and/or reduction of steel area (Chakrabarti *et al.* 1989, Campione and Cannella 2020). In addition, improving the concrete properties (e.g., the compressive strength) is imperative, particularly for the GFRP-RC corbel, as it is usually over-reinforced in such a way that concrete crushing governs the failure. Hence, in response to the previous circumstances (e.g., applying higher loads, the exposure to harsh environment, the design criterion of GFRP-RC structures) considering the latest advancement in the concrete industry, the utilization of high-strength concrete (HSC), which is one of the common forms of high-performance concrete (HPC), has gained significant ground in the construction field. Compared to normal-strength concrete (NSC), HSC had various advantages pertaining to its higher compressive strength (more than 55 MPa (ACI Committee 363 2011; ACI Committee 222 2019)), enhanced durability properties, and higher modulus of elasticity, which helped the designers to reduce the required cross-sectional area and reduce the creep and shrinkage rates of structural members under severe loading and/or environmental conditions (Fattuhi 1994a; Foster *et al.* 1996; Almomani *et al.* 2022). On the other hand, the increased strength of concrete is associated with increased brittleness, which would hinder the application of HSC with GFRP in shear-critical concrete members such as corbels.

The current Canadian standards for FRP-RC buildings, CSA S806-12 (CSA 2021) and bridges, CSA S6-19 (CSA 2019b), permitted applying the STM used for deep beams along with special provisions to compute the load-carrying capacity of corbels and brackets. These special provisions, which controls the corbel's effective depth, the usage of crack-control reinforcement, etc., were reproduced from the equations stipulated in the standards for the steel-RC structures, CSA A23.3-19 (CSA 2019a). The former standards considered the compressive strength of concrete and the strains formed in the tie. Conversely, even the recently published American code for GFRP-RC structures, ACI 440.11-22 (ACI Committee 440 2015), still does not offer any provisions for the design of corbels and brackets. Nevertheless, the American code for steel-RC structures, ACI 318-19 (ACI Committee 318 2019) adopted two approaches for the design of corbels: the "empirical method" in Chapter 16, when the $a/d$ ratio is less than 1.0, which is identical to

those mentioned in the studies conducted by Mattock et al. in 1976 (Mattock *et al.* 1976), and the STM in Chapter 23 for any $a/d$ less than 2.0. The former method relies on calculating the load-carrying capacity at the interface between the column and the corbel (the critical shear section/location), while the latter method uses the concrete compressive strength and the strut's dimensions to compute the load-carrying capacity of the strut. Thus, either approach can be applied for corbels and brackets with an $a/d$ less than 1.0.

Generally, in steel-RC corbels, the STM assumed that the tie would yield first (the governing mode of failure) so that sufficient ductility could be provided, while in FRP corbels, the load capacity is governed by the concrete strut failure to achieve a less brittle failure. In addition, if a strut under compression develops transverse tensile cracking at the mid-height, it may never reach its design capacity and undergo early failure. Moreover, in a typical corbel, there are two forces exerted on a distance measured from the column face: vertical force ($V_u$) and horizontal action ($N_u$), as shown in Figure 4.1. This is among the reasons why various code provisions have requirements to provide secondary horizontal reinforcement throughout the depth of the corbel.

To date, serval experimental research has been conducted to assess the shear capacity of steel-RC corbels cast with NSC or HSC (Fattuhi 1994a; Yong and Balaguru 1994; Hwang *et al.* 2000; Abdul-Razzaq and Dawood 2020). These studies confirmed the efficiency of STM in analyzing RC corbels, which thoroughly defined the failure of RC corbels due to crushing of the strut, yielding of the tie, or nodal failure. However, there is a dearth of experimental data on the behavior of NSC or HSC corbels reinforced with GFRP bars, which led to a significant lack of knowledge on how to adopt the STM for GFRP-RC structures. This paper attempts to fill this gap and to remove any ambiguity associated with the application of the STM in designing GFRP-RC corbels. To this end, this study is divided into two main phases: experimental and analytical. In the experimental phase, eight large-scale GFRP-RC corbels were constructed and tested until failure. All the corbels were simply supported with two equal corbel spans. All corbels had a rectangular cross-section measuring 300 mm in width and 450 mm in height at the corbel-column interface. The test variables were the concrete strength, the shear span-to-depth ratio, and the reinforcement ratio. In addition,

one steel-RC corbel was constructed and tested for comparison purposes. As for the analytical phase, the feasibility of applying the current STM provisions stipulated in the available design codes and standards to compute the load-carrying capacity of corbels was assessed.

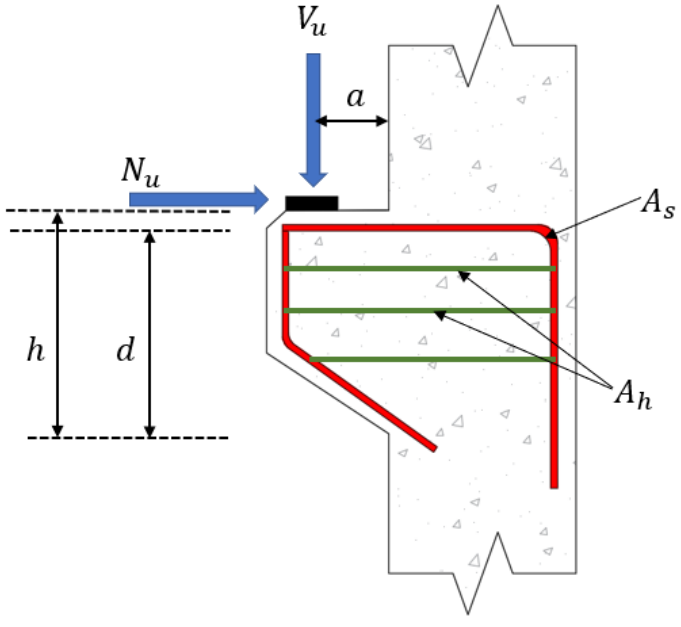


Figure 4.1. Typical reinforced concrete corbel.

## 4.3 Experimental Program

### *4.3.1 Test Specimens*

In this study, a total of nine corbels were constructed and tested until failure. These specimens represent a cantilever beam segment integrated with short columns. All the corbels were simply supported with two equal corbel spans and designed according to the STM provisions of CSA S806-12 (CSA 2021), except for the steel-RC corbel that was designed following the requirements of CSA A23.3-19 (CSA 2019a). The corbel was tapered with a rectangular cross-section having a width of 300 mm and a height of 450 and 300 mm at the corbel-column interface and at the free end, respectively. The column segment of the specimen had dimensions of 300 × 350 mm and extended 400 and 600 mm below and above the corbel surfaces, respectively, as shown in Figure 4.2. Except the steel-RC control specimens, all test specimens were internally reinforced with sand-coated GFRP bars located at an effective depth ($d$) of approximately 400

mm. Moreover, the column was adequately reinforced with four No. 20M longitudinal bars and No. 10M closed stirrups spaced at 250 mm, as shown in Figure 4.2. To prevent any premature anchorage failure of the GFRP bars (e.g., slippage), the corbel was extended beyond the point of load application.

The designation of the corbels can be explained as follows. The first letter refers to the reinforcement type ("S" for steel and "G" for GFRP). The second letter refers to the type of concrete ("H" for high-strength concrete and "N" for normal-strength concrete). The fraction refers to shear-span-to-depth ratio ($a/d$ = 0.33 or 0.66), while the last Latin number indicates the main reinforcement / secondary horizontal crack control reinforcement ratio in percentage ("I" for 0.5 / 0.7% and "II" for 0.7 / 1.3%). The details of the corbels are listed in Table 4.1.

Table 4.1. Details of Test Corbels

| Beam ID | *a/d* | *d* (mm) | Main reinforcement | Transverse reinforcement | | $f'_c$ (MPa) |
|---|---|---|---|---|---|---|
| | | | | Nominal diameter (mm) | Spacing (mm) | |
| GN-0.33-I | 0.33 | 403.5 | 3-No. 15 | 9.50 | 65 | 39.9 |
| GH-0.33-I | 0.33 | 403.5 | 3-No. 15 | 9.50 | | 59.3 |
| GN-0.33-II | 0.33 | 401.7 | 3-No. 20 | 12.7 | | 44.0 |
| GH-0.33-II | 0.33 | 401.7 | 3-No. 20 | 12.7 | | 58.5 |
| GN-0.66-I | 0.66 | 403.5 | 3-No. 15 | 9.50 | | 40.8 |
| GH-0.66-I | 0.66 | 403.5 | 3-No. 15 | 9.50 | | 62.3 |
| GN-0.66-II | 0.66 | 401.7 | 3-No. 20 | 12.7 | | 41.5 |
| GH-0.66-II | 0.66 | 401.7 | 3-No. 20 | 12.7 | | 59.8 |
| SH-0.66-I | 0.67 | 404.0 | 3-15M | 11.3 | | 54.3 |

*$a$ is the shear span, $d$ is the effective depth of main flexural reinforcement, $f'_c$ is the concrete compressive strength.

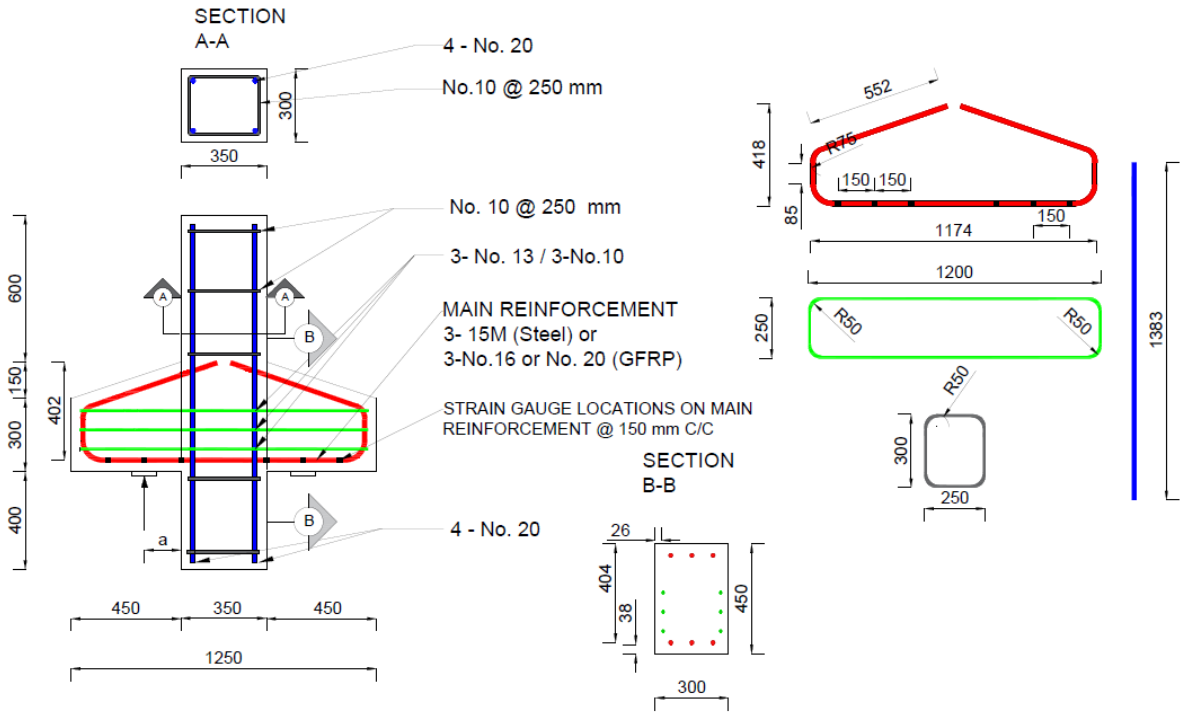


Figure 4.2. Geometry and reinforcement details of the corbel. (Dimensions in mm.)

### *4.3.2 Materials*

All the test specimens were constructed using normal-weight, ready-mix concrete provided by a local supplier with a target 28-day compressive strength of 35 and 60 MPa for the NSC and HSC, respectively. The actual concrete compressive strength was determined by testing standard 100 × 200 mm cylinders on the day of testing according to CSA A23.1-19/A23.2-19 (CSA 2019c), as listed in Table 4.1. The corbel and the cylinders were cast in the laboratory and wet-cured for 7 days.

For all GFRP-RC specimens, either size No. 15 or No. 20 GFRP bars was used as the main reinforcement along with size No. 13 or No. 10 GFRP as horizontal closed stirrups. The column was reinforced with 4-No. 20 GFRP bars and No. 10 GFRP stirrups spaced at 250 mm. All GFRP straight bars and stirrups were sand coated.

For the steel-RC control specimen, size 15M and 10M deformed steel bars were used for the main and horizontal reinforcement, respectively. For column, 4-20M steel bars and No. 10M steel stirrups spaced at

250 mm were used for the main and transverse reinforcements, respectively. The mechanical properties of the used steel and GFRP bent bars were provided by the manufacturer through certified tests that were carried out according to the CSA S807-19(CSA 2019d) standards. The properties of the used reinforcement are listed in Table 4.2.

Table 4.2. Mechanical properties of the corbel reinforcement

| Bar Size | Bar Type | Nominal Diameter (mm) | Area ($mm^2$) | Modulus of Elasticity (GPa) | Tensile Strength (MPa) | Ultimate strain (%) |
|---|---|---|---|---|---|---|
| No. 10M | Steel | 11.3 | 100 | 200 | 460[a] | 0.23[a] |
| No. 15M | Steel | 15.9 | 200 | 200 | 450[a] | 0.225[a] |
| No. 10 | GFRP | 9.5 | 71 | 54.3 | 1,199 | 2.21 |
| No. 13 | GFRP | 12.7 | 127 | 54.7 | 1,209 | 2.21 |
| No. 16 | GFRP | 15.9 | 198 | 55.6 | 1,194 | 2.15 |
| No. 20 | GFRP | 19.1 | 285 | 55.6 | 1,197 | 2.14 |

[a] Yield stress/strain for steel reinforcement

### *4.3.3 Test Setup and Instrumentation*

All specimens were tested in a 5,000-kN capacity hydraulic actuator to failure under a displacement-controlled loading rate of 2.5 mm/minute. The specimens were tested in an inverted configuration and only the vertical load was considered. Each specimen was supported on a roller support at one end and a hinged support at the other. Figure 4.3 shows a schematic drawing of the test setup. The hydraulic actuator was equipped with a built-in load cell, which was used to obtain the axial load applied to the column. The vertical load was applied through a steel loading plate (350×300×50 mm), and the specimen was supported on two identical bearing plates (150×300×50 mm). The tested corbels were instrumented with linear variable displacement transducers (LVDTs) to monitor deflection during the test. Two LVDTs were

attached to the midpoint of the bottom surface of the column. Several strain gauges were attached to the main bars and horizontal crack-control reinforcement to measure strain distribution along the length of reinforcement (Figure 4.2**)**. In addition, four 200-mm long PI gauges were used to calculate the crack width at two locations: at the mid-height of the struts and at the column-corbel interface at the tie level. A data-acquisition system monitored by a computer was used to record the readings of the load cell, LVDTs, strain gauges, and PI gauges.

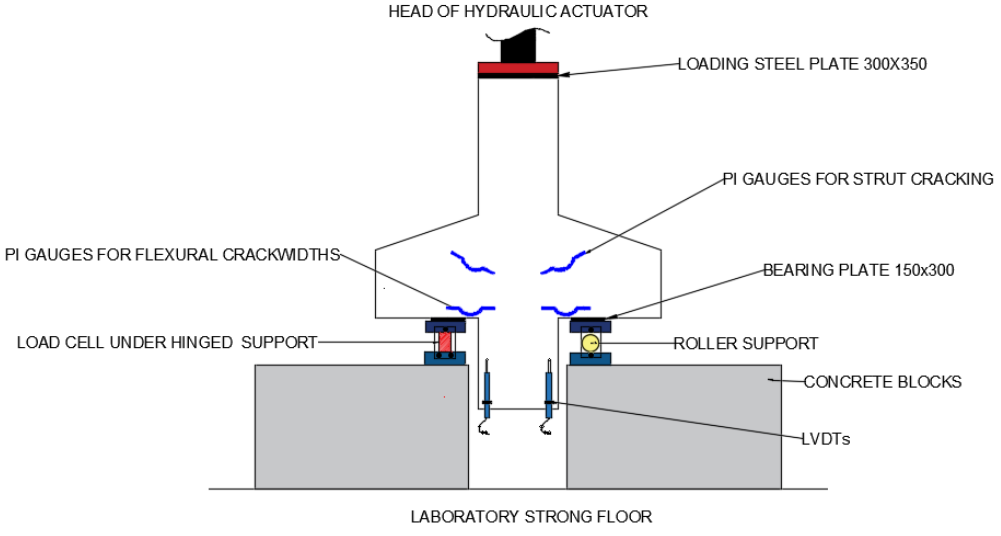


(a)

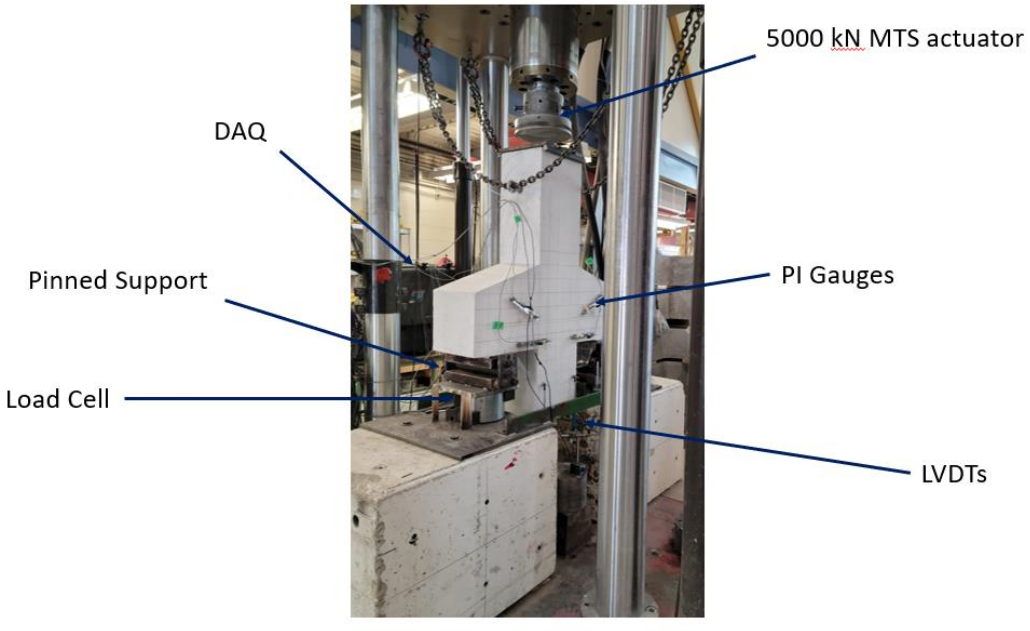


(b)

Figure 4.3. Test Set-up. (a) Schematic drawing, (b) photo (Dimensions in mm)

## 4.4 Results and Discussions

### *4.4.1 Crack Pattern and Mode of Failure*

To better observe the initiation and propagation of the cracks during testing, all the corbels were whitewashed and gridded into 75 mm squares, and the cracks were monitored and marked at 100 kN intervals. Irrespective of the parameters investigated in this study, no premature localized failure resulting from either the bearing under the supporting/loading plates or the slippage of the bars was observed for all specimens. Similar cracking behaviour was noted throughout the test; the initial crack started at the column-corbel interface and propagated vertically to reach 70-80% of the corbel depth. While the load was monotonically increasing, additional wider flexural-shear cracks were formed in the shear span between the edge of the support plate and the column-corbel interface. With the increase in load, approximately at 30-40% of the ultimate load, the inclined diagonal cracks initiated, triggering the arch action in the corbel. Since the load tends to be transferred directly from the loading points to the supports through the inclined strut, no additional inclined cracks were observed; yet the width of the existing diagonal cracks kept increasing until failure, which was defined by a sudden drop in the applied load by approximately 25%. It is worth noting that the intensity of the cracks was higher, and the spacing between two adjacent cracks was smaller in the area where the stirrups are located (approximately the bottom two-thirds of the effective depth).

As depicted in Figure 4.4, several modes of failure were observed in this study: compression strut failure (C-ST), shear compression failure (S-CO), and diagonal splitting failure (D-SP). This was in good agreement with those modes reported by Abu-Obida et al.(Abu-Obaida *et al.* 2018), who tested GFRP-RC corbels with lower concrete grades and higher $a/d$ ratio. The shear compression failure occurred in three corbels (GH-0.66-I, GN-0.66-I, and GN-0.66-II). The shear-compression failure was characterized by the crushing of the concrete at the tip of the diagonal crack at the column-corbel interface. Compression strut failure, the most brittle and abrupt failure, took place in four specimens (GN-0.33-II, GH-0.33-I, GH-0.33-

II, and GN-0.33-I), which can be described by several cracks linking the nodal zones at the top and bottom, defining the compression strut. In addition, the diagonal splitting failure was described by an inclined crack extended from the top edge of the column-corbel junction and the inside edge of the support plate, which happened in GH-0.66-II. Finally, the tie yielding with shear compression failure (TY/S-Co) was observed in the steel-RC specimen (SH-0.66-I), where the ties had already reached yield strains near ultimate loads. This was the least brittle failure and showed good ductility.

In addition, it is worth mentioning that the specimens with a lower *a*/*d* of 0.33 failed in a more brittle manner where wide excessive cracks accompanied by concrete spalling and loud noise "bang" were observed, compared to that of the counterpart specimens with *a*/*d* of 0.66.

### *4.4.2 Cracking Load and Ultimate Capacity*

The recorded loads for the tested corbels at different stages of loading are summarized in Table 4.3. The cracking load was captured when the first flexural crack appeared on the surface of the specimen, while the ultimate load was recorded from the load cell before the sudden drop occurred. Regardless of the reinforcement ratio for the tested corbels, the first flexural cracks for the specimens cast with HSC had higher values compared to their counterpart specimens cast with NSC. For example, the average cracking load for the GFRP HSC corbels (GH-0.33-I, GH-0.33-II, GH-0.66-I, and GH-0.66-II) was 177.5 kN for an average compressive strength of 60 MPa, while this value was 122 kN for the NSC corbels with an average compressive strength of 41.5 MPa. On the other hand, as expected, increasing the longitudinal and transverse reinforcement ratio had an insignificant effect on the cracking load, which depends mainly on the concrete strength. For instance, the cracking load for the specimens with the same *a*/*d* of 0.33 and cast with HSC, yet with different reinforcement ratios (GH-0.33-I and GH-0.33-II), was nearly identical. On the other hand, changing the material of the main or transverse reinforcement had a little effect on the cracking load. For example, using the GFRP for the main and transverse reinforcement in specimen GH-

0.66-I in lieu of the steel bars in specimen SH-0.66-I resulted in a slightly different cracking load of 172 and 185 kN respectively.

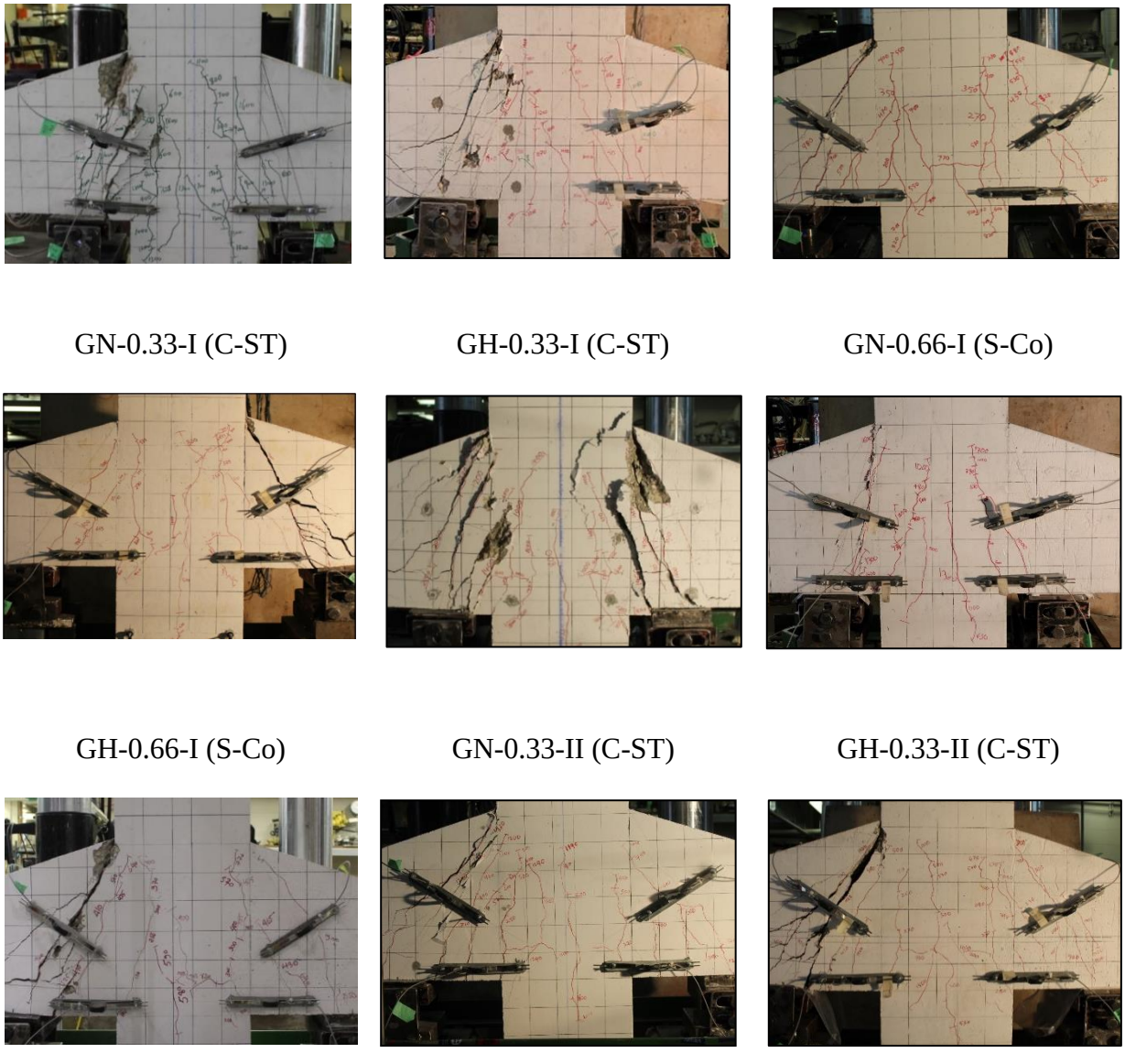

GN-0.33-I (C-ST) GH-0.33-I (C-ST) GN-0.66-I (S-Co)

GH-0.66-I (S-Co) GN-0.33-II (C-ST) GH-0.33-II (C-ST)

GN-0.66-II (S-Co) SH-0.66-I (TY/S-Co) GH-0.66-II (D-SP)

Figure 4.4. Mode of failure of test corbels

Table 4.3. Summary of Test results

| Specimens | $a$ (mm) | $d$ (mm) | $P_{cr}$ (kN) | $P_u$ (kN) | $f'_c$ (MPa) | $w_c$ (mm) | $\delta_{sl}$ (mm) | $\delta_{max}$ (mm) | Mode of Failure |
|---|---|---|---|---|---|---|---|---|---|
| GN-0.33-I | 133.1 | 403.5 | 123 | 1,035 | 39.9 | 0.192 | 0.85 | 5.3 | C-ST |
| GH-0.33-I | 133.1 | 403.5 | 168 | 1,293 | 58.5 | 0.223 | 0.48 | 8.5 | C-ST |
| GN-0.33-II | 132.6 | 401.7 | 145 | 1,115 | 44.0 | 0.166 | 0.54 | 5.7 | C-ST |
| GH-0.33-II | 132.6 | 401.7 | 170 | 1,464 | 59.8 | 0.201 | 0.42 | 8.6 | C-ST |
| GN-0.66-I | 266.3 | 403.5 | 108 | 627 | 40.8 | 1.205 | 2.10 | 4.9 | S-CO |
| GH-0.66-I | 266.3 | 403.5 | 172 | 690 | 62.3 | 1.439 | 1.92 | 6.2 | S-CO |
| GN-0.66-II | 265.1 | 401.7 | 112 | 680 | 41.5 | 0.807 | 1.80 | 5.9 | S-CO |
| GH-0.66-II | 265.1 | 401.7 | 182 | 828 | 59.8 | 0.976 | 1.74 | 9.5 | D-SP |
| SH-0.66-I | 266.6 | 404.0 | 185 | 887 | 54.3 | 0.363 | 0.61 | 9.9 | TY/S-CO |

*Note: $P_{cr}$ = first flexural-cracking load; $P_u$ = ultimate load; $w_c$ flexural crack width at service load; $\delta_{sl}$ = deflection at service load; $\delta_{max}$ = maximum deflection at failure; C-ST is compression-strut failure; S-CO is shear-compression failure; D-SP is diagonal-splitting failure; TY is tie yielding.*

Alternatively, in addition to concrete compressive strength, the aforementioned parameters that did not affect the cracking load (e.g., the reinforcement ratio or the *a*/*d* ratio), had a prominent impact on the ultimate capacity of the tested specimens. Figure 4.5 presents the effect of the investigated parameters on the ultimate load-carrying capacity. Increasing the compressive strength means enhancing the capacity of the diagonal strut, which accordingly increases the transmitted shear forces through the truss formed in the corbel (the arch action). For example, maintaining the same *a*/*d* ratio and the reinforcement ratio; however, increasing the strength of the concrete used in the specimens GH-0.33-I and GH-0.33-II by 47 and 35%, compared to that of the counterpart NSC specimens GN-0.33-I and GN-0.33-II, increased the capacity by 25 and 31%, respectively. A similar trend was observed for the set of corbels that had a higher *a*/*d* ratio of 0.66. For instance, specimens GN-0.66-I and GN-0.66-II with NSC compressive strength of 41.5 and 40.8 MPa failed at 545 and 680 kN, respectively. For the counterpart HSC specimens, GH-0.66-I and GH-0.66-II, these values were 62.3 and 59.3 MPa, and 690 and 828 kN, respectively.

Consistently, the *a*/*d* was one of the main parameters remarked in this study. Increasing the *a*/*d* ratio by 100% from 0.33 to 0.66 led to a 42% reduction in the average ultimate capacity of the specimens GN-0.66-I, GH-0.66-I, GN-0.66-II, and GH-0.66-II, compared to the counterpart specimens with an *a*/*d* ratio of 0.33. This was expected since increasing the *a*/*d* ratio decreases the inclination angle of the strut, which accordingly increases the horizontal component of the shear force that resisted by the tie rather than the vertical one that defines the capacity of the corbel, and in turn, saps the strength of the strut (negatively affect the arch-action mechanism).

Finally, increasing the reinforcement ratio (including the longitudinal reinforcement and the horizontal stirrups) inside the tie had an implicit effect in enhancing the comprehensive capacity of the corbel. For further clarification, increasing the axial rigidity (cross-sectional area of the bars [A] × modulus of elasticity [E]) of the bars located in the tie zone resulted in lower generated strains at the same load level, which consequently decreased the transverse strains developed in the strut according to the modified compression field theory (MCFT) that accounts for the strains in cracked concrete (Vecchio and Collins 1986).

Irrespective of the concrete grade or the *a*/*d* ratio, the average ultimate load of the "I" group with a low reinforcement ratio was 911 kN, while the average capacity for the "II" specimens was 1,022 kN. The former explanation was evident and confirmed when the ultimate capacity of the steel specimen SH-0.66-I (887 kN) was compared with the GFRP specimen GH-0.66-I (690 kN), as maintaining the reinforcement ratio in both specimens will not alter the fact that the axial rigidity of the former specimen is higher compared to the latter specimen. This consequently decreased the transverse strains in the compression strut and improved the overall capacity of the tested corbel.

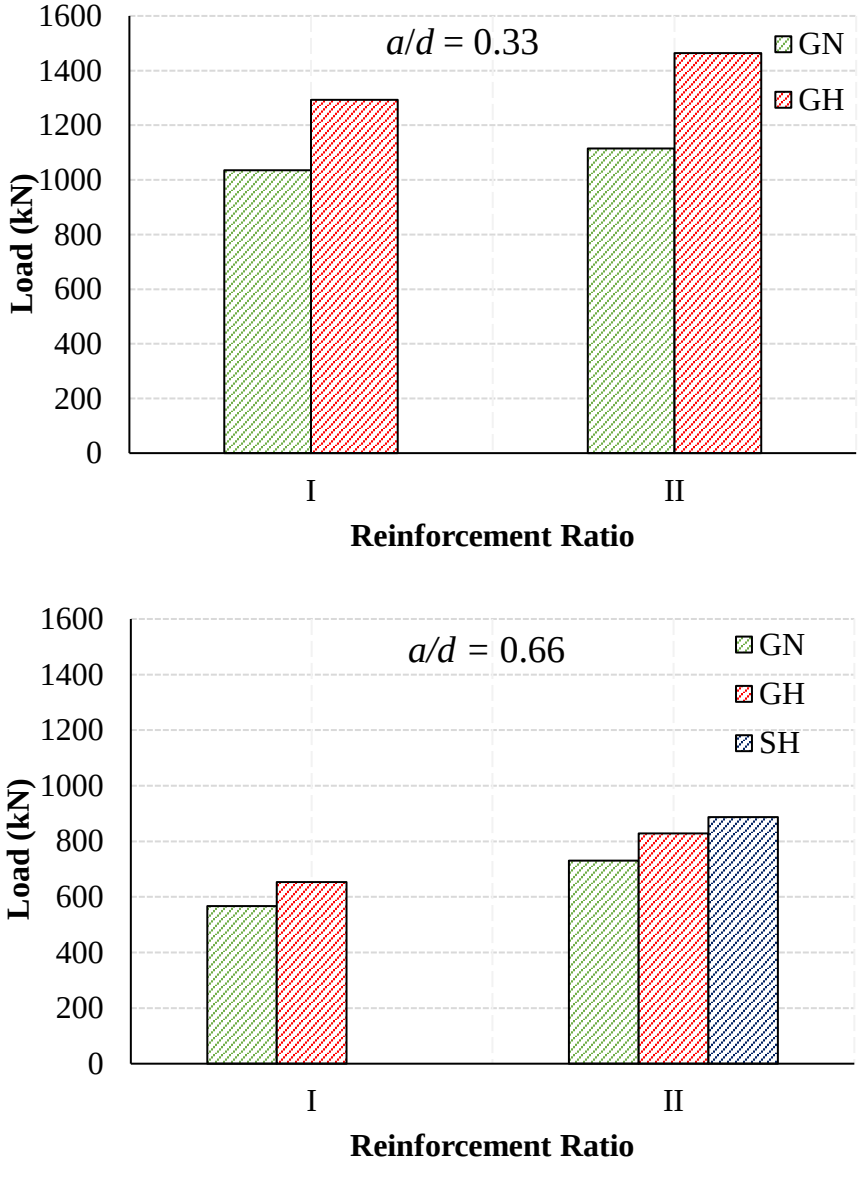


Figure 4.5. Effect of investigated parameters on the ultimate load capacity.

### *4.4.3 Load-Deflection Behaviour*

The load-deflection responses for specimens with an *a*/*d* of 0.33 and 0.66 are illustrated in Figure 4.6. Two LVDT's were installed at the column stub to measure the deflection of each corbel face. The side of the corbel that failed first was presented in the results. Before the formation of the flexural cracks, all specimens experienced small deflections; however, the stiffness of the HSC specimens was similar (equal slope of graphs) compared to the NSC counterparts, no matter what reinforcement ratio or *a*/*d* was considered. This response was more affected by the main tie reinforcement compared to the concrete strength of the struts in compression although the stiffness of the HSC is higher than the NSC (CSA 2019c). In addition, prior to reaching the peak load, all specimens showed a bi-linear load-deflection response, yet with different trajectories due to the different reinforcement ratios adopted in this study. After the early stage (dominated by the beam action), where the stiffness was decreased due to cracking, the enhanced stiffness that occurred in most specimens can be attributed to the activation of the arching action where the diagonal crack was initiated**.** Table 4.3 gives the maximum deflection of the corbel at failure and the deflection corresponding to the service load. It is worth mentioning that the service load of the corbel (SL) was considered as the load corresponding to a strain in the main tension reinforcement of 0.00135 (60% of the yield strain of 0.00225) of the steel-RC corbel. This load was experimentally determined to be 320 kN. For specimens with an *a*/*d* of 0.33, GH-0.33-II carried the highest load of 1,464 kN and experienced the highest corresponding deflection of 8.6 mm at failure, which is in good agreement with the mode of failure where the full capacity of the diagonal strut was utilized. In addition, the specimens with HSC (GH-0.33-I and GH-0.33-II) failed abruptly when reach the peak load and did not show any post-peak gradual drop in the load. While the counterpart NSC specimens (GN-0.33-I and GN-0.33-II) showed a relatively gradual load drop with a descending load-deflection behavior reaching deflections of 11.0 and 13.5 mm and 0.85 and 0.54 mm at the ultimate load and service load, respectively. This may be attributed to the fact that the descending post-peak stress-strain curve for the HSC is much steeper than that of NSC since cracks in NSC usually propagate through the paste rather than the aggregate that has less ductile tendency (Neville 1996;

Ayub *et al.* 2014). In addition, the higher the reinforcement ratio used, the lower deflection was observed at the same service load level except for the specimens with HSC and *a/d* ratio of 0.66 where the difference was insignificant. Although the predominant effect of other parameters (e.g., the concrete type or the *a/d* ratio) on the load-deflection response was more prominent, there was a significant difference in the observed deflection when the reinforcement ratio was increased. For example, the increase in the reinforcement ratio in the NSC and HSC groups from GN-0.33-I and GH-0.33-I to GN-0.33-II and GH-0.33-II respectively was accompanied by an significant reduction in the deflection of 36.5 and 12.5%, respectively, at the service load level of specimens with lower reinforcement ratio. On the contrary, the behavior for specimens with *a*/*d* ratio of 0.66 showed a similar trend with much less load-carrying capacity and higher corresponding deflection (Figure 4.6(b)). For example, increasing the *a/d* ratio from 0.33 to 0.66 for the NSC specimens with lower reinforcement ratio "I" led to an increase in the deflection from 0.85 to 2.10 mm, at the service load level. This is associated with the larger ties available in the STM model with larger shear-spans which can deform more. It is also noteworthy that the deflections at failure for the same specimens was 5.3 mm and 4.9 mm for an increase in *a/d* ratio from 0.33 to 0.66 respectively. This can be associated to the premature modes of failure that occurred within this group (GN-0.66-I, GH-0.66-I, GN-0.66-II, and GH-0.66-II), which stemmed from the larger *a*/*d* ratio. This larger ratio, in turn, made the strut angle much flatter leading to a reduction in the effect of the arch action mechanism, which resulted in a reduced strut capacity. This can be substantiated by the post-crack deflection behavior of specimen GH-0.66-II prior to the peak load (failed by diagonal splitting crack), where the stiffness (reflected by the slope of the load-deflection curve) was not retrieved; thus, the full arch capacity was not attained. Also, the type of the main reinforcement had a clear effect on suppressing the deflection rate of the tested corbel. For example, using steel as the main reinforcement in specimen SH-0.66-I instead of the GFRP in specimen GH-0.66-I resulted in a significant reduction in the deflection by 68%, at the service load level.

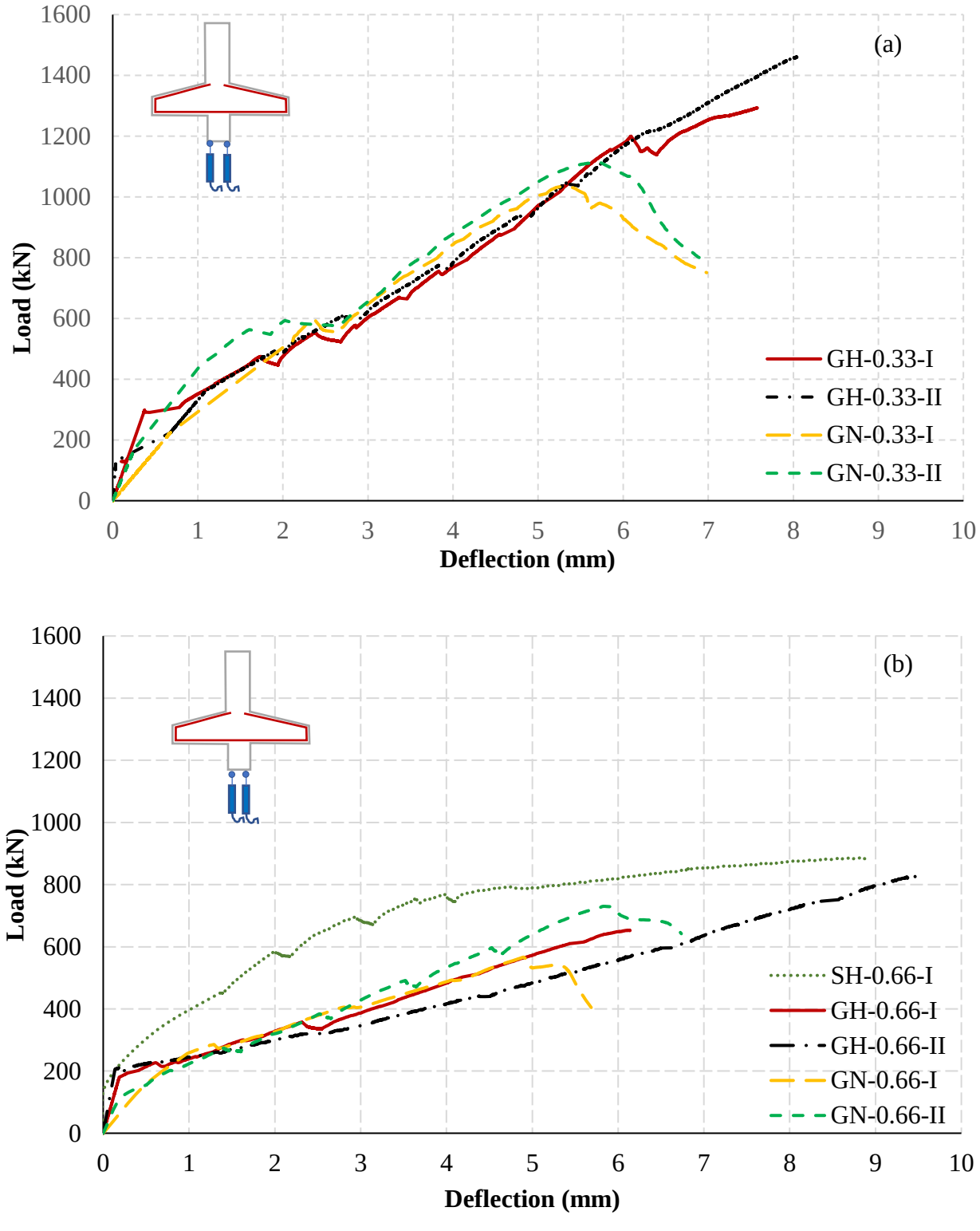


Figure 4.6. Load-deflection relationship for corbels with *a/d* ratio of (a) 0.33, and (b) 0.66

### *4.4.4 Crack Width*

Figure 4.7 illustrates the measured flexural crack width throughout the test. The PI gauges were placed to measure flexural crack widths at the level of reinforcement. It was noticed that the GFRP specimens with *a/d* of 0.66 showed larger flexural crack widths at SL with respect to the counterpart specimens with a*/d* of 0.33. This observation can be attributed to the fact that the angle of the strut in the truss model adopted in the STM was much flatter for an *a/d* = 0.66, which accordingly developed higher tensile forces in the horizontal ties. Increasing the concrete strength made the capacity of the inclined struts higher and, in turn, increased the tensile strains in the ties. Accordingly, it was also found that HSC specimens had larger crack widths at the SL. The highest crack width was 1.439 mm for the GH-0.66-I. Also, at the service load level, the crack width for the GN-0.33-II and GH-0.33-II was 0.17 and 0.2 mm, respectively.

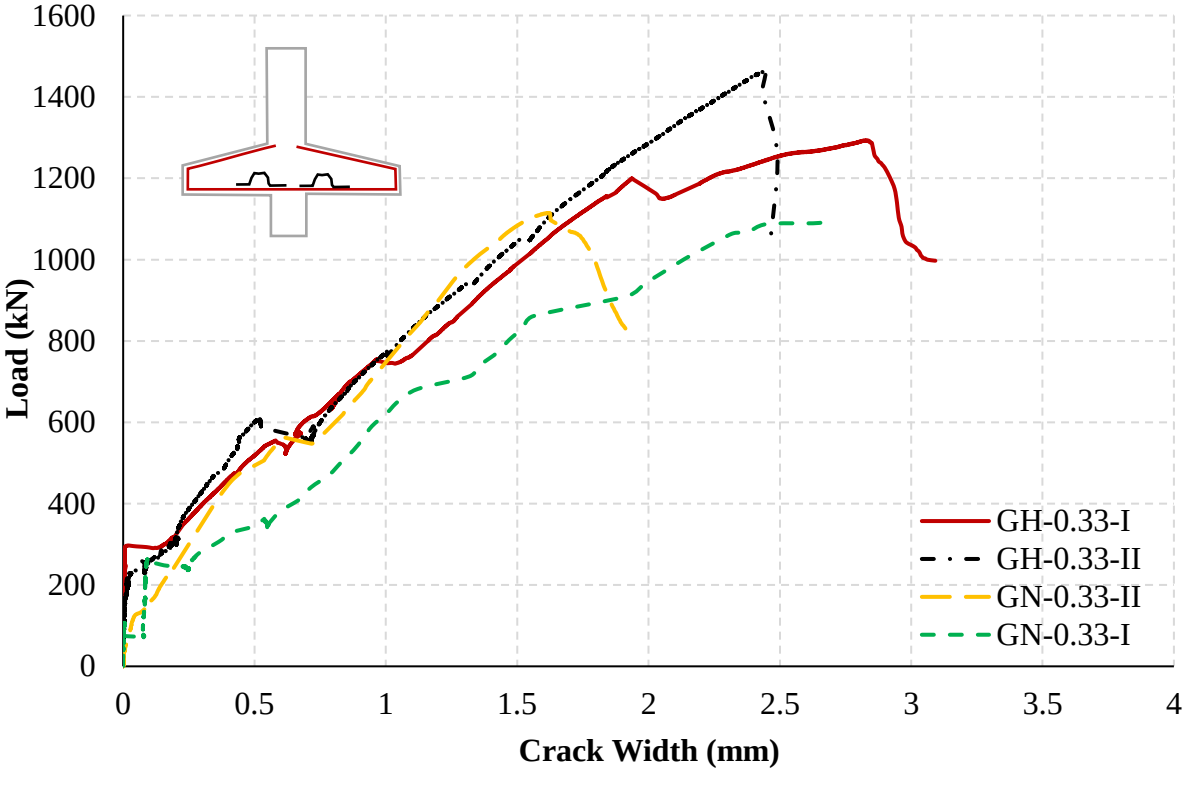

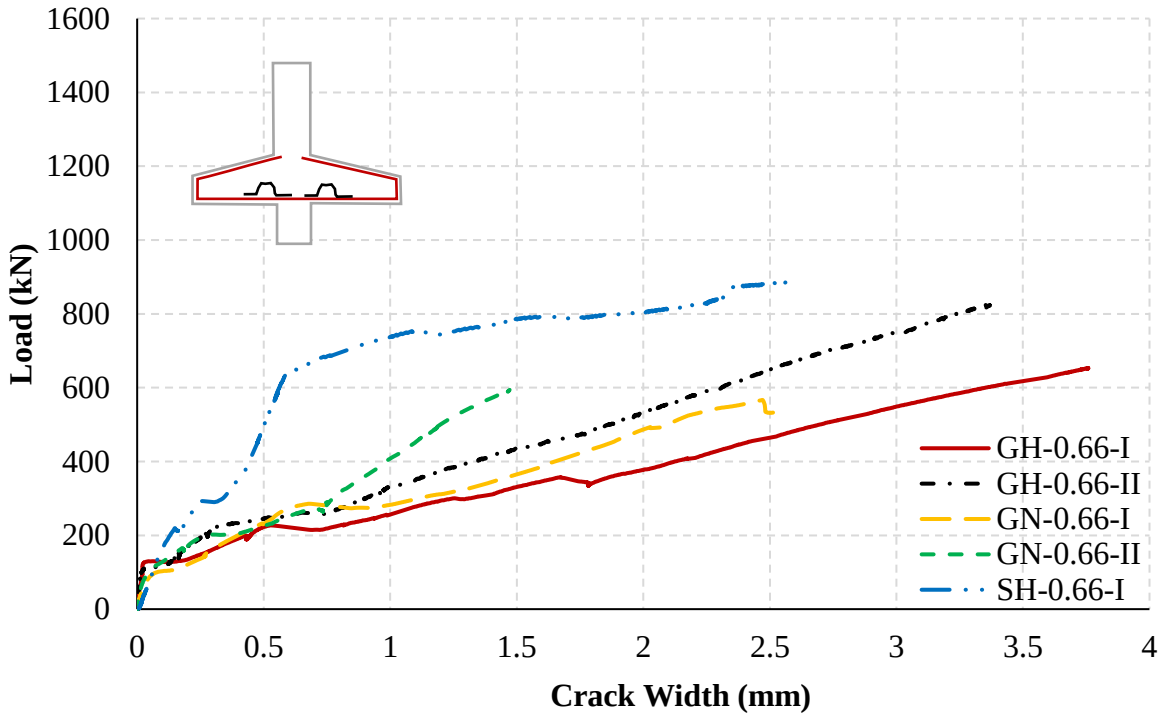


Figure 4.7. Load-flexural crack width relationship for corbels with *a/d* ratio of (a) 0.33, and (b) 0.66

As for Specimen SH-0.66-I with *a*/*d* ratio of 0.66, as expected, using the steel bars instead of the GFRP bars, preserving all other test parameters, showed a marked enhancement in reducing the flexural crack width. For example, at the service load level, the flexural crack width for specimens SH-0.66-I and GH-0.66-I were 0.66 and 1.43 mm, respectively. This can be attributed to the relatively lower modulus of elasticity of the bent GFRP bars, which is approximately one quarter of the steel bars.

In addition, the effect of the reinforcement ratio on the flexural crack width was more evident for the specimens with larger *a/d* = 0.66 for both the NSC and HSC specimens. The crack width for GN-0.66-I and GN-0.66-II at the service load level was 1.21 and 0.81 mm, respectively. While the shorter *a/d* = 0.33 showed an insignificant disparity between the specimens with HSC, indicating the dominance of the other parameters (e.g., the concrete type or the *a*/*d* ratio) over the reinforcement ratio. For instance, increasing the reinforcement ratio from 0.7% in specimen GH-0.33-I to 1.1% in GH-0.33-II led to a negligible change in the flexural crack width from 0.19 mm to 0.2 mm.

For NSC, while the crack propagates, the crack will tend to pass through the paste (the weak component in the normal-strength concrete matrix) rather than the aggregate, leaving the aggregate protruded, correspondingly, further enhancement in the aggregate interlock mechanism and leading to lower crack width. On the other hand, for HSC, when the concrete starts to fracture, the crack will pass through the aggregate (the weak component in the high-strength concrete matrix) in lieu of the paste resulting in a flattened fracture surface, consequently, higher crack widths (Tongaroonsri and Tangtermsirikul 2009).

### *4.4.5 Reinforcement Strain*

The strain profile at various stages of loading for all specimens is depicted in Figure 4.8. The strain profile was determined by measuring the strain along the longitudinal reinforcement at three points, which is used to verify whether and to what extent a full arch action developed in the specimens. There was a slight variation in the GFRP bars strains until the first flexural crack took place. Afterward, the rate of increase in the strains was higher closer to the column-corbel interface, usually in the maximum moment region. With further increase in the load, there were additional cracks formed in the shear span region between the column-corbel face and the support plate, which was reflected by a growth in the measured strains close to the support. In the locations without major cracks, no variation in the strain was observed. In addition, the increase in the measured strain in the GFRP bar past the edge of the support plate was minimal, which can be reflected by the measurement of the strain gauge located at 150 mm from the edge of the support plate. Localized strain leap was observed when the crack coincided with the strain gauge location (GH-0.66-II). To obtain a full arch action, where the reinforcement will perform as a tie, the measured strain along the longitudinal bar should be similar. In the specimens with an $a/d$ ratio of 0.33, the strain variation along the GFRP bar between the support and the column-corbel interface was uniform, confirming the formation of a full arch mechanism, with respect to the corresponding specimens with $a/d$ ratio of 0.66.

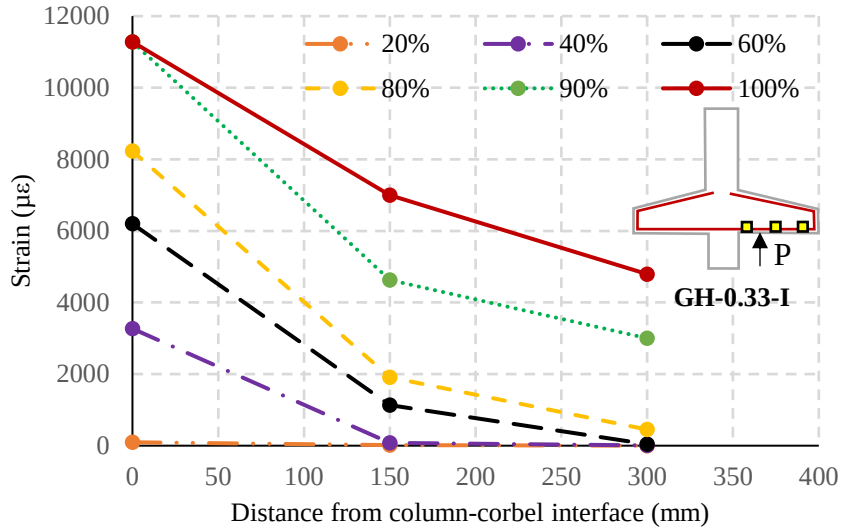
12000
10000
8000
6000
4000
2000
0
Strain (με)
0
50
100
150
200
250
300
350
400
Distance from column-corbel interface (mm)
20%
40%
60%
80%
90%
100%
P
GH-0.33-I

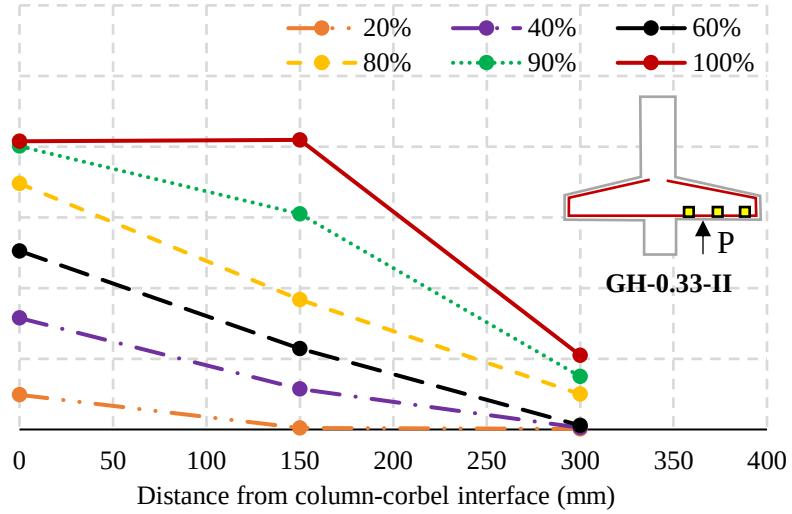
20%
40%
60%
80%
90%
100%
P
GH-0.33-II
0
50
100
150
200
250
300
350
400
Distance from column-corbel interface (mm)

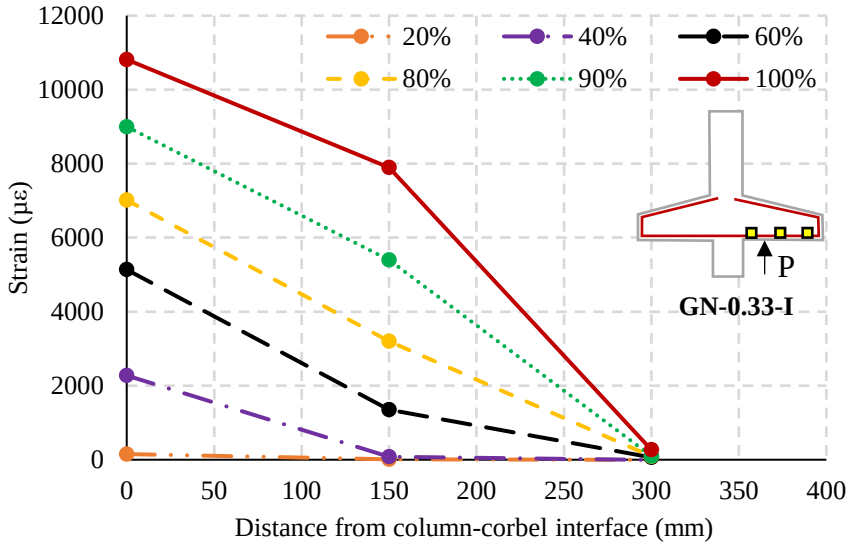
12000
10000
8000
6000
4000
2000
0
Strain (με)
0
50
100
150
200
250
300
350
400
Distance from column-corbel interface (mm)
20%
40%
60%
80%
90%
100%
P
GN-0.33-I

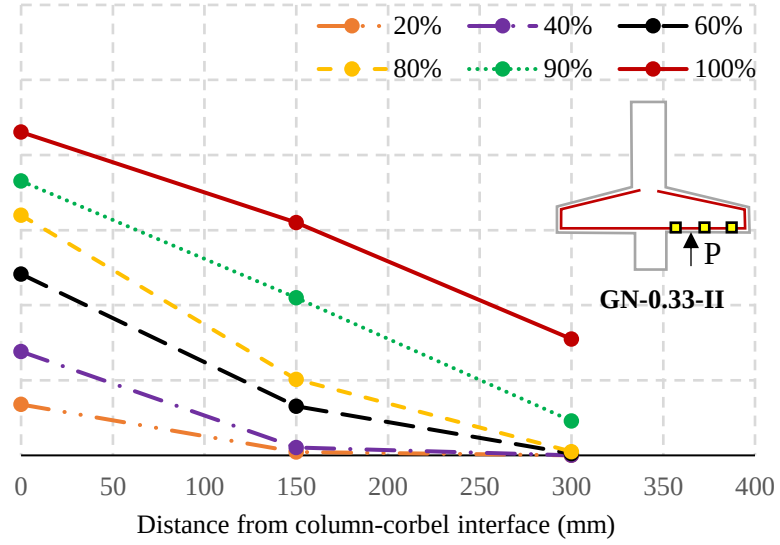
20%
40%
60%
80%
90%
100%
P
GN-0.33-II
0
50
100
150
200
250
300
350
400
Distance from column-corbel interface (mm)

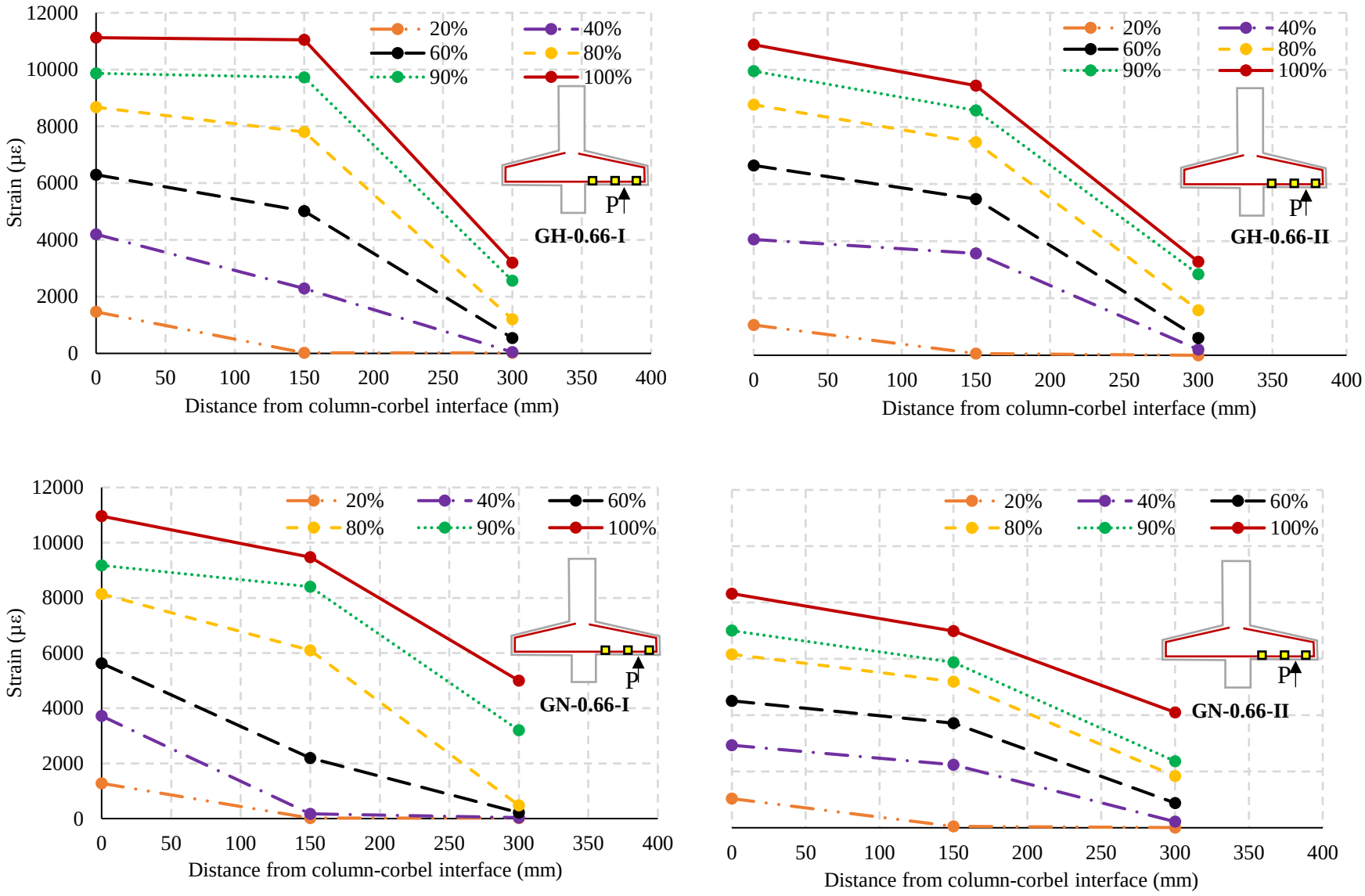


Figure 4.8. Strain profile in corbels

### *4.4.6 Code Provisions for Strut-and-Tie Model*

To investigate the reliability and adaptability of the STM stipulated in the Canadian standards CSA S806-12 (CSA 2021), American code ACI 318-19 (ACI Committee 318 2019), and the European code EC2 (BS EN 1992-1-1 2004) in calculating the capacity of the FRP-RC corbels, a comparison between the experimental and predicted capacity was made. A summary of the STM equations in the above listed standards and codes was provided in Table 4.4. It is worth noting that the material resistance and safety factors ($\alpha_{cc}$ and $\phi$) were set to unity for comparison purposes. As previously mentioned, the CSA S806-12 (CSA 2021) encompassed equations and special provisions for STM for FRP-RC corbels and brackets. On the other hand, although the new code that released by the ACI for FRP-RC structures (ACI Committee 440 2022) did not allow/permit the use of STM in predicting the capacity of FRP-RC corbels, the use of provisions mentioned in the steel-RC standard for FRP-RC structures would be feasible, since the failure occurred in the corbels was governed by the strut capacity in lieu of the capacity of the tie or the node, and the STM specified in the ACI code does not consider the transverse strain in the strut. In addition, the special requirements to apply the STM in corbels or brackets were satisfied, where the shear force shall not exceed the least of (i) $0.2f'_c\, b_w\, d$, (ii) $(480+.08\, f'_c\,)b_w\, d$, or (iii) $1600\ b_w\, d$, where the $f'_c$ is the concrete compressive strength, $b_w$ is the width of the corbel, and $d$ is the effective depth of the corbel. Similarly, the Eurocode (Committee CEN/TS 250)(BS EN 1992-1-1 2004) released the first-ever version for the design of structures reinforced with FRP bars; however, no provisions for the utilization of STM were included, but the application of the equations in the steel version on FRP-RC structures is still convenient/appropriate due to that the capacity of the tested specimens was dominated by the strut capacity. The STM in either the American or the European standards linked the capacity of the structural member solely to the compressive strength, while the Canadian standards adopted more reasonable provisions since the capacity of the structure relied on the concrete compressive strength along with the transverse strains generated in the strut that stemmed from the strains generated in the tie.

A single-panel direct STM mechanism, without vertical ties, was adopted to predict the capacity of the tested specimens, as depicted in Figure 4.9. The comparison between the load obtained from the tested specimens and the anticipated load based on the different design provisions was tabularized in Table 4.5. The Canadian standards CSA S806-12 (CSA 2021) showed conservative predictions of the ultimate capacity with an average value of $P_{pre}/P_{exp}$ of 0.59 and a coefficient of variation (CoV) of 6%. This was expected since CSA S806-12 (CSA 2021) considers the effect of concrete softening that would occur due to the high strains experienced by the main tie GFRP reinforcement and the fact that GFRP-RC corbels are designed to fail by crushing of the concrete strut. In contrast, the ACI and the Eurocode, which do not consider such concrete softening effect, overestimated the capacity of the tested corbels with a mean value of $P_{pre}/P_{exp}$ of 1.18 and 1.25 and CoV of 13% and 17%, respectively.

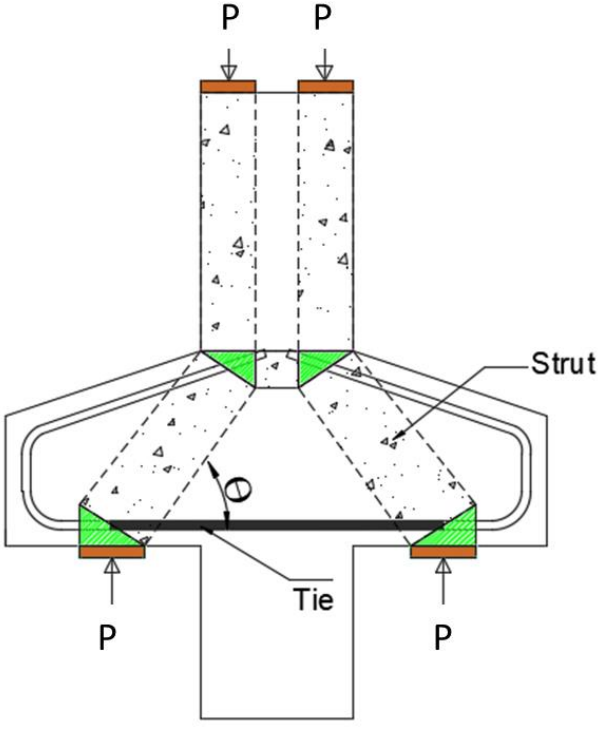


Figure 4.9. Strut-and-tie model (STM) for double-sided corbels

Table 4.4. Design standards and code provisions for STM

| STM Component | CSA S806-12 (CSA 2021) | Eurocode 2 (BS EN 1992-1-1 2004) | ACI 318-19 (ACI Committee 318 2019) |
|---|---|---|---|
| Strut | Compressive force in the strut = $\phi_c f_{cu} A_{cs}$<br>$f_{cu}$ is the limiting compressive stress<br>$f_{cu} = \frac{f_c'}{0.8 + 170\varepsilon_1}$ where,<br>$\varepsilon_1 = \varepsilon_f + (\varepsilon_f + 0.002)\cot^2\theta_s$<br>$f_c'$ = concrete strength<br>$\varepsilon_1$ = transverse tensile strain<br>$\varepsilon_f$ = tensile strain in the tie<br>$\theta_s$ = the smallest angle between the strut and the adjoining ties | The allowable compressive stress of struts $\sigma_{Rd,max} = f_{cd}$<br>$f_{cd}$ is design value of concrete compressive strength = $\alpha_{cc} f_{ck}/\gamma_c$<br>Where $f_{ck}$ is characteristic compressive cylinder strength of concrete at 28 days<br>$\alpha_{cc}$ is the coefficient taking account of long-term effects on the compressive strength (Recommended value is 1.0)<br>$\gamma_c$ is the partial safety factor for concrete | Strength of struts = $F_{ns} = f_{ce} A_{cs}$ and<br>$f_{ce} = 0.85\beta_s\beta_c f_c'$ where<br>• $\beta_s$ is strut coefficient = 1.0 for boundary struts, 0.75 for interior struts satisfying one of the following equations<br>$\frac{0.0025}{\sin^2\alpha_1}$ & $V_u \le \phi 5 \tan\phi\lambda\lambda_s\sqrt{f_c'} b_w d$ and 0.4 for other cases<br>• $\beta_c$ is strut confinement factor, which is the lesser of: $\sqrt{\frac{A_2}{A_1}}$ or 2.0, where $A_1$ is the loaded area and $A_2$ is the area of the lower base of the largest frustum of a pyramid, cone, or tapered wedge contained wholly within the support and having its upper base equal to the loaded area |
| Tie | Tensile force in the tie $\le 0.65\phi_F A_{FT} f_{FU}$<br>$\phi_F$ = resistance factor for FRP, $A_{FT}$ = area of reinforcement, $f_{FU}$ = ultimate strength of the bar | The nominal tensile strength of a tie, $F_{nt}$, shall be calculated by $F_{nt} = A_{st} f_y$, $A_{st}$ = area of steel reinforcement<br>$f_y$ = yield strength of steel reinforcement | |
| Node | Compressive stress in the node regions $\le 0.85\phi_c m f_c'$ in node regions bounded by struts and nearing areas, $0.75\phi_c m f_c'$ in node regions anchoring a tie in only one direction and $0.65\phi_c m f_c'$ in node regions anchoring ties in more than one direction | Compressive stress in the node regions $\le v f_{cd}$ in node regions bounded by struts and nearing areas, 0.85 $v f_{cd}$ in node regions anchoring a tie in only one direction and 0.75 $v f_{cd}$ in node regions anchoring ties in more than one direction | The nominal compressive strength of a nodal zone, $F_{nn}$, is calculated by $F_{nn} = f_{ce} A_{nz}$<br>where $f_{ce} = 0.85\beta_n f_c'$, $\beta_n$ is nodal zone coefficient.<br>• $\beta_n$ =1.0, nodal zones bounded by struts and bearing areas or both, $\beta_n$ = 0.8, nodal zones anchoring one tie, and $\beta_n$ = 0.6, nodal zones anchoring two or more ties. |
| Special Provisions for Corbels | • Closed stirrups or ties parallel to the primary tensile tie reinforcement, and having a total area of not less than 0.65 $A_{FT}$, shall be distributed within two-thirds of the effective depth adjacent to $A_{FT}$<br>• The ratio $A_{FT}/bd$ calculated at the face of the support shall be not less than 0.04 ($f_c'$ /0.01$E_f$), where $E_f$ is the design modulus for FRP reinforcement. | • If $a_c < 0.5\ h_c$, closed horizontal stirrups should be provided with $A_{shorizontal}$ more than $k_1\ A_{s,main}$, and If $a_c > 0.5\ h_c$, closed vertical stirrups should be used<br>• $a_c$ is shear span, and $h_c$ is the height of the corbel<br>• The main tension reinforcement should be anchored at both ends | • Primary tension reinforcement shall be developed at the face of the support<br>• Closed stirrups or ties shall be spaced such that $A_h$ is uniformly distributed within (2/3) $d$ measured from the main tension reinforcement |

Table 4.5. Comparison between experimental and predicted failure loads.

| Corbel ID | $P_{exp}$ (kN) | Strut-and-tie-model (STM) | | | | | |
|---|---|---|---|---|---|---|---|
| | | CSA S806-12 (CSA 2021) | | ACI 318-19 (ACI Committee 318 2019) | | Eurocode 2 (BS EN 1992-1-1 2004) | |
| | | $P_{CSA}$ (kN) | $P_{CSA}/P_{exp}$ | $P_{ACI}$ (kN) | $P_{ACI}/P_{exp}$ | $P_{EC2}$ (kN) | $P_{EC2}/P_{exp}$ |
| GN-0.33-I | 1,035 | 568 | 0.55 | 1,161 | 1.12 | 1,223 | 1.18 |
| GH-0.33-I | 1,293 | 712 | 0.55 | 1,223 | 0.95 | 1,223 | 0.95 |
| GN-0.33-II | 1,115 | 700 | 0.63 | 1,292 | 1.16 | 1,745 | 1.56 |
| GH-0.33-II | 1,464 | 841 | 0.57 | 1,745 | 1.19 | 1,745 | 1.19 |
| GN-0.66-I | 627 | 349 | 0.55 | 746 | 1.19 | 746 | 1.19 |
| GH-0.66-I | 690 | 444 | 0.64 | 746 | 1.08 | 746 | 1.08 |
| GN-0.66-II | 680 | 410 | 0.60 | 999 | 1.47 | 1,065 | 1.57 |
| GH-0.66-II | 828 | 506 | 0.61 | 1,065 | 1.29 | 1,065 | 1.29 |
| SH-0.66-I | 887 | *284 | 0.32 | 284 | 0.32 | 284 | 0.32 |
| **Mean | | | 0.59 | | 1.18 | | 1.25 |
| ***CoV | | | 0.06 | | 0.13 | | 0.17 |

* The steel specimen (SH-0.66-I) was computed using CSA A23.3 [1]

** The mean value was calculated based on the GFRP specimens only

*** CoV = Coefficient of variation

## 4.5 Conclusions

The main objective of the current study is to investigate the behavior of GFRP-RC corbels, emphasizing the effect of using high-strength concrete. Nine large-scale GFRP-RC corbels with *a*/*d* ratios equal to 0.33 and 0.66 and with different reinforcement ratios were tested to failure. Based on the test results, the main findings of this study can be summarized as follow:

1. Different modes of failure were noted in this study for the GFRP-RC corbels: compression strut failure (C-ST), shear-compression failure (S-CO), and diagonal-splitting failure (D-SP). In general, the specimens with the lower *a*/*d* ratio of 0.33 failed in a more brittle manner, where wide excessive

cracks accompanied by concrete spalling and loud noise "bang" were observed, compared to that of the counterpart specimens with *a*/*d* ratio of 0.66.

2. Both concrete strength and a/*d* ratio had a significant impact on the capacity of the tested specimens at failure. Increasing the concrete strength increased the capacity of GFRP-RC specimens while increasing the *a/d* ratio changed the mode of failure from the desired strut-crushing to the brittle diagonal-splitting. A similar trend was observed when the reinforcement ratio was increased.
3. The concrete strength had minimal effect on load-deflection relationship for both *a/d* ratios (0.33 and 0.66). However, increasing the main reinforcement ratio caused a reduction in the deflection at the service load level.
4. The Canadian standards, CSA S806-12 (CSA 2021), produced reasonable safe predictions of the corbel capacity, while the ACI 318-19 (ACI Committee 318 2019) and the Eurocode (BS EN 1992-1-1 2004) overestimated the capacity of the tested corbels.

# Chapter 5. Analytical Modelling

## 5.1 Load-Carrying Mechanisms in RC Corbels.

The analytical model in terms of Modified Compression Field Theory (MCFT) for Discontinuity regions can only be a pure shear model due to the nature of the formation of stresses around discontinuity regions. Therefore, a prediction of the strains using plane sections is not possible. The primary mechanism (I) shown in Figure 5.1 is calculated following the provisions of the CSA S806 (CSA 2021) codes. The secondary mechanism (II), as shown in Figure 5.2, stems from the fact that the primary mechanism induces strains on the horizontal stirrups and these stirrups, in turn, orient them to a new mechanism which can carry the load. A stronger corbel resistance is generated with both mechanisms I and II, as shown in Figure 5.3.

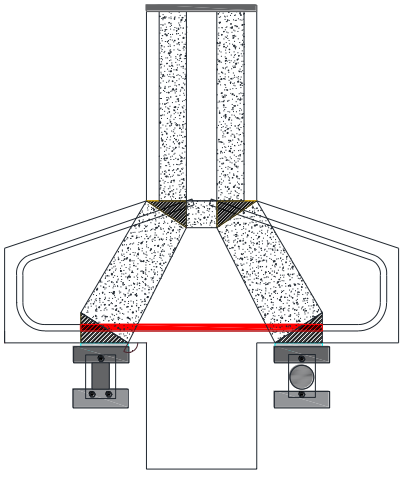

Figure 5.1. Primary Load carrying Mechanism.

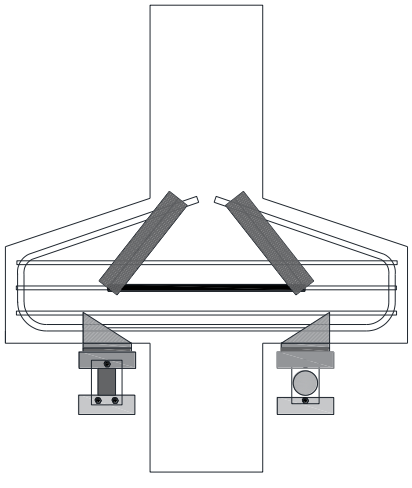

Figure 5.2. Secondary Mechanism to calculate additional stirrup capacity.

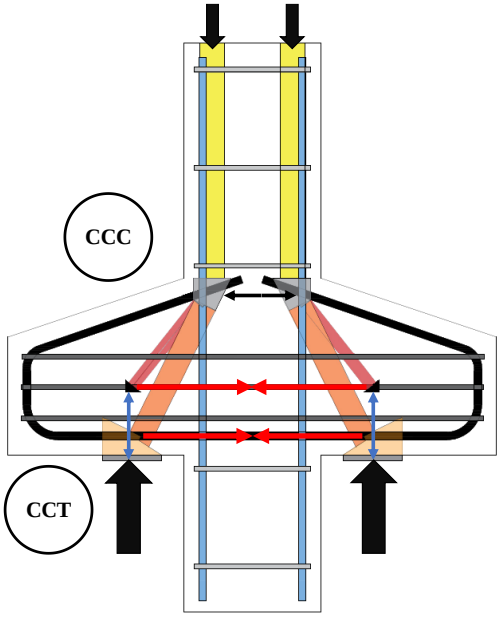


Figure 5.3.Combined Mechanism I and II.

The capacity of corbels predicted with the Canadian codes is often underpredicted as the Modified compression field theory equations cannot be fully utilized in the discontinuity regions. A slightly modified approach in MCFT is used in D-Regions where the angle of inclination of the compressive strains is dependent geometrically on the location of the supports and the load points. The constitutive relationship used for the concrete in compression is given by

$$f_{c2} = f_{c2max}\left[2\left(\frac{\varepsilon_2}{\varepsilon_c'}\right) - \left(\frac{\varepsilon_2}{\varepsilon_c'}\right)^2\right]$$

Equation 5-1

Where $\frac{f_{c2max}}{f_c'} = \frac{1}{0.8+170\varepsilon_1} \leq 1$

Equation 5-2

In the STM method used by the CSA, the strut is considered to have a maximum strength of $f_{c2max}$ and the geometrical relationship of the Mohr circle of strain is used to compute the average principal tensile strains using the formula as shown below:

$$\tan^2\theta = \frac{(\epsilon_x + \epsilon_2)}{(\epsilon_z + \epsilon_2)}$$

Equation 5-3

The cracked concrete is considered a new material which transmits tension. In a location where a crack has occurred, the reinforcement shows higher tensile local stresses than the average stresses, and the concrete regions without any cracks or in between two cracks transmit tensile stresses. The average concrete principal tension stress of uncracked concrete between two cracks for smaller elements is given by the empirical expression as follows:

$$f_{c1} = \frac{f_{cr}}{1 + \sqrt{200\varepsilon_1}}$$

Equation 5-4

This expression is chosen as the secondary truss formed by the stirrups is considerably smaller than the main truss formed by the direct strut mechanism (I).

## 5.2 Equilibrium Equations

The force in horizontal stirrups is calculated by using the same concept for calculating forces carried by vertical stirrups.

Taking equilibrium on a slice of corbel along the crack results in the following equations, as shown in Figure 5.4. This equilibrium was established on a single layer of horizontal crack-control reinforcement, and therefore, the effective area of the compressive stress on the concrete was $b_w \times s_x$ where $s_x$is the spacing of the crack-control reinforcement laid in the x-direction.

$$-A_x f_x = f_1(s_x \sin\theta \times b_w)\sin\theta - f_2(s_x \cos\theta \times b_w)\cos\theta$$

$$\Rightarrow \frac{-A_x f_x}{s_x b_w} = f_1(\sin\theta)\sin\theta - f_2(\cos\theta)\cos\theta$$

$$\Rightarrow (-\rho_x f_x) = f_1(\sin^2\theta) - f_2(\cos^2\theta)$$

Equation 5-5

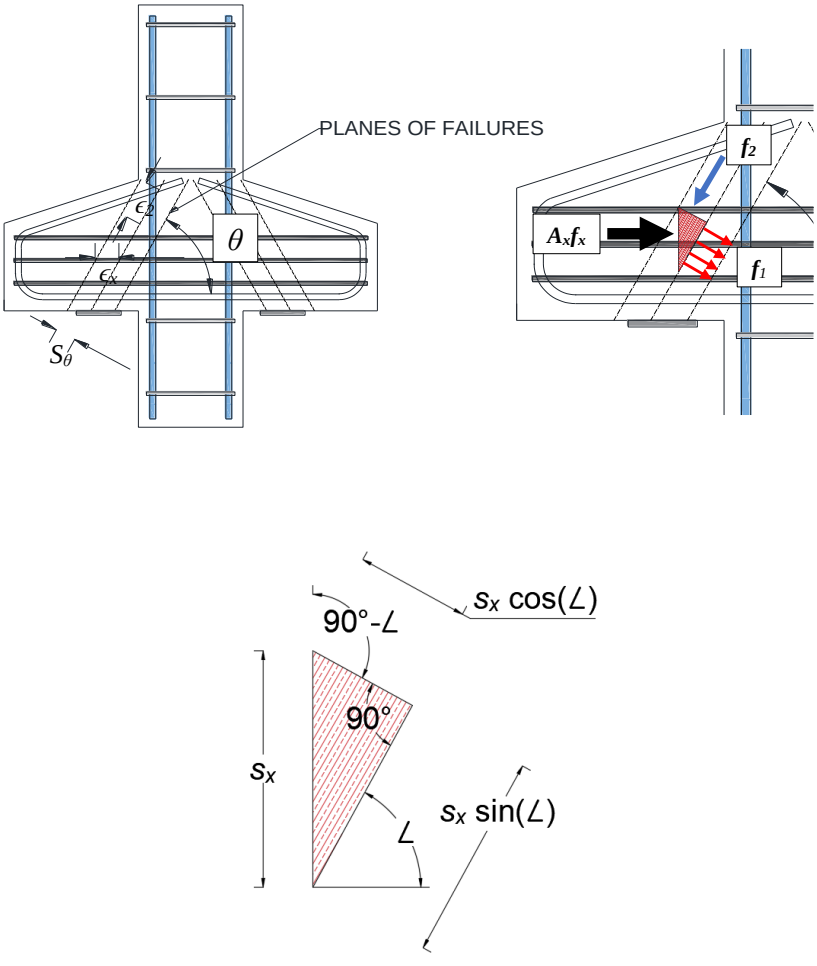


Figure 5.4.MCFT variables used in the development of analytical model.

When near ultimate strength, in an uncracked portion of the corbel the strut strength is given by:

$$f_2 = f_{c2max} = \frac{f_c'}{0.8 + 170\varepsilon_1}$$

Equation 5-6

$$f_1 = f_{c1} = \frac{f_{cr}}{1 + \sqrt{200\varepsilon_1}}$$

Equation 5-7

$$f_x = E_x \varepsilon_x$$

Equation 5-8

$$\varepsilon_1 = \varepsilon_x + (\varepsilon_x - \varepsilon_2) \cot^2 \theta$$

Equation 5-9

Replacing Equation 5-6, Equation 5-7, Equation 5-8 and Equation 5-9 in Equation 5-5, an equation in $\varepsilon_x$ is developed which can be solved.

The strains in the axial direction of reinforcement $\varepsilon_x$ which are computed by the equilibrium Equation 5-5 stated above, can be used to calculate the stress in the stirrups. This tensile strain in the ties (stirrups) is considered a part of a newer STM which is connected to a much flatter strut which increases the stiffness of the primary mechanism (I), as shown in Figure 5.3.

The capacity of the stirrups in the longitudinal directions can be broken into vertical components $V_{stirrups} = T \tan\theta = A_{Total} \times E_x \varepsilon_x \tan\theta$. This is the extra capacity of the corbels provided by the stirrups. The angle $\theta$ is the angle between the centroid of the confinement caging around the corbel to the newer strut formed as a result of the secondary mechanism of the horizontal crack-control reinforcement. This newer strut begins above the bearing surface at the centroid of the crack-control reinforcement distribution and extends to the location of the CCC node of the STM in the column. The strut for the primary mechanism is much steeper than the newer strut due to the secondary mechanism.

The assumption that the horizontal crack-control reinforcement is provided uniformly along the length of the main reinforcement holds true here.

## 5.3 Type of Failure in Mechanism II

The horizontal crack-control reinforcement capacity is a secondary mechanism by which the corbel gains additional capacity near the ultimate strength as the equilibrium condition used only occurs after the cracks

are well developed and the reinforcement arresting the cracks are activated. These strains are average values and may differ from the actual strains in the reinforcement, as this may be due to the presence of cracks.

The primary strut mechanism (mechanism I) is the direct strut which has the maximum contribution to the strength of the corbels. The maximum strain that can occur in the stirrups is the sum of the strains in both mechanisms. The stirrups nearest to the tie reinforcement can rupture if the strain limit is lower than the maximum strain value given by the summation of mechanism (1) (direct strut) and mechanism (II) (horizontal stirrups).

Another mechanism by which failure can occur is the shearing along the plane of the strut, as shown in Figure 5.5. This is given by the aggregate interlock relationship which occurs between the concrete cracks given by the equation given by Vecchio and Collins (Vecchio and Collins 1986).

$$v_{ci} \leq \frac{0.18 \times \sqrt{f_c'}}{0.3 + \frac{24w}{a + 16}}$$

Equation 5-10

The crack spacing used in Equation 5-10 is given by the equations shown below:

$$w = \varepsilon_1 \times s_\theta$$

Equation 5-11

Where $s_\theta = \frac{s_x}{\sin\theta}$ and $s_x$ is the maximum spacing between horizontal stirrups (In the experiments, it was measured from 65~ 75 mm in the crack-control reinforcement caging). Also, this can be further modified to suit corbels without any crack-control reinforcement by equating the effective shear depth $d_v$ to $s_x$.

At higher shear forces, the cracked concrete transfers shear by the above mechanism, and at the uncracked stage, the principal tensile stresses are responsible for the shear capacity of the strut. Establishing equilibrium between an uncracked plane and a cracked plane leads us to the following two equations:

For uncracked face:

$$V = f_1 \frac{\cos\theta \, b_w jd}{\sin\theta}$$

Equation 5-12

For cracked face:

$$V = v_{ci} b_w jd$$

Equation 5-13

Until the structure still supports the load, both the planes should have equal shear resistance and Equation 5-12 and Equation 5-13 can be equated with each other.

$$f_1 = v_{ci} \tan\theta$$

Equation 5-14

The cracked concrete can resist shear by this mechanism using Equation 5-14, and the shear resistance of concrete given by this formula is $v_{ci} b_w d$ in the vertical direction. The least strength of the two mechanisms: the stirrup mechanism and the cracked concrete mechanism, gives additional strength due to the presence of the stirrups. The $w$ is the width of crack in the face of cracked concrete and is calculated using the formula $w = \epsilon_1 \times s_\theta$ where $\epsilon_1$ is the principal tensile strain calculated using the equilibrium equation shown below:

$$s_\theta = \frac{s_x}{\sin\theta}$$

Equation 5-15

The Bernoulli regions in the shear design depend on two parameters, the $\beta$ and $\theta$ where the former is a parameter of concrete strength, and the latter is a parameter of crack direction or the direction of the principal compressive stresses.

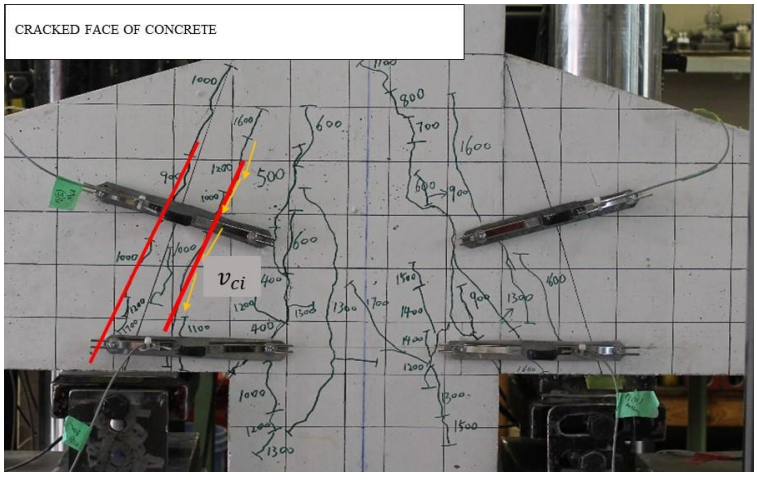


(a) Failure mechanism along shearing plane

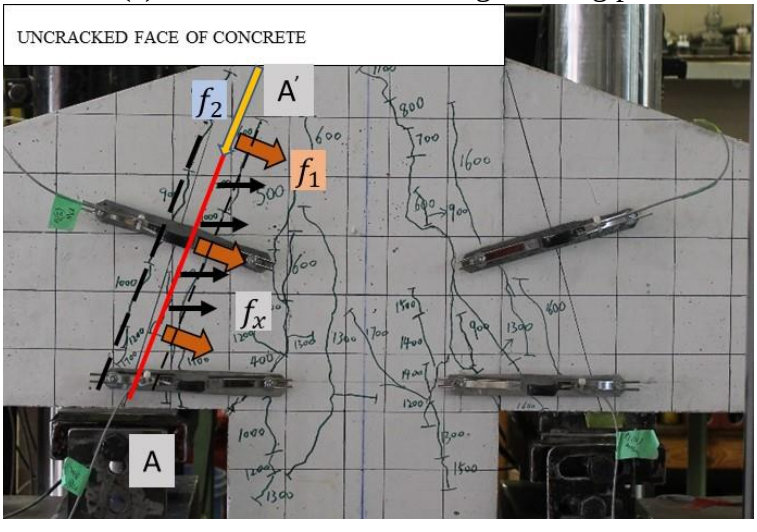


(b) Failure Mechanism in Strut crushing

Figure 5.5. Mechanism of Failure (a) Shearing Plane (Tensile splitting) (b) Strut crushing.

## 5.4 Ultimate Strains in Horizontal Stirrups at a Diagonal Crack

Strains on a reinforcement at a crack are always larger than the strains of reinforcement at an uncracked location. The above analysis will help in evaluating average strains on the crack-control reinforcement (horizontal stirrups). But it is also important to know about the state of stress in the cracks; else, the cracks might lead to the rupture of the bars.

The two cracked and uncracked faces should satisfy equilibrium, applied in the horizontal direction, as shown below.

$$f_1 jd \times b_w + \frac{jd}{s} A_{sx} f_{hx} = v_{ci} b_w jd \cot\theta + \frac{jd}{s} A_x f_{hfinal}$$

Equation 5-16

Shuffling Equation 5-14, we get and using it in Equation 5-16,

$$v_{ci} = {f_1}/{\tan\theta}$$

$$\Rightarrow \frac{A_x}{b_w s}\left(f_{hfinal} - f_{hx}\right) = \left(f_1 - f_1 \cot^2\theta\right)$$

$$\Rightarrow \rho_{secondary}\left(f_{hfinal} - f_{hx}\right) = \left(f_1 - f_1 \cot^2\theta\right)$$

Equation 5-17

Equation 5-17 above can be used to calculate the stresses that can occur at the location of the cracks when the secondary mechanism is followed. If the second mechanism fails to take place and the aggregate interlock takes precedence, Equation 5-5 does not hold true. The excess strength is calculated using the aggregate interlock formulation, as shown in Equation 5-13.

Also, both STM mechanisms affect each other. Therefore, the strains at the bottommost horizontal stirrups (crack-control reinforcement) are the summations of the stresses $\varepsilon_{final\ x,STM\ 2} + \varepsilon_{x,STM\ 1}$.

The effect of strains of the ties due to the presence of the primary STM (1) gradually decreases towards the top of the horizontal stirrups.

The steps required to analyze corbel strength are shown in Table 5.1.

Table 5.1. Flow chart for using the analytical model to calculate strength from various mechanisms.

| | |
|---|---|
| Step 1: | Calculate the capacity of STM Mechanism (1) using the CSA S806 STM model and keep the strut strength and ultimate tie strain to check in STEP 4. |
| Step 2: | Estimate a value for $\varepsilon_x$ in the web reinforcement. Use Equation 5-9 to calculate $\varepsilon_1$. |
| Step 3: | Calculate the $f_1, f_2, \varepsilon_x$ using Equation 5-7, Equation 5-8 and Equation 5-9. |
| Step 4: | Evaluate the $\varepsilon_1$ using Equation 5-5. |
| Step 5: | If the $f_2$ from Equation 5-5 is more than $f_2$ from STM (1) then go to STEP 6. |

| | |
|---|---|
| | Else<br>Consider the new $f_2 = f_{c2max}$ from STM (1) mechanism and repeat from STEP 3. |
| Step 6: | Calculate $v_{ci}$ using Equation 5-10 and Equation 5-11 |
| Step 7: | Using Equation 5-14 calculate $f_1$ and check if it has a value higher than $f_1$ from Equation 5-5 mentioned in STEP 5.<br>If True – the stirrup mechanism works.<br>If False – the aggregate interlock mechanism works. |
| Step 8: | If True<br>$V_{(2)} = T \tan\theta = A_{Total} \times E_x \varepsilon_x \tan\theta$<br>If False<br>$V_{(2)} = v_{ci} b_w jd$ |
| Step 9: | If True<br>$f_{hfinal}$ can be computed from Equation 5-17. |

## 5.5 Validation of Analytical Model against Experimental Results

All input parameters to the analytical model are shown in Table 5.2. The analytical model was validated against all test specimens in Article 2 from Chapter 4. The two columns (H) and (I) of Table 5.3 show the additional strength of the corbels due to two methods of failure:

1. Failure along the Shearing plane due to diagonal splitting
2. Failure due to Strut crushing.

Column (A) was the input strain which was iterated until convergence was found where columns (B) and (D) were equal. This strain was then used to calculate the aggregate interlock resistance $v_{ci}$. The next step was to check whether the diagonal tensile split was occurring by comparing column (E) with column (C). All specimens with an *a/d* of 0.66 had very close values in both Columns (C) and (E). This was an indication of failure due to diagonal splitting over strut crushing. All the specimens with *a/d*=0.33 had almost thrice the required amount of $f_1$ to undergo strut crushing. In the former case, Column (H) was the additional capacity for diagonal tensile splitting due to the aggregate interlock mechanism, while for the specimens with *a/d*=0.33, Column (I) was the additional strength due to the ability of the specimens to undergo strut

crushing. Column (J) shows the predicted total capacity using Mechanism I and Mechanism II, while Column (K) shows the experimental strengths.

Table 5.2. Input parameters of analytical model

| | **Equilibrium at Stirrup Location Geometry of (1)** | | | | | | **LHS of Eqn. 6-5** | **Un-cracked Face** | $f_2$ | **RHS of Eqn. 6-5** | | | **Cracked Face** | **Aggregate interlock** |
|---|---|---|---|---|---|---|---|---|---|---|---|---|---|---|
| | $\varepsilon_x$[i] **(A)** | $\varepsilon_1$ | $\theta$[ii] | $E_s$ | $\rho_{sw}$[iii] | $f'_c$ | $f_1 \sin^2\theta$ **(B)** | $f_1$[iv] **(C)** | $f_{cu}$ | $f_2 \cos^2\theta$ | $-\rho_{sw} f_x$ | $-\rho_{sw} f_x + f_2 \cos^2\theta$ **(D)** | $v_{ci} \tan\theta$ **(E)** | $v_{ci}$[v] |
| **GN-0.33-0.5-10** | 0.007 | 0.010 | 1.044 | 54336 | 0.007 | 39.9 | 0.486 | 0.651 | 12.48 | 3.156 | -2.670 | 0.486 | 2.268 | 1.32 |
| **GN-0.33-0.7-13** | 0.0043 | 0.007 | 1.041 | 54706 | 0.0130 | 440 | 0.5473 | 0.7349 | 14.2035 | 3.6259 | -3.078 | 0.5473 | 2.838 | 1.66 |
| **GH-0.33-0.5-10** | 0.0081 | 0.012 | 1.044 | 54336 | 0.0073 | 58.5 | 0.754 | 1.01 | 15.69147582 | 3.9678 | -3.213 | 0.754 | 2.462 | 1.432 |
| **GH-0.33-0.7-13** | 0.0054 | 0.008 | 1.041 | 54706 | 0.013 | 59.8 | 0.841 | 1.129 | 18.27 | 4.664 | -3.823 | 0.841 | 3.134 | 1.835 |
| **GN-0.66-0.5-10** | 0.0103 | 0.022 | 0.81 | 54336 | 0.01 | 40.8 | 0.36 | 0.68 | 9.18 | 4.41 | -4.06 | 0.36 | 0.66 | 0.64 |
| **GH-0.66-0.7-13** | 0.0084 | 0.018 | 0.802 | 54706 | 0.013 | 59.8 | 0.454 | 0.88 | 13.29 | 6.43 | -5.971 | 0.454 | 0.923 | 0.893 |
| **GH-0.66-0.5-10** | 0.0131 | 0.0272 | 0.805 | 54336 | 0.0073 | 62.3 | 0.41 | 0.782 | 11.66 | 5.606 | -5.200 | 0.406 | 0.68 | 0.65 |
| **GN-0.66-0.7-13** | 0.0067 | 0.0149 | 0.8019 | 54706.0000 | 0.0130 | 41.5 | 0.403 | 0.78 | 10.76 | 5.201 | -4.799 | 0.403 | 0.896 | 0.867 |

[i] Strain on horizontal crack-control reinforcement
[ii] Strut angle from primary mechanism
[iii] Horizontal crack-control ratio
[iv] Principal Tensile strains
[v] Aggregate interlock strength

Table 5.3. Validation of analytical model

| Specimen ID | Crack widths between Two cracks | Spacing between two Diagonal cracks. | Ties Stress | ∠ for (2) | Secondary Mechanism (2) | | | Capacity of Mechanism II | | Capacity of Mechanism I | Total Capacity | Experimental Capacity | $[V_{(1)} + V_{(2)}]/P_{(exp)}$[vi] |
|---|---|---|---|---|---|---|---|---|---|---|---|---|---|
| | | | | | | | | $jd$ | 404 | | | | |
| | $w$ (mm) | $s_\theta$ | $E_s\varepsilon_x$ | $\theta_2$[vii] (F) | $A_{bar}$ | $A_{sw}$[viii] | Stirrup Tie Force (G) | $V_{(2)}$[ix] (H) | $V_{(2)}$[x] (I) | $V_{(1)}$ | $V_{(1)} + V_{(2)}$ (J) | $V_{(exp)}$ (K) | |
| **GN-0.33-0.5-10** | 0.842 | 86.8 | 366.6 | 0.91 | 71 | 426 | 156 | 200.0 | 160 | 568 | 780 | 1,035 | 0.75 |
| **GN-0.33-0.7-13** | 0.564 | 86.9 | 236 | 0.91 | 127 | 762 | 180 | 231 | 200 | 700 | 931 | 1,115 | 0.83 |
| **GH-0.33-0.5-10** | 1.002 | 86.8 | 441.4 | 0.91 | 71 | 426 | 188 | 240.7 | 173 | 712 | 953 | 1,293 | 0.74 |
| **GH-0.33-0.7-13** | 0.686 | 86.9 | 293.5 | 0.91 | 127 | 762 | 224 | 286.3 | 221 | 841 | 1127 | 1,464 | 0.77 |
| **GN-0.66-0.5-10** | 2.25 | 104.1 | 557.1 | 0.68 | 71 | 426 | 237 | 192.1 | 77 | 349 | 426 | 627 | 0.68 |
| **GH-0.66-0.7-13** | 1.889 | 104.4 | 458.4 | 0.68 | 127 | 762 | 349 | 282.7 | 108 | 506 | 614 | 828 | 0.74 |
| **GH-0.66-0.5-10** | 2.83 | 104.1 | 714.1 | 0.68 | 71 | 426 | 304 | 246.2 | 79 | 444 | 523 | 690 | 0.76 |
| **GN-0.66-0.7-13** | 1.556 | 104.4 | 368.4 | 0.68 | 127 | 762 | 280 | 227.2 | 105 | 410 | 637 | 680 | 0.94 |
| Average | | | | | | | | | | | | | 0.78 |

[vi] Ratio of predicted capacity due to both mechanisms I and II to experimental load at failure
[vii] Angle of secondary strut mechanism
[viii] Total area of secondary horizontal reinforcement
[ix] Strength due to secondary reinforcement mechanism
[x] Strength due to secondary aggregate interlock mechanism

# Chapter 6. Conclusions

## 6.1 Summary

This study investigated the behaviour of fourteen large-scale NSC and HSC corbels reinforced with GFRP and steel longitudinal and crack-control reinforcement. The specimens were tested under a monotonic displacement-controlled load. The parameters studied were the shear-span-to-depth ratio (*a/d*), reinforcement type (steel or GFRP), amount of main reinforcement ratio ($\rho_{main}$) and crack-control reinforcement ($\rho_{sw}$) and concrete strength ($f'_c$). Predictions of the capacity of the corbels were calculated using strut-and-tie models in accordance with the relevant American and Canadian Standards and European codes. Experimental results were then compared against the code predictions. Finally, an analytical model was presented that successfully predicted strengths much closer to the actual strengths and could also be used to predict the type of failure: Strut crushing or strut splitting.

## 6.2 Conclusions

1. Different modes of failure were noted in this study for the GFRP-RC corbels in the absence/ presence of crack-control reinforcement: Compression strut failure (C-ST), Shear-compression failure (S-CO), and Diagonal-splitting failure (D-SP). In general, the specimens with the lower *a*/*d* ratio of 0.33 failed with excessive cracking accompanied by concrete spalling compared to that of the counterpart specimens with an *a*/*d* ratio of 0.66, which failed by strut splitting and shear compression.
2. The parameters: concrete strength ($f'_c$) and shear-span-to-depth ratio (*a/d*) had a noticeable impact on the capacity of the tested specimens. Increasing the concrete strength increased the capacity of GFRP-RC specimens while increasing the *a/d* ratio changed the failure

mode from the desired strut-crushing to the brittle diagonal-splitting. A similar trend as that of concrete strength was observed when the reinforcement ratio was increased.

3. The concrete strength had minimal effect on the load-deflection relationship for both *a/d* ratios (0.33 and 0.66). However, increasing the main reinforcement ratio caused a reduction in the deflection at the service load level. The load-deflection responses at failure for specimens for *a/d* of 0.33 were larger in magnitude with respect to specimens of larger shear spans of *a/d* of 0.66. This can be attributed to the premature failure of diagonal struts due to excessive principal tensile strains. On the other hand, the specimens with *a/d* of 0.33 showed lower deflection at service load levels when compared to *a/d* of 0.66. The steel-RC specimens showed yielding with the plateau-like formation in load-deflection responses.
4. The main reinforcement and horizontal crack-control reinforcement had minimal effect on the formation of initial flexural cracking; however, it enhanced the ultimate load capacity of the corbel. The crack-control horizontal reinforcement distributed within two-thirds of the effective depth had a notable effect on the ultimate deflection of the specimens with a shorter *a/d* ratio of 0.33. The horizontal crack-control reinforcement also reduced crack spacing in the web of the corbel and helped distribute cracks uniformly.
5. The load-flexural crack width relationship showed that the specimens with HSC and *a/d* of 0.66 had lower crack-opening resistance. Moreover, the specimens with NSC and an *a/d* of 0.66 showed less flexural crack width when it was compared to their HSC counterparts. An increase in concrete strength and *a/d* ratio increased flexural crack widths. An increase in main reinforcement ratio also showed an increase in crack-control resistance.
6. In general, the codes and standards generated strength predictions of shorter spanned specimens with *a/d* of 0.33 with smaller $P_{pre}/P_{exp}$ ratios when compared to a larger shear

span for *a/d* of 0.66. This is due to the excessive tensile stresses on the strut for a longer *a/d* of 0.66. The Canadian standards, CSA S806-12 (CSA 2021), produced conservative predictions of the corbel capacity with an average value of $P_{CSA}/P_{exp}$ of 0.6 and a CoV of 17.6 % (average values in Article I and Article II). The minimum crack-control reinforcement requirement was conservative, and even specimens without it also had predicted strengths lower than the experimental results. On the other hand, the ACI 318 (ACI Committee 318 2019) overestimated the capacity of the tested corbels in the presence of crack-control reinforcement with a mean value of $P_{ACI}/P_{exp}$ of 1.04 and a mean value of $P_{ACI}/P_{exp}$ of 0.84 for specimens without crack-control reinforcement respectively.

7. The analytical model presented in Chapter 5 can be used to predict type of failure (either strut crushing or tensile splitting) in GFRP-RC STM. The add-on model helps to find the residual strength of corbels with crack-control reinforcement according to CSA S806 (CSA 2021) by computing the strains in the crack-control reinforcement. The model can also be used to predict the failure of specimens without crack-control reinforcement.

## 6.3 Future Work

Based on the work conducted in the current study, several questions remain unanswered, and some gaps need to be filled. Additional research is required to allow the adoption of the strut-and-tie modelling technique to GFRP-RC members. The following recommendations for future work are suggested:

1. The effect of using fibres in the concrete mix needs to be studied particularly for the corbels with *a/d* greater than 0.33. The current study indicates that control of crack widths in concrete struts can be crucial to inclined struts to enhance their capacity and reduce premature failure. Fibres can be beneficial in arresting cracks and reducing crack widths.

Further testing can help introduce a minimum limit on the use of fibres and horizontal crack-control reinforcement to prevent diagonal tensile failure.

2. Additional research can be done on corbels strengthened or confined with sprayed-GFRP composites to check its effectiveness as a confinement material to resist the tensile splitting of concrete struts.

3. An analytical model devoted to vertical crack-control reinforcement can be developed.

4. Conduct a numerical finite element analysis to investigate further and cover a broader range of parameters.

# References

Abdul-Razzaq, K.S. and Dawood, A.A., 2020. Corbel strut and tie modeling – Experimental verification. *Structures*, 26, 327–339.

Abdul-Razzaq, K.S. and Dawood, A.A., 2021. Reinforcing Struts and Ties in Concrete Corbels. *ACI Structural Journal*, 118 (4), 153–162.

Abu-Obaida, A., El-Ariss, B., and El-Maaddawy, T., 2018. Behavior of Short-Span Concrete Members Internally Reinforced with Glass Fiber–Reinforced Polymer Bars. *Journal of Composites for Construction*, 22 (5).

ACI Committee 222, 2019. ACI PRC-222-19: Guide to Protection of Metals in Concrete Against Corrosion. *American Concrete Institute (ACI)*, Detroit, MI.

ACI Committee 318, 2019. "Building Code Requirements for Structural Concrete" (ACI 318-14) and Commentary (ACI 318R-19), *American Concrete Institute*, Detroit, MI, 1-628.

ACI Committee 363, 2010. “Report on High-Strength Concrete” (ACI PRC-363-10), *American Concrete Institute*., Detroit, MI.

ACI Committee 363, 2011. “Guide to Quality Control and Assurance of High-Strength Concrete.” (ACI 363.2R-11), *American Concrete Institute*., Detroit, MI.

ACI Committee 440a, 2015. "Guide for the Design and Construction of Structural Concrete Reinforced with FRP Bars." (ACI 440.1R-15), *American Concrete Institute*, Detroit, MI, 1-88.

ACI Committee 440b. 2022. “Building Code Requirements for Structural Concrete Reinforced with Glass Fiber-Reinforced Polymer (GFRP) Bars—Code and Commentary.” (ACI 440.11-22). *American Concrete Institute* Farmington Hills, MI: ACI.

ACI-ASCE Committee 445, 2021. “Strut-and-Tie Method Guidelines for ACI 318-19—Guide.” (ACI PRC-445.2-21), *American Concrete Institute*, Detroit, MI.

Adebar, P. and Zhou, Z., 1993. Bearing Strength of Compressive Struts Confined by Plain Concrete. *Structural Journal*, 90 (5), 534–541.

Almomani, M., Mahmoud, K., and El-Salakawy, E.F., 2022. Experimental Investigation of Large-Scale Eccentrically Loaded GFRP-Reinforced High-Strength Concrete Columns. *Journal of Composites for Construction*, 26 (2).

Andermatt, M.F. and Lubell, A.S., 2013. Behavior of Concrete Deep Beams Reinforced with Internal Fiber-Reinforced Polymer—Experimental Study. *Structural Journal*, 110 (4), 585–594.

ASTM C31, 2019. Standard Practice for Making and Curing Concrete Test Specimens in the Field. *ASTM International*, 04.

ASTM C39, 2016. *ASTM Standard C39/C39M-16, Standard Test Method for Compressive Strength of Cylindrical Concrete Specimens*. ASTM International.

ASTM. (2016). “Standard test method for tensile properties of fiber reinforced polymer matrix composite bars.” ASTM D7205/D7205M-06, West Conshohocken, PA.

ASTM. (2017). “Standard test methods and definitions for mechanical testing of steel products.” ASTM A370-17, West Conshohocken, PA.

Ayub, T., Shafiq, N., and Fadhil Nuruddin, M., 2014. Stress-strain response of high strength concrete and application of the existing models. *Research Journal of Applied Sciences, Engineering and Technology*, 8 (10).

Bediwy, A.G. and El-Salakawy, E.F., 2021. Ductility and performance assessment of glass fiber-reinforced polymer-reinforced concrete deep beams incorporating cementitious composites reinforced with basalt fiber pellets. *ACI Structural Journal*, 118 (4).

Bentz, E.C. and Collins, M.P., 2006. Development of the 2004 Canadian Standards Association (CSA) A23.3 shear provisions for reinforced concrete. *Canadian Journal of Civil Engineering*, 33 (5).

Berg, A.C., Bank, L.C., Oliva, M.G., and Russell, J.S., 2006. Construction and cost analysis of an FRP reinforced concrete bridge deck. *Construction and Building Materials*, 20 (8).

BS EN 1992-1-1, 2004. Eurocode 2: Design of concrete structures - Part 1-1 : General rules and rules for buildings. *British Standards Institution*, 1 (2004).

Campione, G. and Cannella, F., 2020. Analytical model for flexural response of reinforced concrete corbels externally strengthened with fiber- reinforced polymer. *ACI Structural Journal*, 117 (4).

Campione, G., 2012. Flexural Behavior of Steel Fibrous Reinforced Concrete Deep Beams. Journal of Structural Engineering, 138 (2).

Chakrabarti, P.R., Farahani, D.J., and Kashou, S.I., 1989. Reinforced and precompressed concrete corbels - an experimental study. *ACI Structural Journal*, 86 (4).

Collins, M.P. and Kuchma, D., 1999. How safe are our large, lightly reinforced concrete beams, slabs, and footings? *ACI Structural Journal*, 96 (4).

Collins, M.P. and Mitchell, D., 1986. Rational Approach to Shear Design--The 1984 Canadian Code Provisions. *Journal Proceedings*, 83 (6), 925–933.

CSA, 2021. "Design and Construction of Building Structures with Fibre-Reinforced Polymers" CSA S806-12. *Canadian Standard Association* (*CSA*), Toronto, Ontario, Canada.

CSA, 2019a. "Design of Concrete Structures" CSA A23.3-19. *Canadian Standard Association (CSA)*, Toronto, Ontario, Canada.

CSA, 2019b. "Canadian Highway Bridge Design Code" CSA S6-19. *Canadian Standard Association (CSA*) Toronto, Ontario, Canada.

CSA, 2019c. "Concrete Materials and Methods of Concrete Construction/Test Methods and Standard Practices for Concrete" CSA A23.1:19/CSA A23.2:19. *Canadian Standards Association (CSA)*, Toronto, Ontario, Canada.

CSA, 2019d. "Specification for fibre-reinforced polymers." CSA S807-19. *Canadian Standard Association (CSA)*. Toronto, Ontario, Canada.

El-Sayed, A.K., El-Salakawy, E.F., and Benmokrane, B., 2012. Shear strength of fibre-reinforced polymer reinforced concrete deep beams without web reinforcement. *Canadian Journal of Civil Engineering*, 39 (5).

Elzanaty, A.H., Nilson, A.H., and Slate, F.O., 1986. Shear Capacity of Reinforced Concrete Beams Using High-Strength Concrete. *Journal Proceedings*, 83 (2), 290–296.

Fattuhi, N.I., 1990a. ColumnLoad Effect on Reinforced Concrete Corbels. *Journal of Structural Engineering*, 116 (1), 188–197.

Fattuhi, N.I., 1990b. Strength of SFRC Corbels Subjected to Vertical Load. *Journal of Structural Engineering*, 116 (3), 701–718.

Fattuhi, N.I., 1994a. Strength of FRC Corbels in Flexure. *Journal of Structural Engineering*, 120 (2), 360–377.

Fattuhi, N.I., 1994b. Reinforced Corbels Made With High-Strength Concrete and Various Secondary Reinforcements. *Structural Journal*, 91 (4), 376–383.

Foster, S.J., Powell, R.E., and Selim, H.S., 1996. Performance of High-Strength Concrete Corbels. *Structural Journal*, 93 (5), 555–563.

Hoult, N.A., Sherwood, E.G., Bentz, E.C., and Collins, M.P., 2008. Does the Use of FRP Reinforcement Change the One-Way Shear Behavior of Reinforced Concrete Slabs? *Journal of Composites for Construction*, 12 (2).

Hwang, S.J., Lu, W.Y., and Lee, H.J., 2000. Shear strength prediction for reinforced concrete corbels. *ACI Structural Journal*, 97 (4), 543–552.

Joint ASCE-ACI Task Committee 426, 1973. The Shear Strength of Reinforced Concrete Members. Journal of the Structural Division, 99 (6), 1091–1187.

Kani, M.W., Huggins, M.W., and Wittkopp, R.R., 1979. Kani on shear in reinforced concrete.

Koch, G., Varney, J., Thompson, N., Moghissi, O., Gould, M., and Payer, J., 2016. *International measures of prevention, application, and economics of corrosion technologies study*. NACE International Impact.

Kriz, L.B. and Raths, C.H., 1965. Connections in Precast Concrete Structures—Strength of Corbels. *PCI Journal*, 10 (1), 16–61.

Mattock, A.H., Chen, K.C., and Soongswang, K., 1976a. The Behavior of Reinforced Concrete Corbels. *PCI Journal*, 21 (2), 52–77.

Mohamed, A., Mahmoud, K., and El-Salakawy, E.F., 2021. Shear Capacity of Glass Fiber-Reinforced Polymer-Reinforced Concrete Continuous Deep Beams without Web Reinforcement. *ACI Structural Journal*, 118 (3).

Mohamed, K., Farghaly, A.S., and Benmokrane, B., 2017. Effect of Vertical and Horizontal Web Reinforcement on the Strength and Deformation of Concrete Deep Beams Reinforced with GFRP Bars. *Journal of Structural Engineering*, 143 (8).

Nagrodzka-Godycka, K., 1999. Behavior of corbels with external prestressing bars - Experimental study. *ACI Structural Journal*, 96 (6).

Neville, A., 1995. Chloride attack of reinforced concrete: an overview. *Materials and Structures*, 28 (2).

Neville, A.M., 1996. *Properties of Conrete, NEVILLE 4th Edition Book.pdf*. London: Pitman Publishing.

Omeman, Z., Nehdi, M and El-Chabib, H. (2008). "Optimal efficiency factor in strut-and-tie model for FRP-reinforced concrete short beams with ($1.5 < a/d < 2.5$)." Materials and structures, 41(10), 1713-1727.

Schlaich, J., Schaefer, K., and Jennewein, M., 1987. Toward a Consistent Design of Structural Concrete. *PCI Journal*, 32 (3), 74–150.

Schmidt, M. and Fehling, E., 2005. Ultra-high-performance concrete: Research, development and application in Europe. *In*: *American Concrete Institute, ACI Special Publication*.

Tan, K.H., Kong, F.K., Teng, S., and Weng, L.W., 1997. Effect of web reinforcement on high-strength concrete deep beams. ACI Structural Journal, 94 (5).

Tongaroonsri, S. and Tangtermsirikul, S., 2009. Effect of mineral admixtures and curing periods on shrinkage and cracking age under restrained condition. *Construction and Building Materials*, 23 (2).

Vecchio F and M. P Collins, 1982. *The response of reinforced concrete to in-plane shear and normal stresses*. Dept. of Civil Engineering, University of Toronto.

Vecchio, F.J. and Collins, M.P., 1986. The Modified Compression-Field Theory for Reinforced Concrete Elements Subjected to Shear. *Journal Proceedings*, 83 (2), 219–231.

Wight, J.K. and MacGregor, J.G., 2009b. *Reinforced Concrete: Mechanics and Design*. Pearson Education, Inc., Upper Saddle River, New Jersey.

Williams, C.; Deschenes, D.; and Bayrak, O., 2012. "Strut-and-Tie Model Design Examples for Bridges,. *Bridges," Center for Transportation Research, the University of Texas at Austin, Austin, TX*, 7.

Yong, Y. and Balaguru, P., 1994. Behavior of Reinforced High-Strength-Concrete Corbels. *Journal of Structural Engineering*, 120 (4).

# APPENDIX A. SPECIMEN DETAILS WITH RESPECT TO ARTICLE 1 AND ARTICLE 2

## A.1 Test Specimens

A total of fourteen (14) large-scale corbels, twelve GFRP-RC specimens and two steel-RC specimens were fabricated and tested at the W.R McQuade's Structural Engineering Laboratory at the University of Manitoba.

All the corbel specimens were simply supported with two equal corbel spans. Each specimen had a rectangular cross-section with a width of 300 mm and a height of 450 mm at the corbel-column interface. The span length between two bearing supports of the inverted simply supported corbels was 1250 mm, with a shear span-to-depth ratio of 0.33 and 0.66, respectively. The clear unsupported length of the two bearings supports in the inverted corbel setup was spaced at 466 mm and 733 mm for *a/d=0.33* and *a/d=0.66*, respectively while the centre-to centre length between the bearings support in the inverted test setup was 616 mm to 883 mm for *a/d* from 0.33 to 0.66.

The $\rho_{main}$ of 0.5% and 0.7% was chosen and designed according to the CSA S806-12 and literature (Kriz and Raths 1965, Mattock *et al.* 1976). The remaining parameters such as the *a/d* ratio of less than unity was also chosen to represent D-regions entirely without any B-region effects according to the North American Standards and Codes (ACI Committee 318 2019, CSA 2019a). The column for the GFRP-RC specimens was reinforced with 4-No. 20 GFRP bars and No. 10 GFRP stirrups spaced at 250 mm. All GFRP straight bars and stirrups were sand coated.

Two conventional steel-RC corbels were designed according to ACI 318 (ACI Committee 318 2019) provisions with similar ratios for *a/d=0.33* and *a/d =0.66*. They were constructed and tested to assess the difference in behaviour between the two reinforcing materials. For the steel-RC control specimens, three 15M and 10M deformed steel bars were used for the main and horizontal crack-control reinforcement, respectively. For the column, 4-20M steel bars and No. 10M steel stirrups spaced at 250 mm were used for the main and transverse reinforcements, respectively.

The test specimens were categorized into three groups. The first series (I) was intended for testing the absence of crack-control reinforcement, while the second series (II) was employed for examining the presence of crack-control reinforcement. The third series (III) was allocated to investigate the concrete strength parameter. Chapter 3 deals with Series (I) and Series (II), while Chapter 4 deals with Series (II) and Series (III), respectively.

Series I had four simply supported GFRP-RC corbels with a main longitudinal reinforcement ratio ($\rho_{main}$) of 0.5 % and 0.7% and a shear span-to-depth ratio *(a/d)* of 0.33 and 0.66. Horizontal crack-control reinforcement was absent in Series I. Series II had five specimens, and crack-control reinforcement was the distinguishing parameters from the specimens of Series I. The specimens of Series II had *a/d* ratio varying from 0.33 to 0.66 and a primary reinforcement ratio ($\rho_{main}$) of 0.5% and 0.7% similar to Series I. The parameter of the crack-control reinforcement ratio was 0.7% and 1.3% and coupled with $\rho_{main}$ of 0.5% and 0.7%, respectively.

Series III had the same configuration of reinforcement and testing setup details as in Series II but with High Strength concrete (HSC). While Series I and II had a target strength of concrete of $f'_c$ = 35 MPa, the Series III had a target strength of $f'_c$ = 60 MPa.

In this study the corbels were identified with a name consisting of four terms. For e.g. *SH-0.66-0.5-10* the first term denotes the type of reinforcement ("*SH*" for HSC steel or "*GH/GN*" for HSC/NSC GFRP), the second term is *a/d* ratio (0.33 and 0.66), the third term indicates the main reinforcement ratio (0.5% for steel, 0.5% and 0.7% for GFRP) while the last term defines the crack-control reinforcement ( "10" for three horizontal stirrups of No.10 corresponding to 0.7% and "13" for three stirrups of No 13 corresponding to 1.3% reinforcement ratio respectively ).

A detailed breakdown of the test matrix is listed in Table 6.1 and some of the dimension variables used in the test matrix are represented in Figure A.1 . Figure A.2 and Figure A.3 provided the diagrammatic representation of the reinforcement detailing with dimensions for specimens with and without crack-control reinforcement, respectively.

Table 6.2 listed the specimens used in the two journal articles along with their corresponding names in the articles.

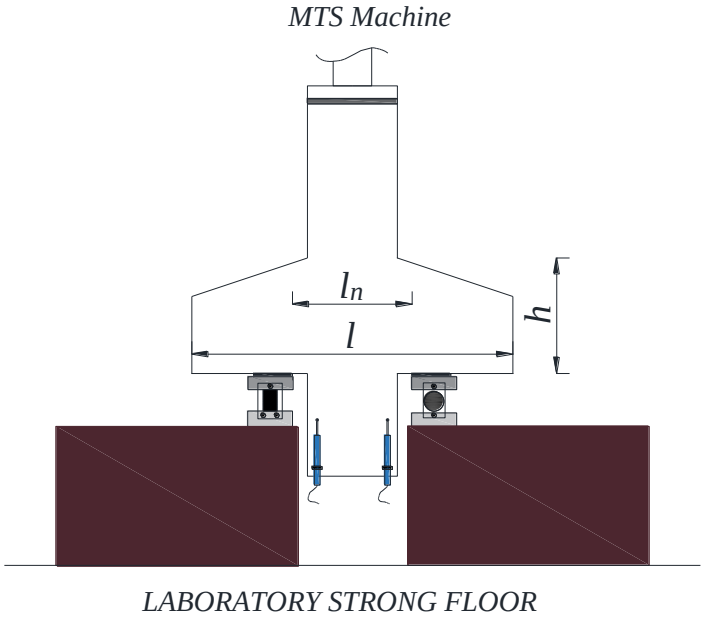


Figure A.1. Dimensions symbols used in Table A.1

Table 6.1. Details of Test specimens.

| Series | Beam ID | *a/d* | *d* (*mm*) | *b* (*mm*) | *l*[4] (*mm*) | $l_n$[5] (*mm*) | Main Reinforcement (Tie) | | Secondary Horizontal Crack-control reinforcement | | $f'_c$ (MPa) |
|---|---|---|---|---|---|---|---|---|---|---|---|
| | | | | | | | $\rho_{main}$ (%) | Bars | $\rho_{sw}$ (%) | Bars | |
| I | GN-0.33-0.5-0 | 0.33 | 403.5 | 300 | 1250 | 732.6 | 0.5 | 3-No. 16 | N/A | | 39.1 |
| | GN-0.33-0.7-0 | 0.33 | 401.7 | 300 | 1250 | 465.1 | 0.7 | 3-No. 20 | | | 42.0 |
| | GN-0.66-0.5-0 | 0.66 | 403.5 | 300 | 1250 | 732.6 | 0.5 | 3-No. 16 | | | 42.5 |
| | GN-0.66-0.7-0 | 0.66 | 401.7 | 300 | 1250 | 730.2 | 0.7 | 3-No. 20 | | | 43.0 |
| II | SN-0.33-0.5-10 | 0.33 | 404.0 | 300 | 1250 | 466.7 | 0.5 | 3 No. 15M | 1 | 3-10M @ 65 mm | 45.2 |
| | GN-0.33-0.5-10 | 0.33 | 403.5 | 300 | 1250 | 466.3 | 0.5 | 3 No. 16 (#5) | 0.7 | 3-10M (#3) @ 65mm c/c | 39.9 |
| | GN-0.33-0.7-13 | 0.33 | 401.7 | 300 | 1250 | 465.1 | 0.7 | 3 No. 20 (#6) | 1.3 | 3-No.13 (#4) @ 65 mm c/c | 44 |
| | GN-0.66-0.5-10 | 0.66 | 403.5 | 300 | 1250 | 732.6 | 0.5 | 3 No. 16 (#5) | 0.7 | 3-No.10 (#3) @ 65mm c/c | 40.8 |
| | GN-0.66-0.7-13 | 0.66 | 401.7 | 300 | 1250 | 730.2 | 0.7 | 3 No. 20 (#6) | 1.3 | 3-No.13 (#4) @ 65 mm c/c | 41.5 |
| III | GH-0.33-0.5-10 | 0.33 | 403.5 | 300 | 1250 | 732.6 | 0.5 | 3 No. 16 (#5) | 0.7 | 3-No.10 (#3) @ 65mm c/c | 58.5 |
| | GH-0.33-0.7-13 | 0.33 | 401.7 | 300 | 1250 | 465.1 | 0.7 | 3 No. 20 (#6) | 1.3 | 3-No.13 (#4) @ 65 mm c/c | 59.8 |
| | GH-0.66-0.5-10 | 0.66 | 403.5 | 300 | 1250 | 732.6 | 0.5 | 3 No. 16 (#5) | 0.7 | 3-No.10 (#3) @ 65mm c/c | 62.3 |
| | GH-0.66-0.7-13 | 0.66 | 401.7 | 300 | 1250 | 730.2 | 0.7 | 3 No. 20 (#6) | 1.3 | 3-No. 13 (#4) @ 65 mm c/c | 59.8 |
| | SH-0.66-0.5-10 | 0.67 | 404.0 | 300 | 1250 | 466.7 | 0.5 | 3 No. 15M | 1 | 3-10M @ 65mm c/c | 54.3 |

[4] Total span of the double-sided corbel
[5] Clear span of the corbel between two bearing surfaces on the test setup

Table 6.2. Specimen IDs used in the Journal articles and their nomenclature.

| SERIES | SPECIMENS | Chapter 4: ARTICLE 1 | Chapter 5: ARTICLE 2 |
|---|---|---|---|
| I | GN-0.33-0.5-0 | G-0.33-0.5-0 | N/A |
| | GN-0.33-0.7-0 | G-0.33-0.7-0 | N/A |
| | GN-0.66-0.5-0 | G-0.66-0.5-0 | N/A |
| | GN-0.66-0.7-0 | G-0.66-0.7-0 | N/A |
| II | SN-0.33-0.5-10 | S-0.33-0.5-10 | N/A |
| | GN-0.33-0.5-10 | G-0.33-0.5-10 | GN-0.33-I |
| | GN-0.33-0.7-13 | G-0.33-0.7-13 | GN-0.33-II |
| | GN-0.66-0.5-10 | G-0.66-0.5-10 | GN-0.66-I |
| | GN-0.66-0.7-13 | G-0.66-0.7-13 | GN-0.66-II |
| III | GH-0.33-0.5-10 | N/A | GH-0.33-I |
| | GH-0.33-0.7-13 | N/A | GH-0.33-II |
| | GH-0.66-0.5-10 | N/A | GH-0.66-I |
| | GH-0.66-0.7-13 | N/A | GH-0.66-II |
| | SH-0.66-0.5-10 | N/A | SH-0.66-I |

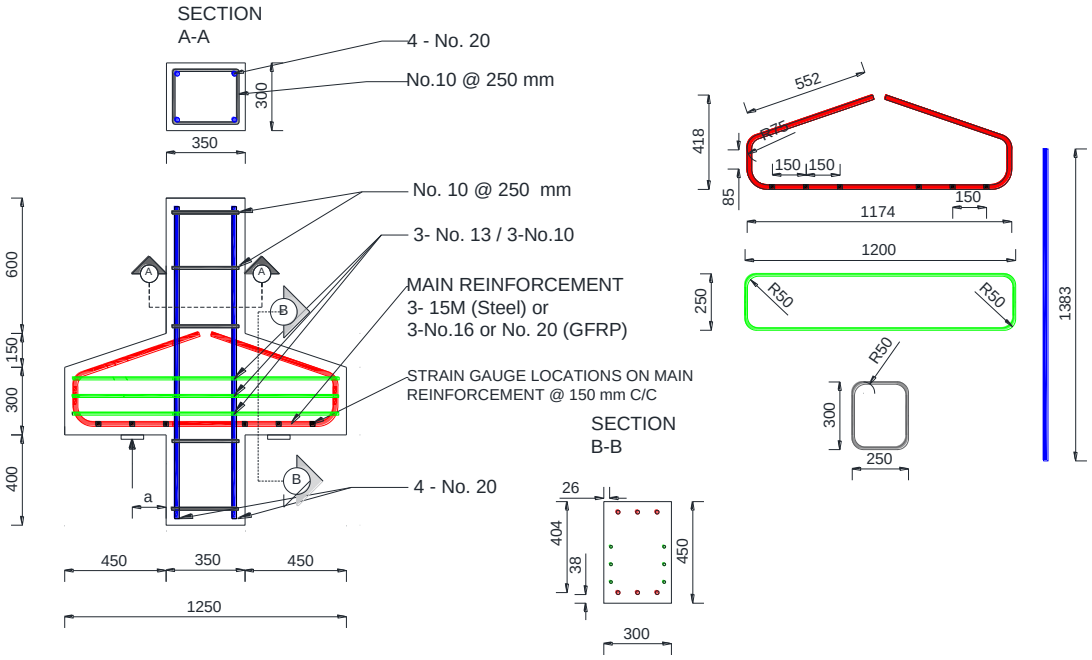


Figure A.2. Geometry and Reinforcement details for corbels with crack-control reinforcement.

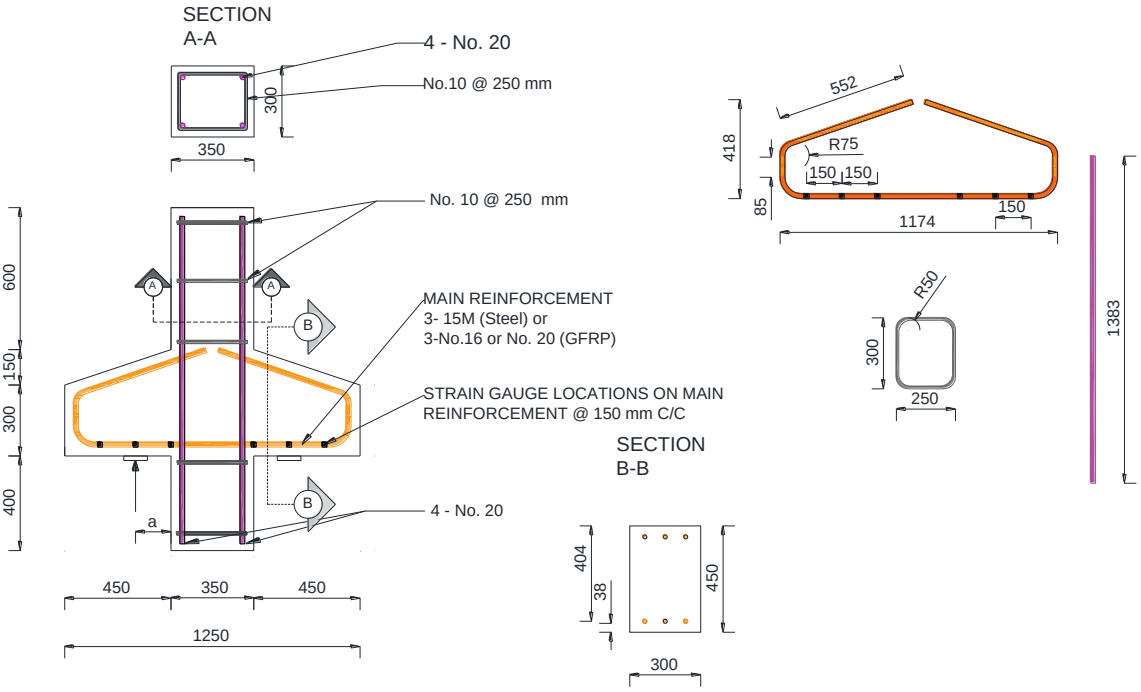


Figure A.3. Geometry and Reinforcement details for corbels without crack-control reinforcement.

## A.2 Test setup and Instrumentation

The specimens were marked with 75 mm grid lines after whitewashing the specimen, and then cracking markings were to be done on the specimen. The tests were conducted using a static simply supported setup, with a 5000 kN MTS closed loop hydraulic actuator applying monotonic loading under displacement-controlled mode. The corbels were set up with a hinged support on one side and the roller on the other end. The MTS machine is equipped with a built-in load cell; this was used to obtain the axial load applied to the column. Two more load cells were used under the pinned support to measure the reactions of the support of the inverted corbel. The rate of loading was 0.25mm/minute which was researched through available literature for D-regions tests including corbel and deep beams tests (Fattuhi 1990b, 1994b, Andermatt and Lubell 2013). To measure strains in the longitudinal main reinforcement, eight electronic strain gauges (ESG) were attached to critical locations on primary bent reinforcement and four ESGs were placed on crack-control reinforcement as shown in the Figure A.4. The two shear spans with the test-setup are shown in Figure A.5. All strains, displacements, and loads were automatically logged into a Data Acquisition System (DAQ) and were recorded and stored on a personal computer as shown in Figure A.6.

Linear variable-displacement transducers (LVDTs) were used to measure deflection at the two corbels surface with respect to the column. In addition, four 200 mm PI gauges were used to calculate the crack widths at two locations: the mid-height of the struts and column-corbel interface at ties level (clear cover from the tension side). These gauges were employed to monitor the widths of the strut and flexural cracks respectively.

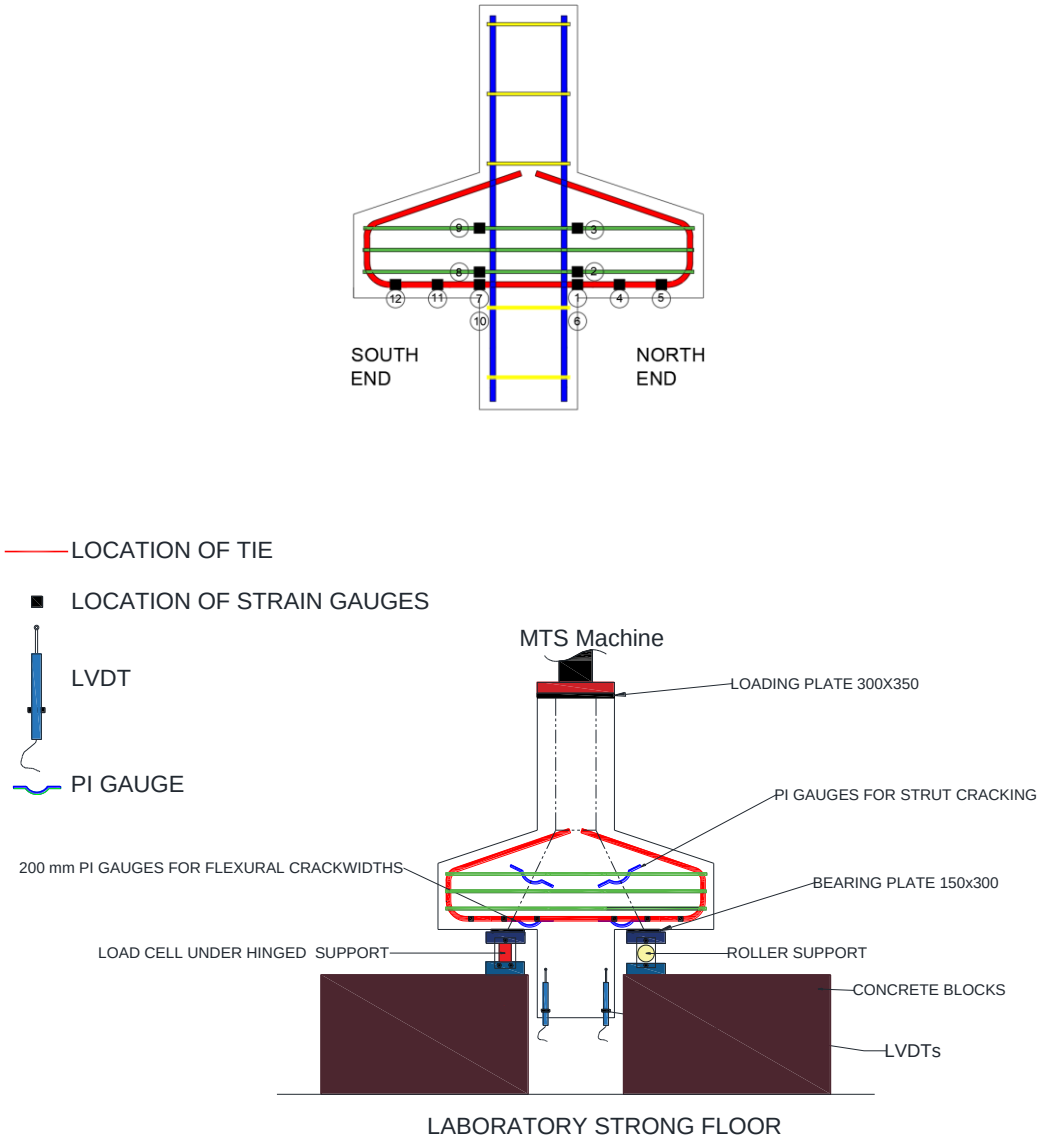


Figure A.4.Test Setup and Instrumentation

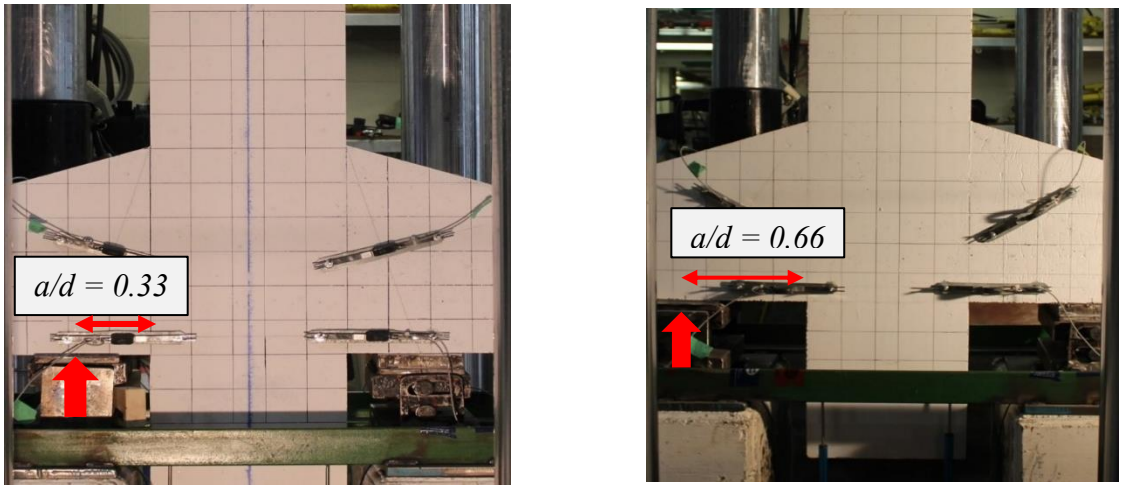


(a) (b)

Figure A.5. Photos showing the two shear-span-to-depth ratios (a) *a/d=0.33* (b) *a/d=0.66*

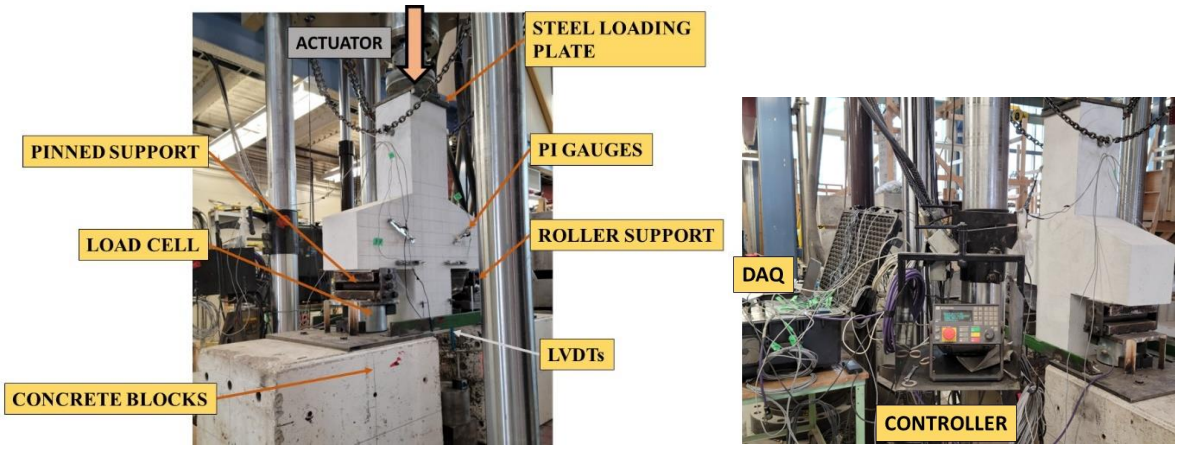


(a) (b)

Figure A.6. Photo of the various components of the test-setup(a) side view (b) rear view.

## A.3 Construction of Test Corbels

The initial construction stage involved mounting the strain gauges on GFRP or steel reinforcement bars at predetermined positions. To prepare for installing strain gauges, the bars were abraded and cleaned. Special adhesive was used to attach the strain gauges to the reinforcement cages. The

reinforcement cages were subsequently assembled, followed by creating formworks out of plywood sheets for various corbel dimensions. Stiffeners were added to each formwork to prevent shape distortion during concrete casting. Once the formworks were ready, the reinforcing cages were inserted into the formwork, followed by casting the concrete. The strain gauges were given a thin layer of silicone coating to shield them from moisture, impact, and damage during casting. To make it simpler to remove the corbel after casting and curing the concrete, a coating of oil was applied to the formwork before the reinforcing cages were installed. Figure A.7 illustrates some of the construction steps for the specimens.

(A) Oiling Formwork before casting of concrete

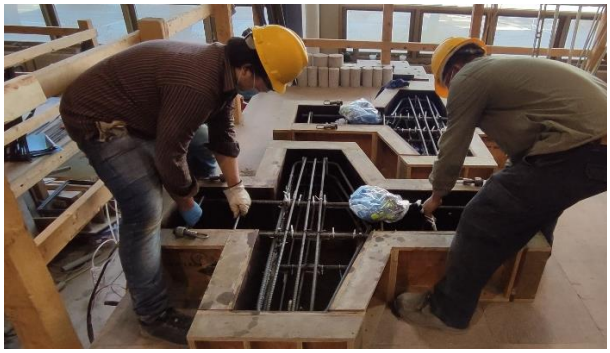

(B) Placing build reinforcement caging into the formwork.

(C) Casting of concrete

(D) Curing of concrete using burlaps and plastic cover

(E) Preparation of bars for installation of strain gauges

(F) Reinforcement with installed strain gauges

Figure A.7. Steps of construction of specimens.

To maintain the depths of the concrete cover and reinforcement, plastic chairs were incorporated. Moreover, an electrical vibrator was utilized during the casting process to ensure proper compaction. Once the casting was complete, the concrete's surface was smoothed to a fine finish and then covered with a plastic film. The curing process for the constructed concrete corbels and the concrete cylinders started the next day and the concrete surface was kept wet until the cylinder tests yielded target strengths.

Standard 100×200 mm and 150×300 mm cylinders were cast from each batch following the standards (ASTM C31 2019) and tested after 3, 14 and at the day of testing to determine the actual concrete compressive and tensile strengths, respectively.

# APPENDIX B. GFRP-RC CORBEL ANALYSIS USING CSA S806-12

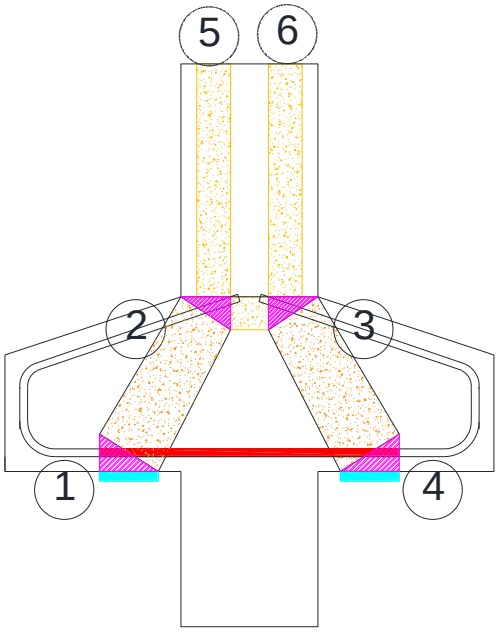


Figure B.1. STM used as primary mechanism I for the prediction calculations.

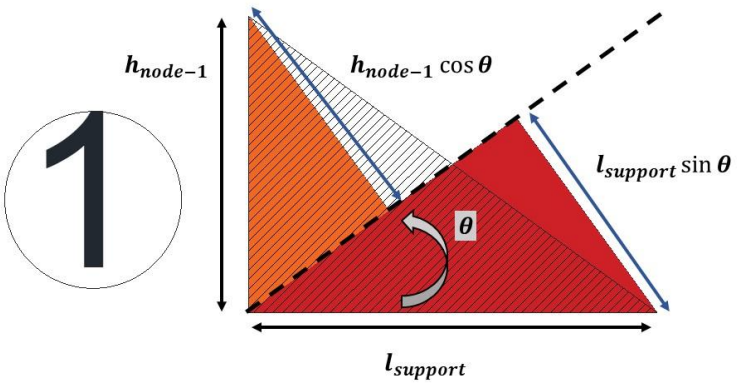


Figure B.2. Parameters on CCT node 1

Sample calculations from CSA S806-12 for specimen **GH-0.33-0.7-13:**

| Parameter | Formulae | Values |
|---|---|---|
| Shear-span-to-depth ratio, $\frac{a}{d}$ | | 0.33 |
| Corbel Width, $w$ | | 300 |
| Clear Cover requirement, $c_c$ | | 38 |
| Height of corbel, $H$ | | $450mm$ |
| Depth of column head, $H_{column}$ | | 350 $mm$ |
| Concrete strength, $f_c'$ | | $59.6MPa$ |
| Main Reinforcement | | |
| Strength, $f_{Fu}, MPa$ | 1* | 1194 $MPa$ |
| Area of 1 bar | 2* | 285 |
| No. of Bars | 3* | 3 |
| Failure load of Ties, $T$ | $= f_{Fu} \times A_{FT} = 1194 \times 285 \times 3$ | 1020870 $N$ |
| Modulus of Elasticity, $E$ | | 55881 $MPa$ |
| Diameter, $d_{main}$ | $= \sqrt{(2^*) \times 4/\pi}$ | 19.05 $mm$ |
| Effective Depth of corbel, $d_{\ actual}$ | $= H - c_c - d_{main}/2$ | $401.7mm$ |
| Depth of corbel for the strut angle $d_{\ angle}$ | $= H - 2c_c - d_{main}$ | 355 $mm$ |
| Load point (from interface), $a$ | $= \frac{a}{d} \times d_{\ actual}$ | $132.5mm$ |
| Load point from the end of node, $B$ | $= a + {Width_{bearing}}/{2}$ | 207.8 $mm$ |
| Angle of the strut | $\tan\theta = d_{\ actual}/B$ | 1.708 |
| Strut angle $\theta_{degrees}$ | | 59.7 |
| Load on one corbel, $P$ | $\Rightarrow \frac{T}{P} = \frac{B}{d_{actual}}$ | 1713474 $N$ |
| Total capacity, $2P$ | | 3427 $kN$ |
| NODE | | 1 (See Figure B.2). |
| $\phi_c$ | | 1 |
| $m$ | | 1 |
| Node capacity for 1, $N_1$ | $= 0.75\phi_c m f_c'$ | $44.7MPa$ |
| Height of Node back face near ties, $h_{node-1}$ | $h_{node-1} = (c_c \times 2) + d_{main}$ | 95.0 $mm$ |

| | | |
|---|---|---|
| Bearing length provided (at Supports), $l_{support}$ | | 150 $mm$ |
| Dimension of interior face of Node, $w_{node-1}$ | $w_{node-1} = (l_{support} \sin\theta) + (h_{node-1} \cos\theta)$ | 178.0$mm$ |
| Iteration 1: | | |
| Assuming, Tie Strain, $\epsilon_s$ | | 0.0103 |
| Principal Tensile Strain, $\epsilon_1$ | $\epsilon_1 = \epsilon_s + (\epsilon_s + 0.002)\cot^2\theta$ | 0.0145 |
| Concrete Strength, $f_c'$ | | 59.8 $MPa$ |
| Limiting compressive stress in concrete strut $f_{cu}$ | $f_{cu} = \frac{f_c'}{(0.8 + 170\epsilon_1)}$ | 18.3 $MPa$ |
| Load on Strut 1-2 and 3-4, $L_{1-2}$ | $L_{1-2} = {}^{P}/_{\sin\theta_{degrees}}$ | 971286 $N$ |
| Area of cross-section,$A_{1-2}$ | $A_{1-2} = L_{1-2}/f_{cu}$ | 53163 $mm^2$ |
| Width of strut $w_{1-2}$ | $= A_{1-2}/w$ | 177 $mm$ |
| The interior face will support Width of strut. ($w_{node-1} = w_{1-2}$) | | |
| Using dimension of interior face of the node as width of strut | $w_{1-2} = w_{node-1}$ | |
| Load on Strut 1-2 | $L_{1-2,actual} = w_{node-1} \times w \times f_{cu}$ | 971286 $N$ |
| Load on one corbel, $P_{actual}$ | $P_{actual} = L_{1-2} \sin\theta$ | 971.3 $kN$ |
| Force on Ties, $T_{actual}$ | $T = L_{1-2} \cos\theta$ | 491 $kN$ |
| Strain on Ties, | $\epsilon_s = T/(A_{1-2} \times E)$ | 0.0103 |
| Same Tie strains as assumptions | | |
| NODE CHECK: | | |
| Dimension of interior face of Node is safe as $N_1 > f_{cu}$ | | |
| Bearing length needed (at Supports), $l_{support,\ needed}$ | $l_{support,\ needed} = P_{actual}/(N_1 \times w)$ | 62.5 $mm$ |
| Safe bearing length 62.5< 150 | | |
| Height of Node back face near ties, $h_{node-1,needed}$ | $h_{node-1,needed} = T_{actual}/(N_1 \times w)$ | 36.6 $mm$ |
| Safe height of back face $36.6\ mm < h_{node-1}$ | | |

# APPENDIX C. GFRP-RC CORBEL ANALYSIS USING ACI 318-19

Sample calculations from ACI 318-19 for specimen **GH-0.33-0.7-13:**

| Parameter | Formulae | Values |
|---|---|---|
| Shear-span-to-depth ratio, $\frac{a}{d}$ | | 0.33 |
| Corbel Width, $w$ | | 300 |
| Clear Cover requirement, $c_c$ | | 38 |
| Height of corbel, $H$ | | 450$mm$ |
| Depth of column head, $H_{column}$ | | 350 $mm$ |
| Concrete strength, $f_c'$ | | 59.6$MPa$ |
| Main Reinforcement | | |
| Strength $f_{Fu}, MPa$ | 1* | 1194 $MPa$ |
| Area of 1 bar | 2* | 336 |
| No. of Bars | 3* | 3 |
| Failure load of Ties, $T_{failure}$ | $= f_{Fu} \times A_{FT} = 1194 \times 285 \times 3$ | 1020870 $N$ |
| Modulus of Elasticity, $E$ | 4* | 55881 $MPa$ |
| Diameter, $d_{main}$ | $= \sqrt{(2^*) \times 4/\pi}$ | 19.0 $mm$ |
| Effective Depth of corbel, $d_{\ actual}$ | $= H - c_c - d_{main}/2$ | 401.7$mm$ |
| Depth of corbel for the strut angle $d_{\ angle}$ | $= H - 2c_c - d_{main}$ | 355 $mm$ |
| Load point (from interface), $a$ | $= \frac{a}{d} \times d_{\ actual}$ | 132.5$mm$ |
| Load point from the end of node, $B$ | $= a + {Width_{bearing}}/{2}$ | 207.8 $mm$ |
| Angle of the strut | $tan\,\theta = d_{\ angle}/B$ | 1.70800 |
| Strut angle $\theta_{degrees}$ | | 59.7 |
| NODE Geometry 1 (See Figure B.2). | | |
| Height of Node back face near ties, $h_{node-1}$ | $h_{node-1} = (c_c \times 2) + d_{main}$ | 95 $mm$ |
| Bearing length provided (at Supports), $l_{support}$ | | 150$mm$ |

| | | |
|---|---|---|
| Dimension of interior face of Node, $w_{node-1}$ | $w_{node-1} = (l_{support} \sin\theta) + (h_{node-1} \cos\theta)$ | $177.0mm$ |
| STRUT | | 1 (See Figure B.1 and B.2). |
| $\beta_s$ | | 0.75 |
| $\beta_c$ | | 1 |
| Strut Strength for 1-2, $\sigma_{S,1-2}$ | $= 0.85\beta_s\beta_c f_c'$ | $37.3MPa$ |
| Strut force for 1-2, $F_{S,1-2}$ | $= \sigma_{S,1-2} \times w \times w_{node-1}$ | 1713474 $N$ |
| | | |
| Tie Force $T_{actual}$ | $= F_{S,1-2} \times \cos\theta$ | 1003206 $N$ |
| Strain on Tie, $\epsilon_s$ | $= T_{actual}/(2^* \times 3^* \times E)$ | 0.021116544 |
| Ultimate strain of Tie $\epsilon_{s-ultimate}$ | $= {T_{failure}}/{(2^* \times 3^* \times E)}$ | 0.0225 |
| The ultimate strain capacity is lower than strain on tie in STM. | | |
| Load on one corbel, $P_{actual}$ | $P_{actual} = \frac{T_{actual}}{P_{actual}} = \frac{B}{d_{actual}}$ $= F_{S,1-2} \sin\theta$ | 1713.5 $kN$ |
| Total capacity, $2P$ | | 3427 $kN$ |
| NODE CHECK: 1 (See Figure B.2). | | |
| $\beta_n$ | | 0.8 |
| $\beta_c$ | | 1 |
| Node capacity for 1, $N_1$ | $= 0.85\beta_n\beta_c f_c'$ | 39.78 $MPa$ |
| Dimension of interior face of Node is safe as $N_1 > \sigma_{S,1-2}$ | | |
| Bearing length needed (at Supports), $l_{support,\ needed}$ | $l_{support,\ needed} = P_{actual}/(N_1 \times w)$ | 143.6 $mm$ |
| Safe bearing length $143.6 < 150$ | | |
| Height of Node back face near ties, $h_{node-1,needed}$ | $h_{node-1,needed} = T_{actual}/(N_1 \times w)$ | 84.1 $mm$ |
| Safe height of back face $84.1mm < h_{node-1}$ | | |